

ABSTRACT

Title of Document: SELF-ASSEMBLY IN AQUEOUS
SOLUTIONS OF A NON-IONIC
HYDROTROPE

Deepa Subramanian, Doctor of Philosophy, 2012

Directed By: Mikhail A. Anisimov
Professor
Department of Chemical and Biomolecular
Engineering

Hydrotropes are amphiphilic molecules, too small to cause spontaneous self-assembly towards equilibrium mesoscale structures in aqueous solutions, but they form dynamic, noncovalent assemblies, which may create microscopic regions of lowered polarity. This enhances the solubilization of hydrophobic compounds, also known as solubilizates, in aqueous solutions and may cause further aggregation to larger structures. In this work, unusual mesoscopic properties of aqueous solutions of a non-ionic hydrotrope, namely tertiary butyl alcohol (TBA) have been investigated by light scattering, microscopy, and chromatography. Aqueous TBA solutions show anomalous thermodynamic and structural properties in the range of concentrations 3–8 mol % TBA and temperatures 0 – 25 °C. These anomalies appear to be associated

with short-lived, short-ranged micelle-like structural fluctuations, distinctly different from usual concentration fluctuations in non-ideal solutions. Molecular dynamics simulations and neutron-scattering experiments show clustering of TBA molecules on a nanometer scale, interacting through hydrogen bonds with a shell of water molecules. In this concentration range, TBA aqueous solutions, although macroscopically homogeneous, occasionally show the presence of “mysterious” inhomogeneities on a 100 nm scale. We have found that the emergence of such inhomogeneities strongly correlates with impurities present in commercial TBA samples. Experiments with controlled addition of a third component, such as propylene oxide, isobutyl alcohol, or cyclohexane, reveal the mechanism of formation of these inhomogeneities through stabilization of micelle-like fluctuations by a solubilizate. These structures are long-lived, *i.e.*, stable from a few days up to many months. We have confirmed that mesoscale structures in aqueous solutions can be generated from self-assembly of small molecules, without involvement of surfactants or polymers. This kind of self-assembly may potentially result in the development of novel nanomaterials.

SELF-ASSEMBLY IN AQUEOUS SOLUTIONS OF A NON-IONIC
HYDROTROPE

By

Deepa Subramanian

Dissertation submitted to the Faculty of the Graduate School of the
University of Maryland, College Park, in partial fulfillment
of the requirements for the degree of
Doctor of Philosophy
2012

Advisory Committee:
Professor Mikhail A. Anisimov, Chair
Professor Robert M. Briber
Professor Sheryl H. Ehrman
Assistant Professor Jeffery B. Klauda
Associate Professor Srinivasa R. Raghavan
Distinguished University Professor Jan V. Sengers

© Copyright by
Deepa Subramanian
2012

Acknowledgements

I would like to thank my family for giving me the opportunity to pursue higher education and enhance my knowledge.

I would also like to thank my research group members for all the fruitful scientific discussions. I would also like to thank the staff at the business offices of Department of Chemical & Biomolecular Engineering and Institute for Physical Science and Technology for their support throughout my graduate career.

Finally, I am highly indebted to my advisor, Professor Anisimov, for his most wonderful mentoring of a graduate student like me. I am very grateful for all his patience and teaching throughout my 5 years as a graduate student. I am much more educated, knowledgeable, and a better person now, than I would have been without the guidance of my advisor.

Table of Contents

Acknowledgements.....	ii
Table of Contents.....	iii
List of Figures.....	vi

Chapter 1: Introduction

1.1 What are hydrotropes?.....	1
1.2 Hydrotropes vs. surfactants.....	2
1.3 Classification of hydrotropic molecules.....	2
1.4 Tertiary butyl alcohol (TBA): A non-traditional hydrotrope.....	3
1.5 Mechanism of hydrotropic action.....	4
1.6 Mysteries of aqueous solutions of hydrotropes.....	6
1.7 Why do we care about hydrotropes?.....	8
1.8 Current research goals and objectives.....	9
1.9 Dissertation outline.....	10

Chapter 2: Thermodynamics of aqueous TBA solutions

2.1 Thermodynamic phase diagram of TBA-water.....	12
2.2 Excess molar volume and partial molar volumes.....	14
2.3 Heat capacity.....	18
2.4 Excess molar and partial molar enthalpies, entropies, and Gibbs free energies	21

2.5 Activity coefficient of water.....	27
2.6 Ultrasonic absorption and isothermal compressibility	28
2.7 Results from X-ray scattering experiments	31
2.8 Results from small-angle neutron scattering experiments	31
2.9 Results from molecular dynamics simulations.....	32
Chapter 3: Mesoscale inhomogeneities in aqueous TBA solutions	
3.1 Controversies surrounding the mesoscopic properties of aqueous TBA solutions – Review of light-scattering investigations.....	44
3.2 Experimental techniques and procedures	47
3.3 Experimental results	52
3.4 Origin of mesoscale inhomogeneities	61
Chapter 4: Macro and mesophases of aqueous solutions of hydrotropes	
4.1 TBA-water-propylene oxide system	72
4.2 TBA-water-cyclohexane ternary system	91
4.3 TBA-water-isobutyl alcohol ternary system	103
4.4 Results from molecular dynamics simulations.....	110
Chapter 5: Nature of mesoscopic inhomogeneities in aqueous solutions of hydrotropes	
5.1 Microheterogeneities in aqueous TBA solutions	123
5.2 Self-assembly in aqueous solutions of non-ionic hydrotropes.....	129

Chapter 6: Outlook.....	134
Bibliography	137

List of Figures

Figure 2.1. Phase diagram of tertiary butyl alcohol (TBA) - water binary system at ambient pressure, showing the liquid-solid equilibrium line.....	13
Figure 2.2. Excess molar volume of aqueous TBA solutions as a function of TBA concentration, at various temperatures.....	14
Figure 2.3. Excess partial molar volume of TBA in its aqueous solution, as a function of TBA concentration, at various temperatures.	15
Figure 2.4. Excess partial molar volume of water in aqueous TBA solutions, as a function of TBA concentration, at various temperatures.	16
Figure 2.5. Partial molal volumes of C1-C4 monohydric alcohols in their aqueous solutions as a function of concentration, at ambient temperatures.	17
Figure 2.6 Heat capacity of aqueous TBA solutions as a function of concentration, at various temperatures.	19
Figure 2.7. Heat capacity of aqueous TBA solutions as a function of temperature, for various concentrations.	20
Figure 2.8. Excess enthalpy of mixing in TBA-water solutions as a function of TBA mole fraction at $T = 26\text{ }^{\circ}\text{C}$	22
Figure 2.9. Partial molar enthalpy of TBA and water in aqueous TBA solutions as a function of TBA mole fraction, at $T = 25\text{ }^{\circ}\text{C}$	23

Figure 2.10. Excess entropy of mixing in aqueous TBA solutions as a function of TBA mole fraction at $T = 25\text{ }^{\circ}\text{C}$	24
Figure 2.11. Partial molar entropy of TBA and water in aqueous TBA solutions as a function of TBA mole fraction at $T = 25\text{ }^{\circ}\text{C}$	24
Figure 2.12 Excess molar Gibbs energy of mixing in aqueous TBA solutions as a function of TBA mole fraction at $T = 25\text{ }^{\circ}\text{C}$	25
Figure 2.13. Partial molar excess Gibbs energy (excess chemical potential) of TBA and water in aqueous TBA solutions as a function of TBA mole fraction, at $T = 25\text{ }^{\circ}\text{C}$	26
Figure 2.14. Activity coefficient of water in aqueous TBA solutions as a function of TBA mole fraction at $T = 10\text{ }^{\circ}\text{C}$	28
Figure 2.15. Absorption of sound in alcohol-water solutions as a function of alcohol concentration at $\sim 25\text{ }^{\circ}\text{C}$	29
Figure 2.16 Isothermal compressibility measurements in TBA-water solutions as a function of TBA mole fraction, at $T = 25\text{ }^{\circ}\text{C}$	30
Figure 2.17. Radial distribution function between central carbon atom of TBA molecules in its aqueous solution, obtained by using TIP4P-ICE model.	34
Figure 2.18. Partial pair distribution functions between central carbon atoms in TBA for three different concentrations of TBA in water.	35

Figure 2.19. Radial distribution functions between oxygen atoms of TBA molecules in its aqueous solution obtained by using TIP4P-ICE model.	36
Figure 2.20. Snapshots from molecular dynamics simulations of 0.038 mole fraction aqueous TBA solutions obtained by using the TIP4ICE model at 285 K, simulated for 100 ns.	38
Figure 2.21. Radial distribution functions between the oxygen on TBA and water obtained by using TIP4P-ICE model.	42
Figure 2.22. Large clustering of neighboring TBA in the same plane and second shell TBA (TIP4ICE-285).	43
Figure 3.1. Experimental set-up (and schematic) used for static and dynamic light scattering experiments.	48
Figure 3.2. Time-dependent intensity auto-correlation function for the 0.083 mole fraction TBA aqueous solution at a scattering angle $\theta = 30^{\circ}$ obtained at $T = 22.8^{\circ}\text{C}$	53
Figure 3.3. Time evolution of the light-scattering intensity upon cooling from 50°C to 8°C for the 0.087 mole fraction TBA aqueous solution at a scattering angle $\theta = 45^{\circ}$	54
Figure 3.4. Time-dependent intensity auto-correlation function for the 0.083 mole fraction TBA aqueous solution at $T = 8.5^{\circ}\text{C}$ and a scattering angle $\theta = 60^{\circ}$	55

Figure 3.5. Wave-number dependence of the decay rate Γ_2 of the mesoscale mode in the 0.083 mole fraction TBA aqueous solution at $T = 20.8$ °C.	56
Figure 3.6. Effective hydrodynamic radius R_m of the mesoscale particles as a function of temperature for the 0.083 mole fraction TBA aqueous solution.	57
Figure 3.7. Wave-number dependence of the inverse light-scattering intensity for the 0.073 mole fraction TBA aqueous solution.	58
Figure 3.8. Confocal microscopy image of the 0.083 mole fraction TBA aqueous solution at about 10 °C.	59
Figure 3.9. Light-scattering intensity in the aqueous TBA solutions as a function of TBA concentration, at a scattering angle $\theta = 45$ ° and at $T = 8.5$ °C.	60
Figure 3.10. Time dependent intensity auto-correlation function for 0.073 mole fraction TBA aqueous solution after repeated cold filtrations by using a 20 nm Anopore filter, at a scattering angle $\theta = 45$ ° and at $T = 8.5$ °C.	62
Figure 3.11. Time dependent intensity auto-correlation function for 0.073 mole fraction TBA aqueous solution, after cold filtering and doping with 10^{-5} mole fraction of PO, at a scattering angle of 60 ° and $T = 8.5$ °C.	63
Figure 3.12. Gas chromatogram of 0.073 mole fraction aqueous TBA solution before and after cold-filtration.	66
Figure 3.13. Time dependent intensity auto-correlation function for 0.073 mole fraction TBA aqueous solution, after cold filtering and doping 10^{-5} mole fraction of PO, at a scattering angle of 60 °, $T = 8.5$ °C, and two different cooling rates.....	68

Figure 3.14. Light-scattering intensity for a 0.073 mole fraction TBA aqueous solution, after cold filtering and saturating with methane gas, at scattering angle of 45° and $T = 8.5^\circ\text{C}$.	69
Figure 3.15. Time dependent intensity auto-correlation function for 0.073 mole fraction TBA aqueous solution, after cold filtering and saturating with methane gas, at a scattering angle of 60° and $T = 8.5^\circ\text{C}$.	70
Figure 4.1. Thermodynamic phase diagram of propylene oxide (PO) – water binary system at ambient pressure.	73
Figure 4.2. Thermodynamic phase diagram of TBA – water – PO ternary system at $T = 25^\circ\text{C}$ and $T = 10^\circ\text{C}$, and at ambient pressure.	74
Figure 4.3. Composition of micro-emulsion-like phase in TBA-water-PO ternary system at $T = 25^\circ\text{C}$, as characterized by static light scattering at a scattering angle 45° .	75
Figure 4.4. Representation of characteristic samples studied in the TBA –water –PO system on the ternary phase diagram.	76
Figure 4.5. Time dependent intensity auto-correlation functions of four characteristic TBA-water-PO samples at $T = 10^\circ\text{C}$ and at a scattering angle $\theta = 45^\circ$.	78
Figure 4.6 Wave-number dependence of relaxation rate of TBA – water - PO sample at $T = 10^\circ\text{C}$.	81
Figure 4.7. Wave-number dependence of inverse intensity of TBA – water-PO sample at $T = 10^\circ\text{C}$.	82

Figure 4.8. Effect of temperature on the properties of micro-emulsion-like phase in a TBA-water-PO sample.	83
Figure 4.9. a) Representation of characteristic samples in TBA-water-PO system to determine its kinetic behavior.	84
Figure 4.9. b) Kinetic behavior of light-scattering intensity in TBA-water-PO samples, at $\theta = 45^\circ$	85
Figure 4.9. c) Kinetic behavior of hydrodynamic radius in TBA-water-PO samples, at $\theta = 45^\circ$	85
Figure 4.10 Results from mass spectrometer	
a) Pure PO system.....	88
b) TBA-water-PO ternary system I.....	89
c) TBA-water-PO ternary system II	90
Figure 4.11. Phase diagram of TBA-water-cyclohexane system at ambient conditions, $T \sim 21^\circ\text{C}$	92
Figure 4.12. Intensity auto-correlation function from a characteristic sample of TBA-water-cyclohexane ternary system, at $T = 25^\circ\text{C}$ and $\theta = 45^\circ$	94
Figure 4.13. Wave-number dependence of relaxation rate of TBA – water-cyclohexane sample at $T = 25^\circ\text{C}$	96

Figure 4.14. Angular dependence of hydrodynamic radius of TBA – water-cyclohexane sample at $T = 25\text{ }^{\circ}\text{C}$	97
Figure 4.15. Wave-number dependence of inverse intensity of TBA – water-cyclohexane sample at $T = 25\text{ }^{\circ}\text{C}$	97
Figure 4.16. Intensity auto-correlation functions for TBA – water- cyclohexane system at $\theta = 45^{\circ}$, and at three different temperatures.	99
Figure 4.17. Intensity auto-correlation functions for TBA – water- cyclohexane system at $\theta = 45^{\circ}$, before and after cold filtration.	100
Figure 4.18. Intensity auto-correlation functions from aqueous and organic layers of a TBA – water- cyclohexane sample in the two-phase region. $T = 25\text{ }^{\circ}\text{C}$, $\theta = 45^{\circ}$	101
Figure 4.19. a) Time dependence of average hydrodynamic radius of inhomogeneities in TBA – water- cyclohexane sample, at $T = 25\text{ }^{\circ}\text{C}$ and determined at $\theta = 45^{\circ}$	102
Figure 4.19. b) Time dependence of static light-scattering intensity in TBA – water-cyclohexane sample, at $T = 25\text{ }^{\circ}\text{C}$ and determined at $\theta = 45^{\circ}$	103
Figure 4.20. Ternary phase diagram of TBA - water – isobutyl alcohol (IBA) system at $T = 25\text{ }^{\circ}\text{C}$	104
Figure 4.21. Ternary phase diagram of TBA – water - IBA system at $25\text{ }^{\circ}\text{C}$ showing compositions of the three samples investigated by light scattering.	105
Figure 4.22. Intensity auto-correlation functions for a ternary TBA – water - IBA sample, at scattering angle $\theta = 45^{\circ}$, and two different temperatures.	106

Figure 4.23. Wave-number dependence of the relaxation rate for a ternary TBA – water - IBA sample.	107
Figure 4.24. Angular dependence of hydrodynamic radii for a ternary TBA – water - IBA sample.	108
Figure 4.25. Wave-number dependence of inverse intensity for a ternary TBA – water - IBA sample.	109
Figure 4.26. Intensity auto-correlation functions for various ternary samples of TBA – water - IBA system at $T = 10\text{ }^{\circ}\text{C}$ and $\theta = 45^{\circ}$	110
Figure 4.27. Snapshots from molecular dynamics simulations for a ternary TBA – water - PO system at $T = 10\text{ }^{\circ}\text{C}$	111
Figure 4.28. Radial distribution function between C1 on cyclohexane molecule and Oxygen on water molecule, for a ternary TBA – water - cyclohexane system at $T = 25\text{ }^{\circ}\text{C}$	112
Figure 4.29. Radial distribution function between C1 on cyclohexane molecule and C on TBA molecule, for a ternary TBA – water - cyclohexane system at $T = 25\text{ }^{\circ}\text{C}$	112
Figure 4.30. Snapshots from molecular dynamics simulations ($\sim 110\text{ ns}$) for a ternary TBA – water - cyclohexane (with cyclohexane unimers) system at $T = 25\text{ }^{\circ}\text{C}$	113

Figure 4.31. Snapshots from molecular dynamics simulations (~ 90 ns) for a ternary TBA – water - cyclohexane (with dimerized cyclohexane) system at $T = 25$ °C.	115
Figure 4.32. Snapshots from coarse-grained simulations of “TBA”-water-cyclohexane system.	118
Figure 4.33. Radial distribution function between O-O on IBA molecules for a ternary TBA – water - IBA system at $T = 25$ °C.	120
Figure 4.34. Radial distribution function between O on IBA and O on for a ternary TBA – water - IBA system at $T = 25$ °C.	121
Figure 4.35. Snapshots from molecular dynamics simulations for a ternary TBA-water-IBA system at $T = 25$ °C.	122
Figure 5.1. Sketches of the ternary phase diagram in TBA – water - solubilizate systems. (Solubilizates include: a) Cyclohexane; b) IBA; c) PO.)	127
Figure 5.2. Image of 2-phase ternary system consisting of TBA – water - cyclohexane.	131
Figure 5.3. Hypothesized ternary phase diagram for water-oil-surfactant system.	132

Chapter 1: Introduction

1.1 What are hydrotropes?

Hydrotropes are small organic molecules that can substantially increase the solubility of sparingly soluble compounds in water [1]. The molecular structure of hydrotropes is amphiphilic, such that one part of the molecule is polar (hydrophilic) and the other part is non-polar (hydrophobic) [2]. They differ from traditional surfactants in a manner such that the non-polar parts of the molecule are smaller (less than C7 – C8) than in surfactants [3].

Unlike traditional surfactants, hydrotropes do not show spontaneous self-assembly above a specific critical micelle concentration to form stable micelles in aqueous solutions [4]. However, micelle-like fluctuations, loose dynamic non-covalent clustering, are observed in solutions of many hydrotropes above a minimum hydrotrope concentration [5,6]. These micelle-like fluctuations, in the presence of a hydrophobic compound, may become stabilized and form mesoscopic aggregates [7-9]. Thus, hydrotropes may also be defined as solubilizers of sparingly soluble hydrophobic compounds in aqueous solutions [1-21]. The sparingly soluble compounds are also referred to as “solubilizates”.

Hydrotropy is different from molecular solubility. It has been shown that hydrotropy is a collective molecular phenomenon wherein the hydrotrope molecules self-assemble in aqueous media to create a microenvironment of lowered polarity [3,10], which helps in solubilizing the added hydrophobic compound.

1.2 Hydrotropes vs. surfactants

Although there are certain similarities between hydrotropic solutions and micellar solutions, such as their amphiphilic nature, their ability to “solubilize” hydrophobic compounds, there are also distinct differences [11,12]. Micellar solubilization and hydrotropic solubilization are very different with respect to the amount of solubilizer (*i.e.* hydrotrope) and solubilizate (*i.e.* hydrophobic compound). Higher amounts of a hydrotrope, compared to surfactants, are needed to solubilize a hydrophobic compound [13]. Moreover, hydrotropic action is known to be solubilizate-specific, meaning not all hydrophobic compounds can be solubilized by a certain hydrotrope [5,14]. In addition, the solubilization of hydrophobic components in hydrotropic solutions is not a linear function of the hydrotrope concentration, but exhibits a sigmoidal relationship [2,14]. The change in surface tension of a hydrophobic component in a hydrotropic solution is more gradual than in micellar solutions [14]. Another distinguishing feature of hydrotropes, vis-à-vis traditional surfactants, is that hydrotropes have a much higher hydrophile-lipophile balance (HLB) [5,13].

1.3 Classification of hydrotropic molecules

The classification of hydrotrope molecules is broad and diverse. Traditionally, industrially used hydrotropes are aromatic salts; with an aromatic ring that helps in creating a microenvironment of lowered polarity and an ionic part that helps in

enhancing solubility in water [5]. Examples of aromatic ionic hydrotropes include sodium xylene sulphonate, sodium benzoate.

Although there is a wide amount of literature available for ionic hydrotropes, the published information on non-ionic hydrotropes is limited. Non-ionic hydrotropes include simple alcohols such as ethanol [17], aromatic alcohols such as resorcinol [6], amides such as urea [20], α -amino acids such as proline [21], which all contain hydrophilic and hydrophobic parts. Short-chain alkyl alcohols (such as ethanol, *n*- and iso- propanols, *tert*-butanol), are not conventionally considered as hydrotropes. This is because higher molecular weight alkyl alcohols (such as pentanols, hexanols, octanols), exhibit phase separation with water, rather than form micellar structures with water (like surfactants).

In this work, we focus on non-ionic alkyl hydrotropes, such as *tert*-butanol, which is completely miscible with water under ambient conditions [22]. We will broaden the definition of hydrotropes to include small amphiphilic molecules such as isopropanol, isobutanol, tertiary butyl alcohol, 3-methylpyridine, tetrahydrofuran, 2-butoxyethanol.

1.4 Tertiary butyl alcohol (TBA): A non-traditional hydrotrope

Tertiary butyl alcohol (TBA), 2-methyl-2-propanol, is a special molecule. The hydroxyl group of the TBA molecule, which promotes dissolution in water, completely balances the hydrophobic *tert*-butyl group of the molecule [23]. It is the highest molecular weight alcohol molecule to be completely miscible with water in all proportions under ambient conditions. Many experimental works and computer

simulations show the presence of clustering in aqueous TBA solutions [23-44]. It is speculated that such a clustering could be due to formation of short-lived, short-ranged micellar-like aggregates or clathrate-like structures, where a hydrogen-bonded water network surrounds TBA molecules [23]. TBA can also “solubilize” hydrophobic compounds in water. Based on these properties of aqueous TBA solutions, TBA can be classified as a nonionic hydrotrope [45].

1.5 Mechanism of hydrotropic action

Hydrotropic action in aqueous media could be due to self-aggregation or mixed-aggregation [3,4,7-10,13-17]. The mechanism of self-aggregation of hydrotropes is still not fully understood. It is possible that hydrotropes self-associate to form micelle-like aggregates, above a minimal hydrotropic concentration [5]. Molecular dynamics simulations in aqueous solutions of ethanol and *n*-propanol show that these aggregates are short-lived and short-ranged [18,19]. Intramolecular stack-like association in hydrotropes has also been reported [10]. However, due to the broad diversity in the classification of hydrotropes, no single mechanism can completely explain their self-aggregation behavior.

The mechanism of mixed aggregation in hydrotropes is explained by Srinivas *et al.* [3]. By carrying out X-ray crystal structure analysis on hydrotropes such as sodium *p*-butylbenzenesulfonate dihydrate, sodium cumenesulfonate hemihydrate, Srinivas *et al.* have shown that hydrotropic molecules are packed in a two-dimensional sandwich manner, consisting of alternating hydrophobic and hydrophilic regions. The solubilizates are expected to enter the hydrophobic regions of these

assemblies and fill these regions in an intermeshing manner, thus producing a cooperative and mutually stabilizing effect. They have further shown that these open-layer assemblies are more favorable in solubilizing larger amounts of the hydrophobic component.

The mechanism of hydrotropic action in the presence of a solubilize is a subject of active research. It is possible that the interaction between the hydrotrope and the solubilize leads to the formation of a complex, which would have a higher solubility in aqueous media. This is evidenced by some molecular dynamics simulations and solubility studies [9,20]. Another possibility is that hydrotropes may change the structure of the solvent around the solubilize, thus acting as structure-makers or structure-breakers [5]. A third possibility is the formation of micelle-like aggregates, where the hydrotrope molecules surround the solubilize molecules [16,19]. This leads to the formation of sphere-like aggregates.

Given the broad diversity in the classification of hydrotropes, it is possible that more than one of the above-proposed mechanisms of action might be associated with the action of specific hydrotropes to solubilize particular solubilizes.

The formation of aggregates in solutions of hydrotropes is through loose non-covalent interactions. Detailed physio-chemical experiments carried out by Balasubramanian *et al.* show no sharp transition in properties as a function of temperature; instead they show a smooth and gradual transition [14].

1.6 Mysteries of aqueous solutions of hydrotropes

The mechanism of hydrotropic action, in the presence of a solubilizate, is not fully understood. The following section exemplifies how aqueous solutions of certain hydrotropes show the presence of mysterious mesoscopic inhomogeneities. We believe that all these mysterious inhomogeneities are due to the presence of a solubilizate, which causes the water-hydrotrope-solubilizate system to aggregate and form larger mesoscopic structures.

In 2000, Georgalis *et al.* [46] reported observation of a mesoscale structure (50 to 500 nm in size) of concentrated electrolyte solutions, namely sodium chloride, ammonium sulphate, and sodium citrate. They attributed this to possible electrostatic interactions or hydrophobic interactions among ions, or water molecules, acting as “cement” responsible for interaction between like-charged ions.

In 2004, Yang *et al.* [47] observed a slow dynamic mode from laser light scattering, with a correlation length of 200 to 600 nm in certain small organic aqueous solutions, namely tetrahydrofuran and 1,4-dioxane. They also observed that these inhomogeneities could be removed by filtration, and thus concluded that the observed mesoscopic inhomogeneities are a result of incomplete mixing of water and the organic solute, at the micro scale.

In 2006, Sedlák [48-50] carried out an extensive static and dynamic light-scattering study of around 100 different solute-solvent pairs and observed the presence of large supramolecular structures in many electrolytic solutions, non-electrolytic solutions, and mixtures of liquids. Sedlák explained this phenomenon as a

result of attractive interactions between solute molecules through hydrogen-bond bridges formed by solvent molecules, which are themselves hydrogen bonded.

In 2007, Kistler *et al.* [51] reported on observing, for the first time, a continuous transition between discrete macro ions, self-assembled blackberry structures, and back to discrete macro ions in $\{\text{Mo}_{132}\}$ /water/acetone systems. The average hydrodynamic radius of the self-assembled blackberry structures ranged from 45 to 100 nm, increasing with increasing acetone content. They attributed the formation of the blackberry structures to possible attractive van der Waals forces, electrostatic repulsions, and hydrophobic interactions.

In 2007, Jin *et al.* [52-53] carried out a static and dynamic light-scattering study in aqueous solutions of tetrahydrofuran, ethanol, urea, and α -cyclodextrin. They also observed a mesoscopic size of around 100 nm in these systems. They attributed this to the existence of small gaseous nanobubbles formed in these solutions. They also claimed that these nanobubbles are rather stable with the adsorption of small organic molecules on the gas-liquid interface, and can be removed by repeated filtrations and regenerated by air injection.

Another evidence for the existence of the mysterious mesoscopic mode in aqueous solutions was obtained by Kostko *et al.* [54] and Subramanian *et al.* [55] in aqueous solutions of 3-methylpyridine. 3-Methylpyridine is completely miscible in water. However, upon cooling, a dynamic mode, of the order of 200 nm in size, became prominent. They also noted that the presence of these inhomogeneities were independent of the sample source. All these observations led Kostko *et al.* to conclude that the energy landscape in aqueous solutions of 3-methylpyridine is such

that the system forms supramolecular structures which could remain stable for times longer than the time needed to carry out light-scattering experiments.

An unusual self-assembled structure, a multilamellar charge-density wave mesophase, was observed by Sadakane *et al.* [56] in aqueous solutions of 3-methylpyridine and small amounts of an antagonistic salt, namely, sodium tetraphenylborate. They confirmed that in order to observe stable equilibrium density-wave mesophases in aqueous solutions of small molecules of nonelectrolytes one needs to stabilize the structure by adding salts, one of whose ions is hydrophobic.

1.7 Why do we care about hydrotropes?

Although the term hydrotropy was coined by a biochemist, Carl Neuberg; chemical engineers and chemists have further developed the science of hydrotropy. Due to their specific solubilizing properties, hydrotropes find a wide variety of industrial applications. The ability of hydrotropes to dramatically alter the solubility of certain hydrophobic molecules is widely explored in the design and formulations of products such as drugs, soaps, detergents, and cosmetics [2,4-7,13-16,20,57].

Hydrotropes are used in the pharmaceutical industry to transport hydrophobic drugs in aqueous media and to enhance the dissolution and permeation of drugs in biological systems. Hydrotropes are used in the soap and detergent industry to “solubilize” surfactants and make products with concentrated amounts of surfactants. In detergent, drug, or cosmetic formulations, they can also be used as co-solvents along with surfactants to enhance or inhibit micelle formation. Hydrotropes are used as catalysts in heterogeneous chemical reactions to enhance reaction rates. The

presence of hydrotropes lengthens the oscillating life times in the Belousov – Zhabotinskii chemical oscillating reactions [58]. Hydrotropes are also used in the separation of mixtures by selective extraction and as agents used to alter the thermodynamic behavior of liquid crystalline phases. Hydrotropes can also be used as molecular probes to determine properties of the microenvironment. Certain hydrotropes, such as proline, are protein compatible, and help in maintaining cellular osmosis.

Thus the various applications of hydrotropes take advantage of its unique properties such as its amphiphilic nature, hydrogen-bonding ability, and specific interactions with solutes.

1.8 Current research goals and objectives

Motivated by controversies in the literature on the microscopic and mesoscopic structure of aqueous solutions of certain hydrotropes, this research is focused on addressing a fundamental, yet highly controversial, issue in the physical chemistry of aqueous solutions, namely, the nature of mesoscale (hundreds of nanometers) inhomogeneities in aqueous solutions of hydrotropes (or small amphiphilic molecules). As mentioned previously, the presence of so-called mysterious inhomogeneities has been reported, discussed, and disputed in the literature for the past forty years; however, a consensus, or even a commonly accepted qualitative understanding of the observed phenomena, has not been achieved.

In order to clarify this issue, molecular, mesoscopic and macroscopic thermodynamics of aqueous TBA solutions without and with the presence of various

solubilizates have been studied. Detailed experiments on static and dynamic light scattering, confocal microscopy, gas chromatography, and mass spectrometry have been carried out.

The main goals of this dissertation include, clarifying whether mesoscale inhomogeneities are indeed observed in aqueous TBA solutions or whether their observation is an experimental artifact? The next goal is to determine what is the origin or what are the conditions where the mesoscopic aggregates are seen, and what is their role in the thermodynamic stability of the system? The final goal is to understand the nature of these mesoscopic aggregates.

1.9 Dissertation outline

The first part of this dissertation is devoted to understanding the thermodynamics of aqueous TBA solutions. Literature data on the macroscopic phase behavior and solution thermodynamics of aqueous TBA solutions are presented. Results from molecular simulations and neutron scattering are also discussed. The second part of the dissertation deals with understanding the mesoscopic properties of aqueous TBA solutions. Results from light scattering and chromatography are presented. The question on the origin of the mesoscopic aggregates in aqueous TBA solutions is answered. The final part of the dissertation deals with understanding the nature of the mesoscopic aggregates in aqueous TBA solutions upon the addition of a hydrophobic component. Thermodynamic phase behaviour and light-scattering experiments on various ternary systems are presented. A discussion on the nature of

these mesoscopic aggregates is then presented along with applications of hydrotropic solutions.

Chapter 2: Thermodynamics of aqueous TBA solutions

In this chapter, a review of the literature on the thermodynamic properties of aqueous TBA solutions is presented. The phase diagram of TBA-Water system at ambient pressure is shown in Figure 2.1. Various solution properties, such as heat capacities, excess molar and excess partial molar volumes, enthalpies, entropies, and Gibbs free energies, along with activity coefficients, ultrasonic velocity measurements, and isothermal compressibility, exhibit anomalies. These anomalies, as well as the results from small angle X-ray and neutron scattering experiments, are discussed in the subsequent sections. Molecular dynamics simulations, carried out by our collaborator, Professor J. B. Klauda, are also presented and discussed.

2.1 Thermodynamic phase diagram of TBA-water

Various research groups have investigated the phase diagram of TBA-water systems over the years [22,59-61]. The liquid-solid phase diagram at ambient pressure, as determined by Kasrian *et al.* by using differential scanning calorimetry, is shown in Figure 2.1 [22].

TBA and water are completely miscible with each other under ambient conditions. The system exhibits two eutectics, one at about 0.2 mass fraction (0.057 mole fraction) TBA in water at about $T = -5$ °C and another one at about 0.9 mass fraction (0.68 mole fraction) TBA in water at about $T = -3$ °C.

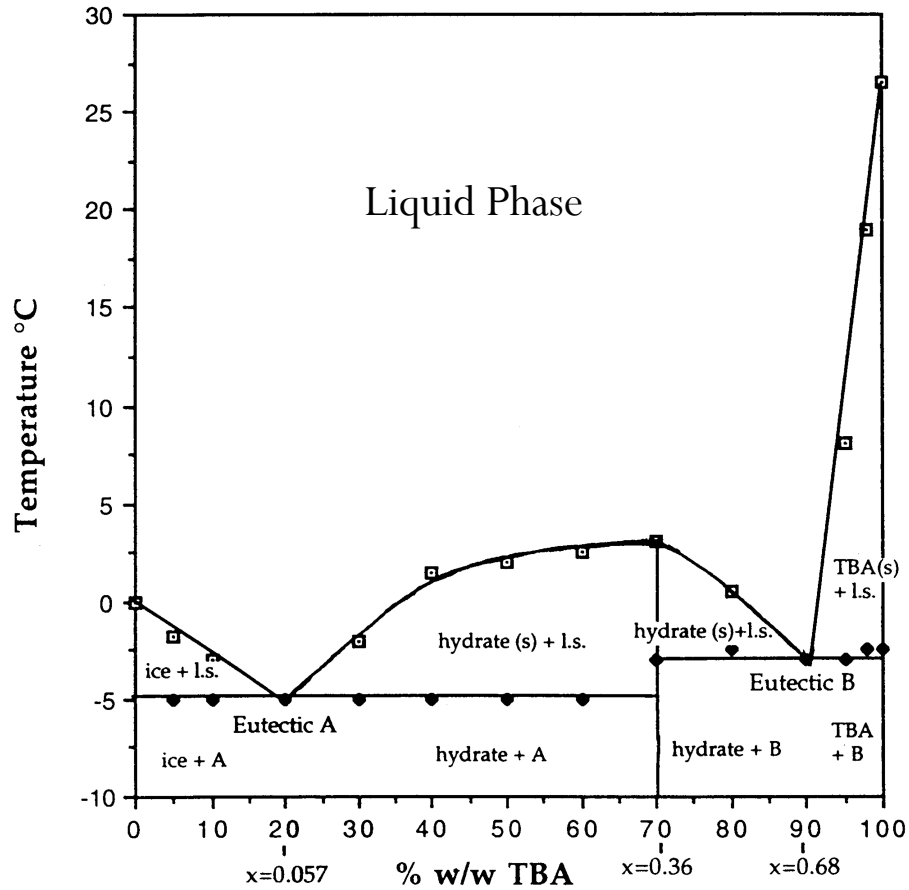


Figure 2.1. Phase diagram of TBA-water binary system at ambient pressure, showing the liquid-solid equilibrium line. (Taken from [22].)

The phase diagram of TBA-water has been investigated at higher pressures, up to 200 MPa, by Woznyj *et al.* [61]. As the pressure is raised the eutectics are observed at a lower temperature and at about the same concentration of TBA in water, as observed under ambient pressures.

2.2 Excess molar volume and partial molar volumes

In ideal solutions, with no preferential interactions between the components of the mixture, the excess volume of mixing is zero. However, for associated liquids, namely, hydrogen-bonded solvent systems, such as aqueous alcohol solutions, significant negative excess volumes are observed [62].

The excess molar volume of aqueous TBA solutions as a function of composition and temperature is shown in Figure 2.2 [63]. It is seen from Figure 2.2 that the excess molar volumes for aqueous TBA solutions are weakly dependent on temperature [63].

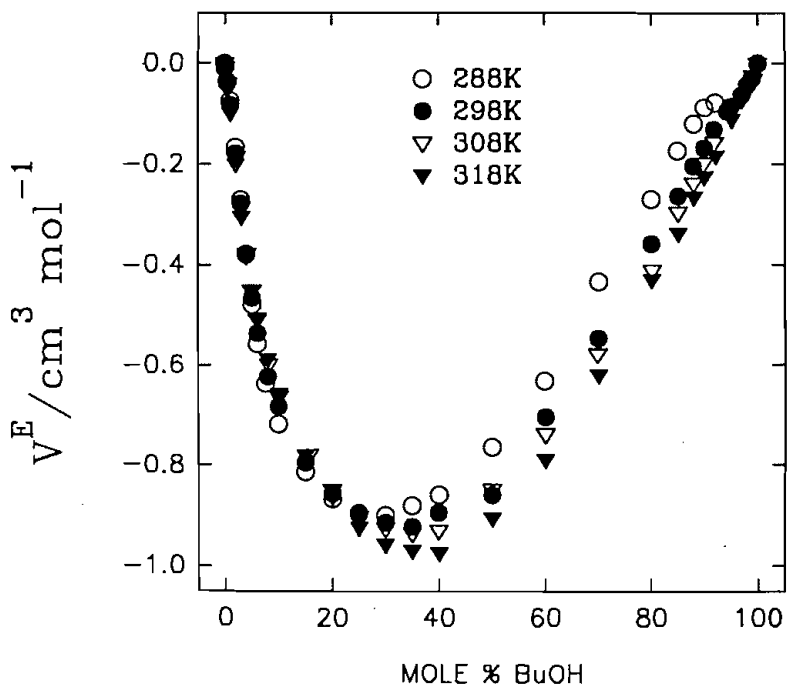


Figure 2.2. Excess molar volume of aqueous TBA solutions as a function of TBA concentration, at various temperatures. (Taken from [65].)

The partial molar volumes of TBA in aqueous TBA solutions as a function of TBA concentration, at various temperatures are shown in Figure 2.3. The partial molar volumes of water in aqueous TBA solutions as a function of TBA concentration, at various temperatures are shown in Figure 2.4 [63]. As seen from Figure 2.3, as the concentration of TBA in the solution is increased, the partial molar volume of TBA initially decreases, passes through a minimum in the water-rich region, and then increases. The minimum in the partial molar volume of TBA becomes sharper and more enhanced as the temperature is lowered. The partial molar volume of water, as seen from Figure 2.4, exhibits a minimum in the TBA-rich region. This minimum becomes more pronounced and shifts to higher TBA compositions as the temperature is increased.

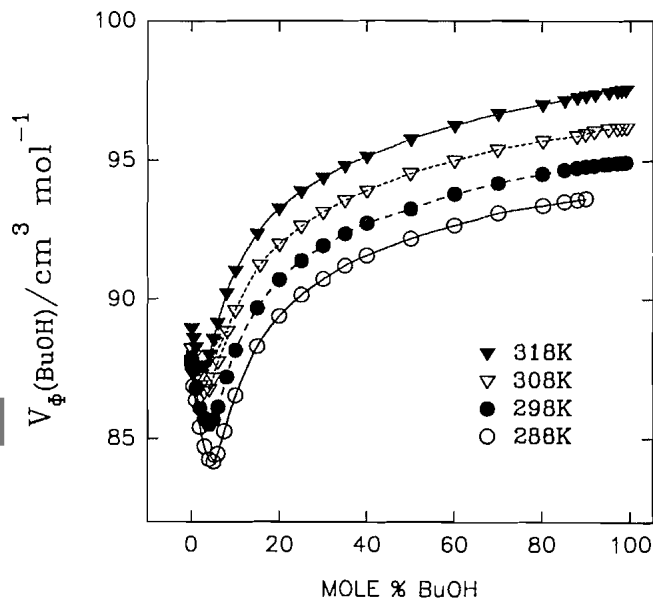


Figure 2.3. a) Excess partial molar volume of TBA in its aqueous solution, as a function of TBA concentration, at various temperatures (Taken from [65].)

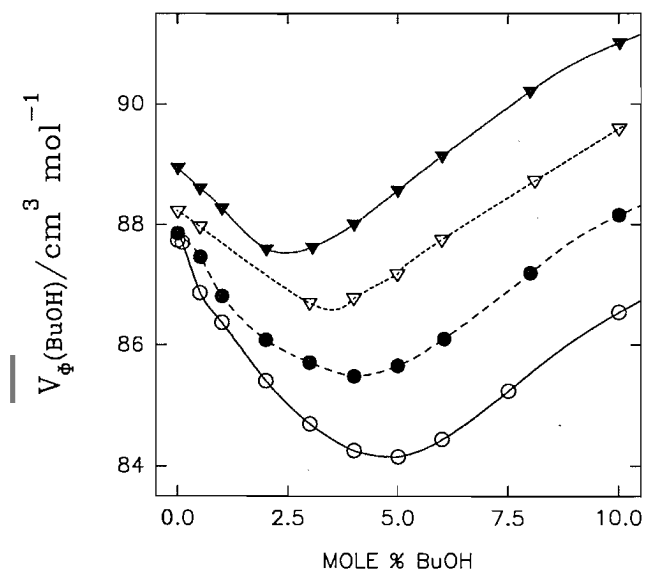


Figure 2.3. b). Enlarged view (Taken from [65].)

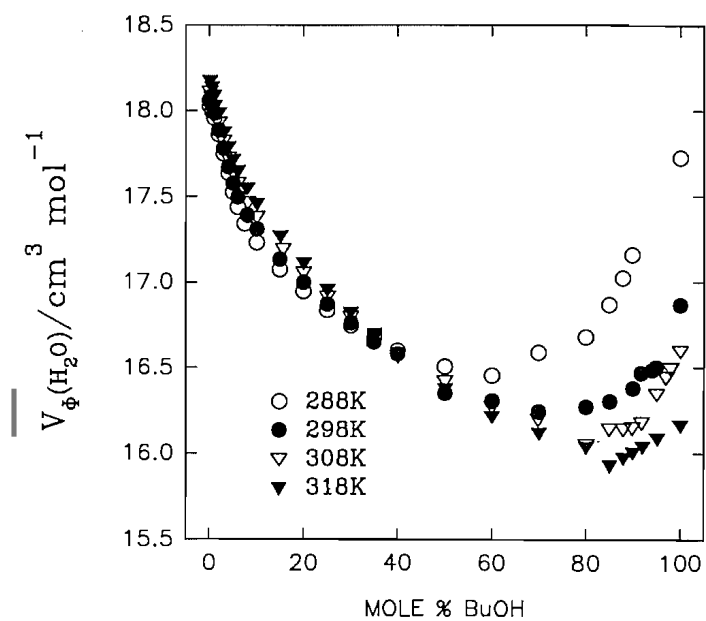


Figure 2.4. Excess partial molar volume of water in aqueous TBA solutions, as a function of TBA concentration, at various temperatures. (Taken from [65].)

It is instructive to compare the partial molar volumes of TBA in aqueous TBA solutions with the partial molar volumes of other C1-C4 alcohols (such as methanol, ethanol, *n*-propanol, isopropanol, *sec*-butanol, ethylene glycol, glycerol) in their respective aqueous solutions, at ambient temperatures [63]. This is shown in Figure 2.5. From this figure it is seen that as the alcohol chain length and branching increases, the minimum in partial molar volume becomes sharper and more pronounced and shifts to a lower alcohol concentration. The most significant effect is seen in aqueous TBA solutions.

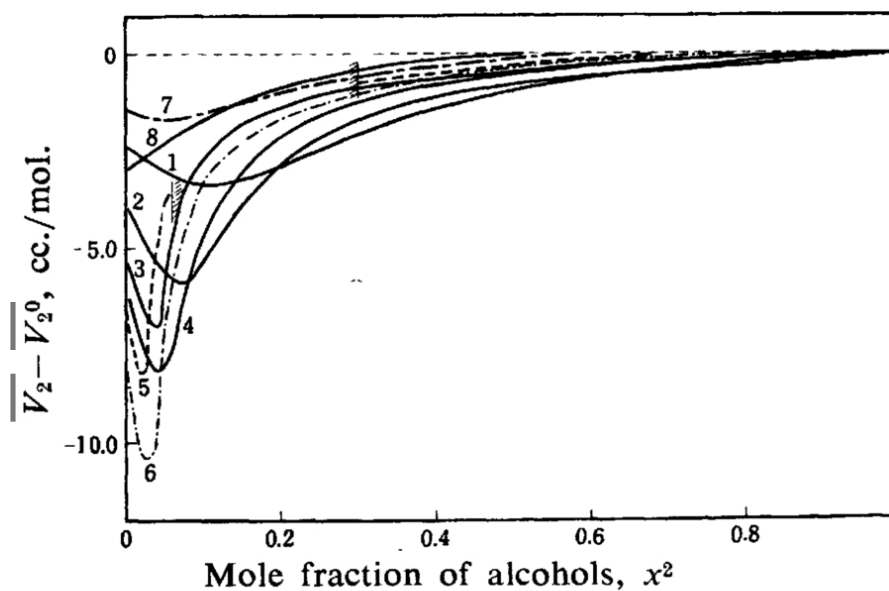


Figure 2.5. Partial molal volumes of C1-C4 monohydric alcohols in their aqueous solutions as a function of concentration, at ambient temperatures. (Taken from [66].)

1: Methanol (15 °C); 2: Ethanol (20 °C); 3: *n*-Propanol (15 °C); 4: Isopropanol (15 °C); 5: *sec*-Butanol (20 °C); 6: *tert*-Butanol (20 °C); 7: Ethylene glycol (20 °C);

8: Glycerol (15 °C)

Although a quantitative description of this phenomenon has not been fully developed, a qualitative explanation can be found in the literature. The behavior of the partial molar volumes in aqueous C1-C4 alcohol solutions can be accounted for as being due to hydrophobic hydration [62], which explains how water molecules surround an apolar solute [63,64]. Water molecules arrange themselves around an apolar solute in a cage-like manner, with the solute molecules occupying the cavities of water. The negative values in excess volumes (as seen in Figure 2.2) can be attributed to the occupation of water cavities by alcohol molecules [65-67].

Another interpretation for the anomalies observed in aqueous alcohol solutions can be obtained by relating the hydrogen bond interactions between the alcohol molecule and water [62]. As the amount of alcohol increases in the water-rich region of the solution, strong hydrogen bonds form between the alcohol molecule and water. This may lead to an initial volume contraction. Thus in the water-rich region of the solution, structural stabilization becomes enhanced with increasing alcohol concentration, until a certain point beyond which increasing the alcohol concentration increases the strain on the water network and the structural integrity of the water breaks down.

2.3 Heat capacity

Heat-capacity measurements yield important mixture information as they are highly sensitive to structural changes in a solution.

The heat capacity of aqueous TBA solutions as a function of TBA concentration, and at various temperatures is shown in Figure 2.6 [68,69]. From this

figure, it is seen that the heat capacity of the solution exhibits a sharp maximum in the water-rich region and rapidly goes down to the molar heat capacity of TBA as the concentration of TBA increases. As the temperature is lowered the magnitude of this heat-capacity maximum increases and the fall towards the molar heat capacity of TBA is more rapid.

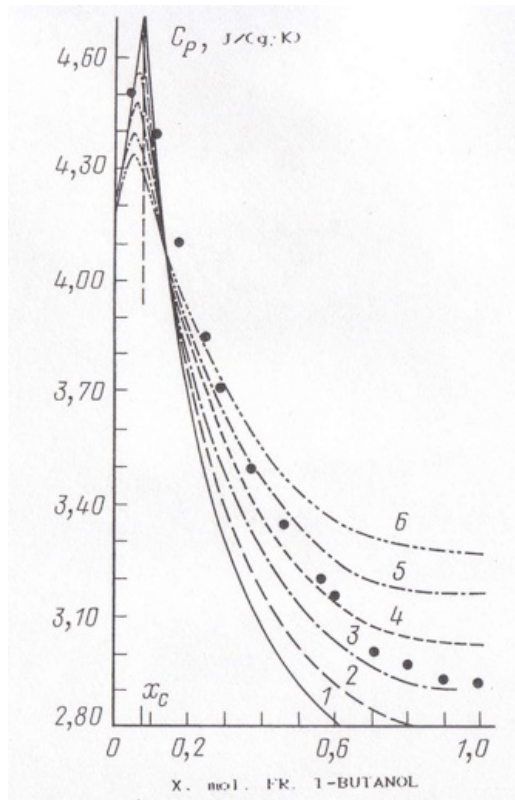


Figure 2.6 Heat capacity of aqueous tertiary butyl alcohol solutions as a function of concentration, at various temperatures. (Taken from [67].)

1: 273 K; 2: 283 K; 3: 293 K; 4: 303 K; 5: 313 K; 6: 323 K; Circles: 304 K.

The temperature dependence of the heat capacity of aqueous TBA solution for various concentrations of TBA in water is shown in Figure 2.7 [68,69]. It is seen that the maximum in heat capacity occurs at about 0.074 mole fraction (0.28 mass fraction) TBA in water at about 0 °C. Interestingly, this concentration is close to the eutectic concentration as seen from Figure 2.1.

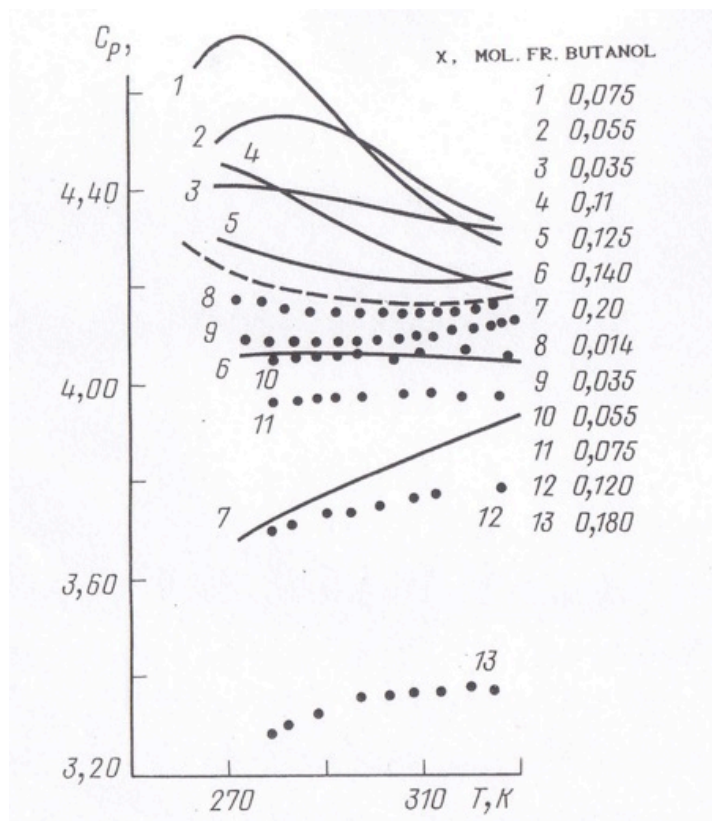


Figure 2.7. Heat capacity of aqueous tertiary butyl alcohol solutions as a function of temperature, for various concentrations. (Taken from [67].) Continuous lines belong to aqueous TBA solutions, dots belong to aqueous tetrahydrofuran solutions, dashed line represents pure water.

Such a trend of heat capacity appears to be typical for associating fluids, such as aqueous TBA solutions [62,67,70]. The maximum in heat capacity observed at about 0.074 mole fraction TBA, as seen in Figure 2.7, has been interpreted by the authors, Anisimov *et al.*, as due to the presence of a structural transformation from an ordered state, at low TBA concentrations, to a disordered state at high TBA concentrations [68,69]. De Visser *et al.* attribute this behavior to solutes such as TBA, which enhances water structure at low solute concentrations [70]. Franks and Ives refer to these effects as being due to hydrophobic hydration [62].

2.4 Excess molar and partial molar enthalpies, entropies, and Gibbs free energies

Excess properties, such as excess enthalpy, entropy, and Gibbs energy of mixing, provide valuable information on mixture properties. Partial molar excess properties provide additional information on solute-solvent interactions within a mixture.

Figure 2.8 shows the excess molar enthalpy of mixing [71], while Figure 2.9 shows the partial molar enthalpies for TBA and water in aqueous TBA solutions at $T \sim 26$ °C [71-73]. It is seen from Figure 2.8 that the excess enthalpy of mixing is negative in the water-rich region, goes through a minimum at a TBA concentration of about 0.06 mole fraction and is then positive in the TBA-rich region with a maximum at about 0.75 mole fraction TBA. From Figure 2.9, it is seen that the excess partial molar enthalpy of TBA is a strong function of TBA concentration till about 0.06 mole fraction TBA, after which it is almost independent of TBA concentration. Figure 2.9

also shows the partial molar enthalpy of water in aqueous TBA solutions. The partial molar enthalpy of water in the water-rich region is quite different than in the TBA-rich region.

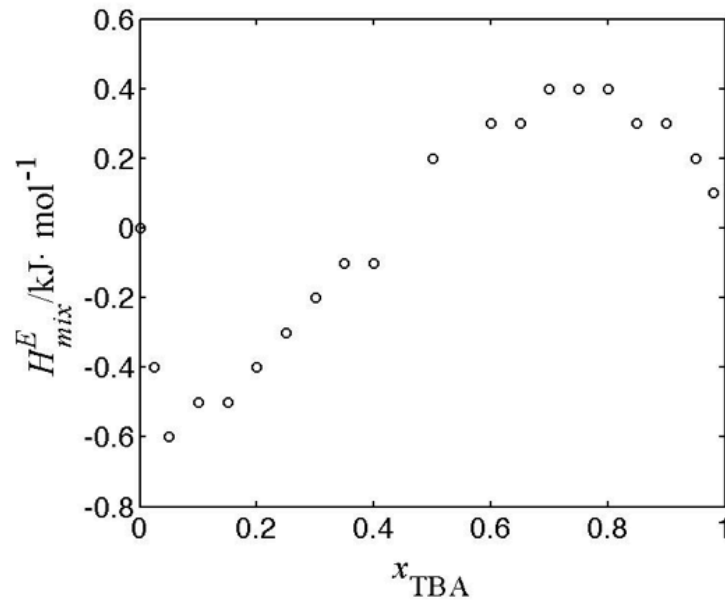


Figure 2.8. Excess enthalpy of mixing in TBA-water solutions as a function of TBA mole fraction at $T = 26 \text{ }^\circ\text{C}$. (Taken from [71].)

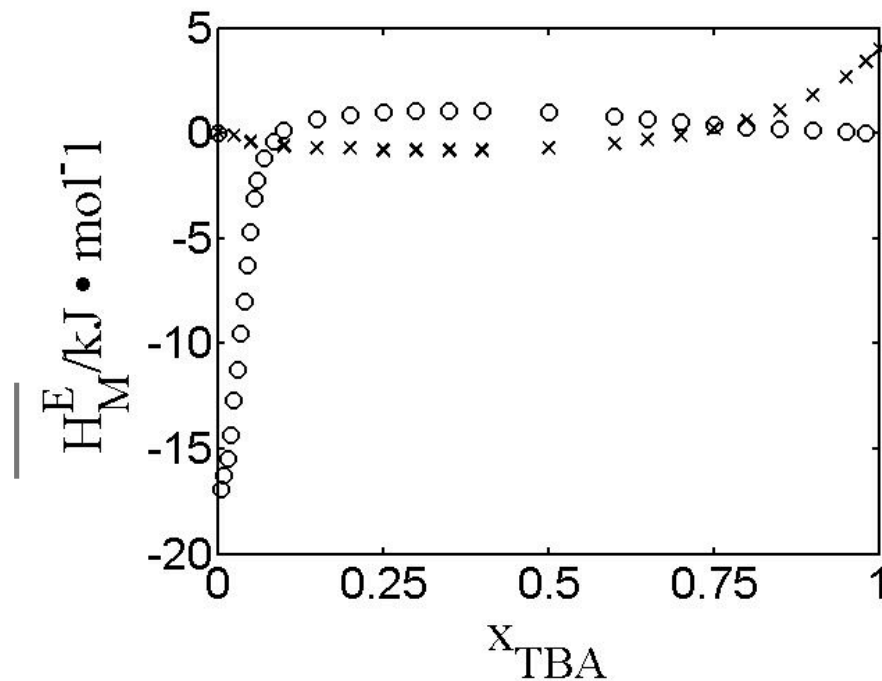


Figure 2.9. Partial molar enthalpy of TBA and water in aqueous TBA solutions as a function of TBA mole fraction, at $T = 25\text{ }^\circ\text{C}$. Open circle: TBA; Crosses: Water.

(Taken from [71-73].)

The excess molar entropy of TBA-water mixtures and the excess partial molar entropies of TBA and water in aqueous TBA solutions are shown in Figures 2.10 and 2.11, respectively [71,74]. The excess molar entropy is negative and exhibits a minimum at about 0.22 TBA mole fraction. The partial molar entropy of TBA shows a strong dependence on TBA concentration till about 0.07 TBA mole fraction; beyond this concentration the partial molar entropy of TBA is almost constant, thus making the system behave like a regular solution. The partial molar entropy of water is negative, but does not show a strong dependence on TBA concentration.

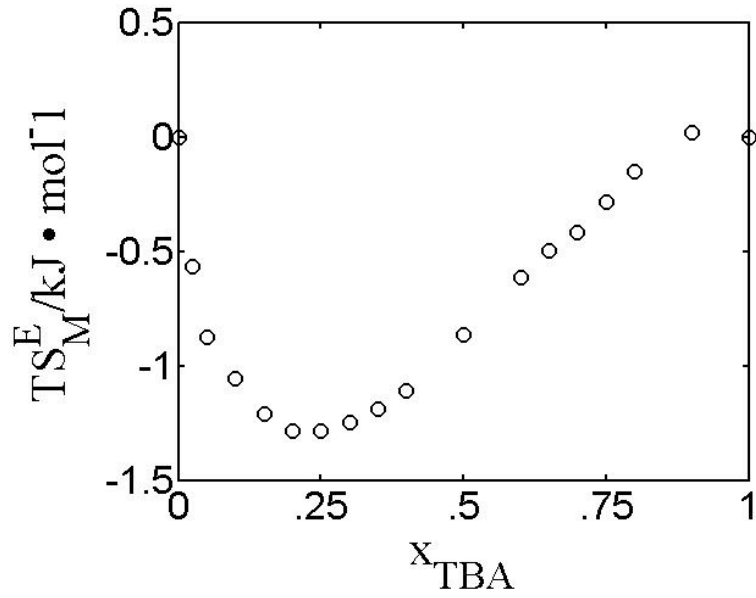


Figure 2.10. Excess entropy of mixing in aqueous TBA solutions as a function of TBA mole fraction at $T = 25 \text{ }^\circ\text{C}$. (Taken from [71,74].)

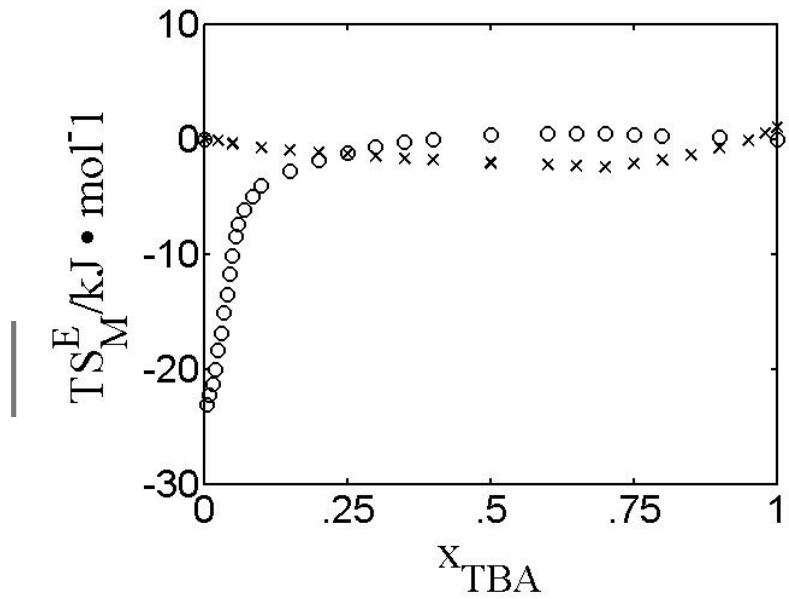


Figure 2.11. Partial molar entropy of TBA and water in aqueous TBA solutions as a function of TBA mole fraction at $T = 25 \text{ }^\circ\text{C}$. Open circles: TBA; Crosses: Water. (Taken from [71,74].)

The excess molar Gibbs energy of mixing and the excess partial molar Gibbs energies of mixing (also known as excess chemical potentials) are shown in Figures 2.12 and 2.13, respectively [71,74]. The excess molar Gibbs energy of mixing is positive, almost symmetric and shows no anomalous behavior. However, the excess partial molar Gibbs energies provide specific information on complex interactions between TBA and water molecules. In particular, the excess chemical potential of TBA shows a peculiar dip at about 0.045 mole fraction TBA. In the same range of TBA concentrations the chemical potential of water shows a strong negative deviation from ideality as discussed in Section 2.5.

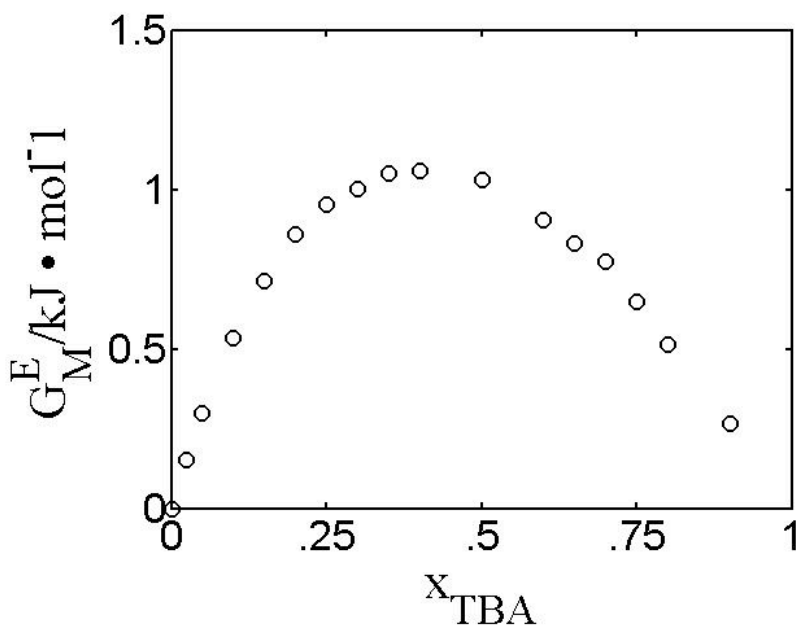


Figure 2.12 Excess molar Gibbs energy of mixing in aqueous TBA solutions as a function of TBA mole fraction at $T = 25^\circ\text{C}$. (Taken from [71,74].)

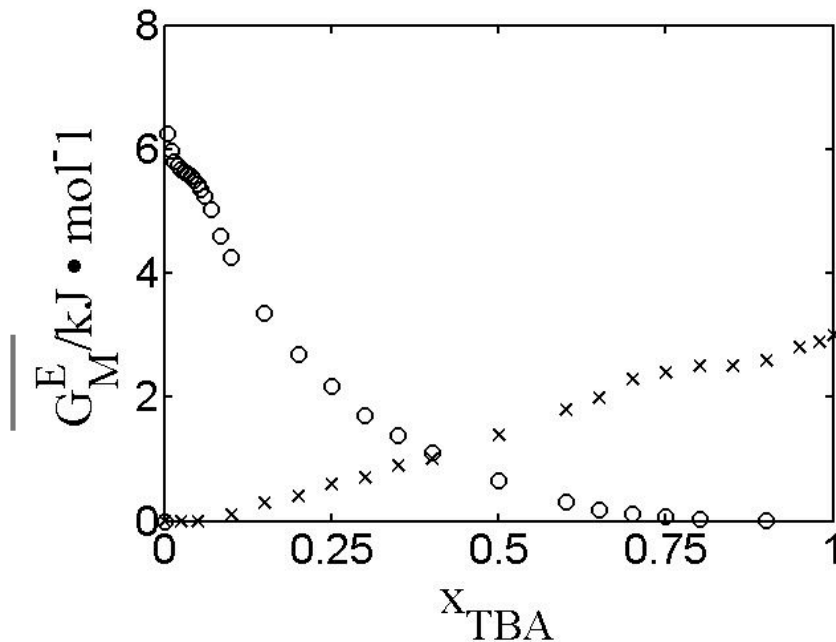


Figure 2.13. Partial molar excess Gibbs energy (excess chemical potential) of TBA and water in aqueous TBA solutions as a function of TBA mole fraction, at $T = 25$ °C. Open circles: TBA; Crosses: Water. (Taken from [71,74].)

The anomalies in the excess partial molar energies and entropies are attributed to the structural changes within the solution. The behavior of the partial molar enthalpies of TBA at TBA concentration below 0.06 mole fraction could be due to the formation of strong hydrogen bonds between TBA and water molecules, bond energy greater than $10 k_B T$. Beyond 0.1 TBA mole fraction, the absence of any dependence of the partial molar enthalpy of TBA on the TBA concentration could be an indication that the energy landscape for the TBA molecules in the solution is almost the same as in pure TBA. The increase of the partial molar enthalpy of water with TBA concentration in the TBA-rich region, beyond 0.6 TBA mole fraction, is speculated to

be due to the destruction of the hydrogen bonded network, where water then mixes into the solution as a single molecule [71-74].

Franks and Ives have pointed out that the opposing features of the excess molar enthalpy of mixing in the water-rich region vs. the TBA-rich region might be due to strong inter-component attractions in the water-rich region, and dissociation of a highly associated network in the TBA-rich region [62].

2.5 Activity coefficient of water

Activity coefficients are uniquely correlated to the excess chemical potentials as $\mu_i^E = RT \ln(x_i \gamma_i)$, where μ_i^E , x_i , and γ_i are the excess chemical potential, concentration, and activity coefficient of species i in solution, T is the temperature, and R is the universal gas constant. Experimentally determined activity coefficients of water in aqueous TBA solutions, shown in Figure 2.14 [75,76], apparently seem to contradict the overall positive excess Gibbs energy of mixing shown in Figure 2.12. The logarithm of the activity coefficient of water in the water-rich region of the mixture shows a strong negative deviation from ideality, with a minimum at about 0.045 mole fraction TBA, and rapidly increases towards positive deviations at higher TBA concentrations. A similar trend is also seen in other aqueous C1-C4 alcohol solutions [75].

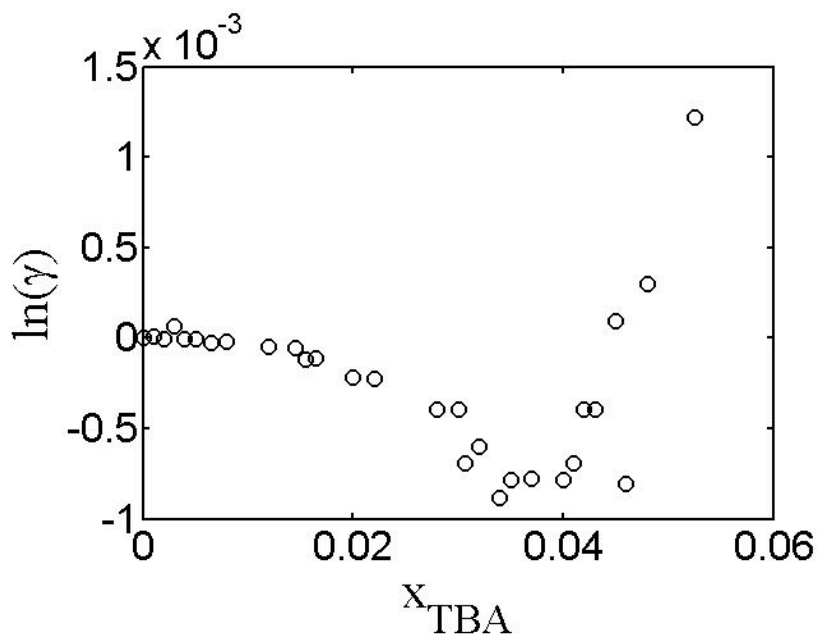


Figure 2.14. Activity coefficient of water in aqueous TBA solutions as a function of TBA mole fraction at $T = 10\text{ }^{\circ}\text{C}$. (Taken from [75].)

This peculiar behavior of the activity coefficient of water is in agreement with the explanation given above. In the water-rich region, strong solute-solvent interactions in the form of strong hydrogen bonds between TBA molecule and water are favored, leading to negative values of the activity coefficient.

2.6 Ultrasonic absorption and isothermal compressibility

Ultrasonic velocity and absorption measurements in aqueous alcohol solutions have been carried out since more than 70 years [77-82].

The absorption of sound in various aqueous C1-C4 alcohol solutions is shown in Figures 2.15 [77]. As seen in this figure, sound absorption exhibits a maximum in the water-rich region of the alcohol-water mixture. The magnitude of the maxima and

the sharpness of the peaks increase as the alcohol chain length and branching increase. The maximum effect is seen in aqueous TBA solutions.

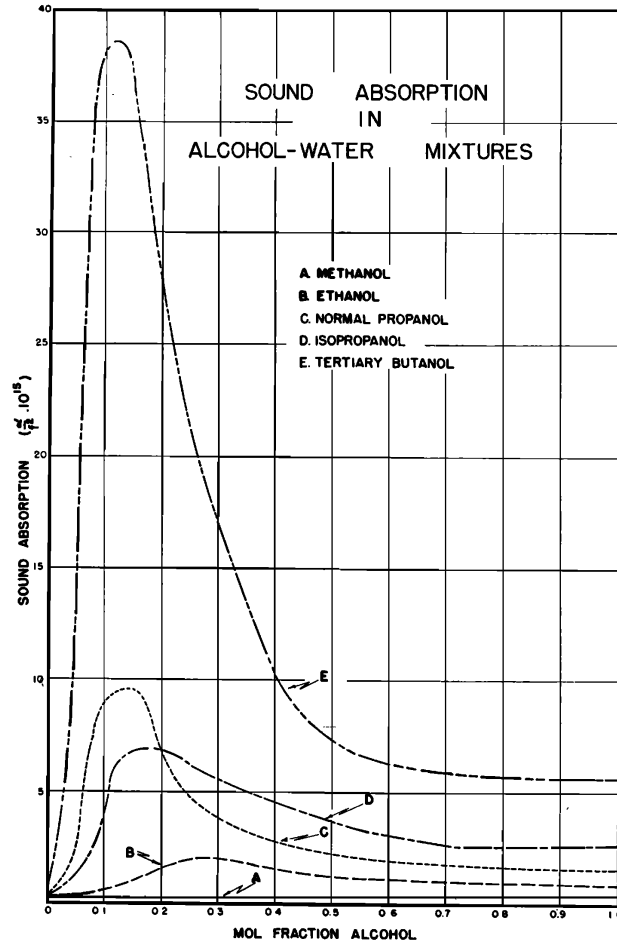


Figure 2.15 Absorption of sound in alcohol-water solutions as a function of alcohol concentration at $\sim 25^\circ\text{C}$. (Taken from [77].)

The isothermal compressibility of aqueous TBA solutions as a function of TBA concentration is shown in Figure 2.16 [81]. It is seen that the isothermal compressibility exhibits a minimum at about 0.045 mole fraction TBA.

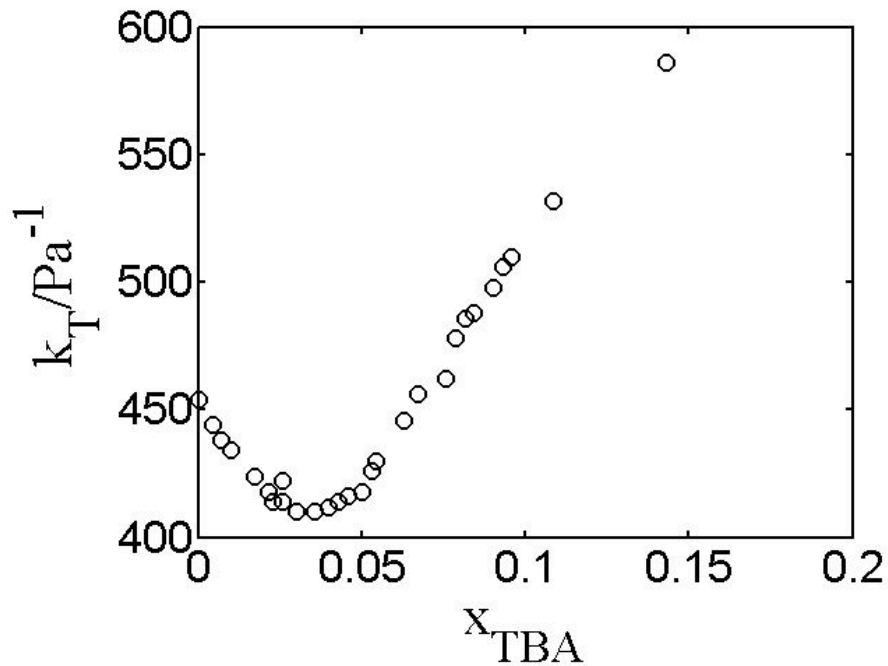


Figure 2.16 Isothermal compressibility measurements in TBA-water solutions as a function of TBA mole fraction, at $T = 25 \text{ }^\circ\text{C}$. (Taken from [81].)

The anomalous behavior of sound absorption in the water-rich region of the aqueous alcohol solutions was speculated to be due to various factors, such as stabilization of the solution by the formation of cage-like or clathrate-like structures at low alcohol concentrations [77], or breakdown of the water structure around the alcohol beyond a certain alcohol concentration, akin to hydrophobic hydration [62]. The anomaly observed in the compressibility of aqueous TBA solutions on the addition of small amounts of TBA may be attributed to the formation or breakdown of a compression-resistant structure, such as due to the making and breaking of hydrogen bonds within the solution [62].

2.7 Results from X-ray scattering experiments

There are many works studying the structural properties of aqueous TBA solutions by small angle X-ray scattering and X-ray diffraction [24-28]. As shown by Nishikawa *et al.* [24-28], the extrapolated zero-angle X-ray scattering intensity exhibits a peak between TBA mole fractions 0.14 and 0.17 [24]. Nishikawa *et al.* also observed that the intensity of this peak increases as the temperature is raised [25]. They attributed the observed phenomenon to concentration fluctuations or aggregates of TBA-water clusters, which increase in size as the TBA concentration and temperature is raised.

X-ray diffraction studies carried out by Nishikawa *et al.* and Tanaka *et al.* in aqueous TBA solutions have been interpreted in the light of formation of a cage-like or clathrate-like structures of the form $(\text{TBA})_m(\text{H}_2\text{O})_l$, wherein raising the temperature may cause a growth of the cluster size [26,28].

2.8 Results from small-angle neutron scattering experiments

D'Arrigio *et al.*, have carried out small-angle neutron scattering (SANS) experiments in heavy-water solutions of various alcohols, namely ethanol, *n*-propanol, isopropanol, *tert*-butanol, and butoxyethanol at various temperatures [29]. They carried out SANS measurements at a fixed concentration of alcohol at a heavy water composition, which corresponds to a concentration where ultrasonic attenuation exhibits a maximum in these systems. They observed an increase in the size of

alcohol molecular clusters for TBA- heavy water and butoxyethanol – heavy water solutions, beyond 25 °C, which they attribute to the tendency of the system to phase separate at higher temperatures.

D'Arrigo *et al.*, interpreted these observations on the basis of two possible scenarios existing in alcohol – heavy water solutions. The first possibility is that alcohols form micelle-like structures within the solutions. The second possibility is the existence of concentration fluctuations, with no sharp separation between the two molecular species. However, they argued that a more elaborated theoretical interpretation is needed to better understand the microscopic behavior in these systems.

2.9 Results from molecular dynamics simulations

Molecular dynamics simulations on pure TBA and on aqueous TBA solutions have been carried out by our collaborator, Professor J. B. Klauda at the University of Maryland, College Park [83]. Among the numerous simulation models available for water the TIP4P/ICE water model has been used for these simulations mainly because it accurately predicts the normal freezing point of water and of solid hydrate phases in water [84]. The compositions of each of the components, temperature, and time taken for simulations are shown in Table 2.1. (Simulations with propylene oxide, PO, will be explained in the subsequent chapters.)

Table 2.1: Compositions (in mole fractions) of each of the components, temperature, and time taken for molecular dynamics simulations.

ID	T (K)	x_{TBA}	x_{water}	$x_{\text{propylene oxide}}$	Time (ns)
TIP4ICE-285	285	0.0380	0.9620	0.0000	1120
TIP4ICE-281-PO	281	0.0384	0.9611	0.0005	1200
7TIP4ICE-281-PO	281	0.0715	0.9281	0.0004	1200
TIP4ICE-283-5PO	283	0.0625	0.8870	0.0505	500
TIP4ICE-283-13PO	283	0.0960	0.7770	0.1270	440
TBA	283	1.0000	0.0000	0.0000	10

Pure TBA

The radial distribution function (RDF) between the central carbons of TBA, is shown in Figure 2.17. This figure shows the presence of a peak at a central carbon distance of 4.7 Å and an additional peak at a distance of about 6 Å. The first peak in the RDF corresponds to strong van der Waals interactions, while the second peak corresponds to weak van der Waals interactions between the methyl groups of TBA.

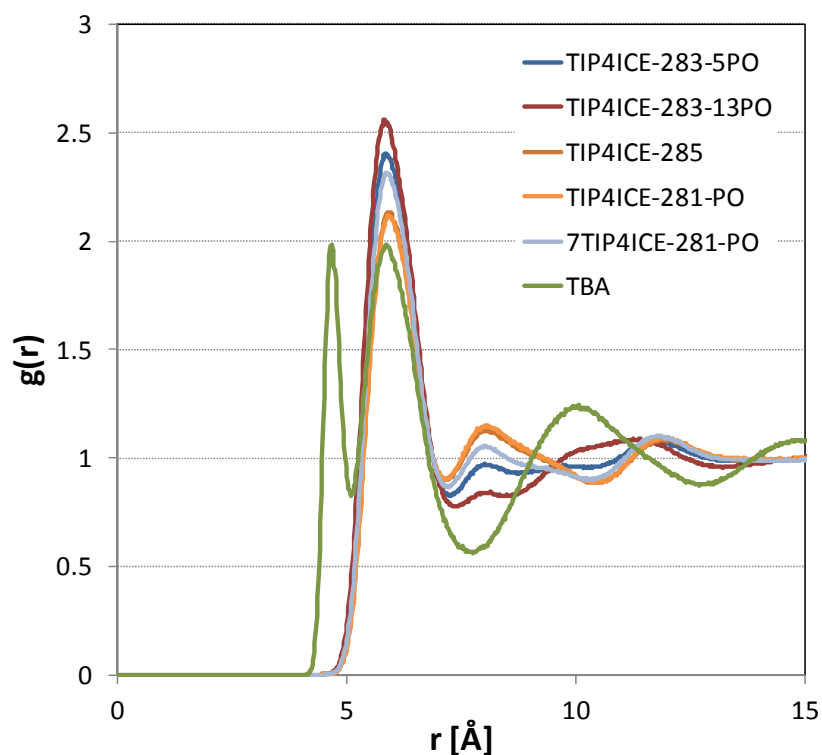


Figure 2.17. Radial distribution function between central carbon atom of TBA molecules in its aqueous solution, obtained from molecular dynamics simulations by using TIP4P-ICE model. The composition of the various components, temperature, and time taken for simulations are shown in Table 2.1. (Taken from [83].)

The radial distribution functions between oxygen's of TBA are shown in Figure 2.18. The initial large peak corresponds to strong hydrogen-bonding between TBA molecules in pure TBA, which disappears when in aqueous solution.

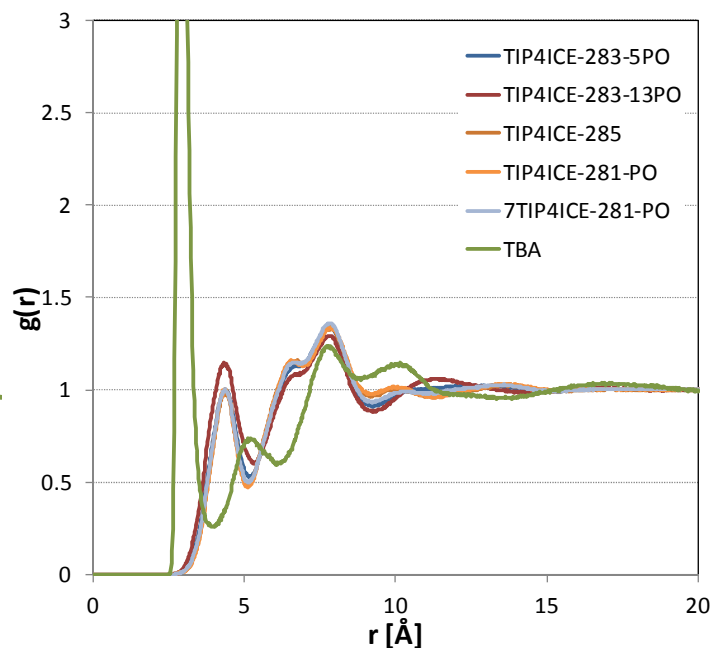


Figure 2.18. Radial distribution function between oxygen atoms of TBA molecules in its aqueous solution obtained by using the TIP4P-ICE model. The composition of the various components, temperature, and time taken for simulations are shown in Table 2.1 (Taken from [83].)

These results and simulations by other researchers, Figure 2.19 [23,36-41], indicate that pure TBA exhibits a mixture of hydrogen bonding interactions between the hydroxyl groups of the TBA molecules and non-polar interactions between the methyl groups of the TBA molecules.

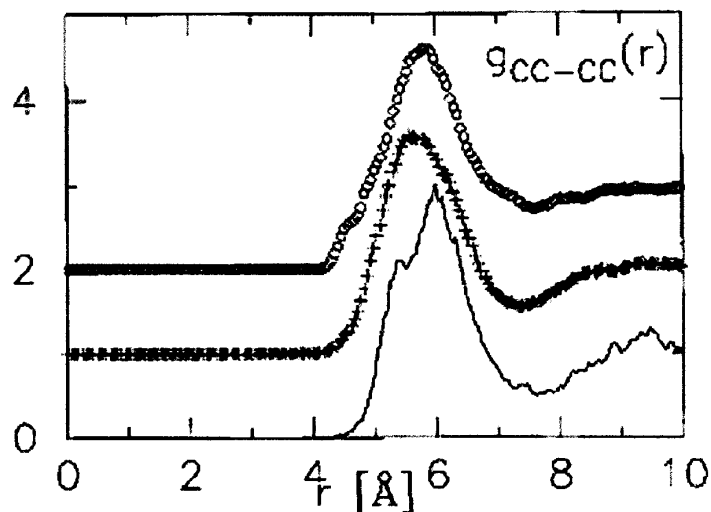


Figure 2.19. Partial pair distribution function between central carbon atoms in TBA for three different concentrations of TBA in water, as calculated from EPSR (empirical structural refinement) models. (Taken from [23].) Compositions in mole fractions: Continuous lines: 0.06 TBA; Crosses: 0.11 TBA; Open circles: 0.16 TBA.

Aqueous TBA Solutions

The RDFs between C-atoms in TBA, as seen from Figure 2.17, show that the first peak, which corresponds to van der Waals interactions in pure TBA, disappears when in aqueous solution and the second peak at a distance of about 6 Å becomes more prominent. A third peak is also seen. These show that in aqueous solutions of TBA, relatively more TBA molecules surround a central TBA as compared to the situation in pure TBA.

Bowron *et al.* have shown that in aqueous TBA solutions, the magnitude of the peak seen at ~ 6 Å gets enhanced as the concentration of TBA increases, as seen in Figure 2.19 [23]. From this figure, it is also seen that aqueous TBA solutions

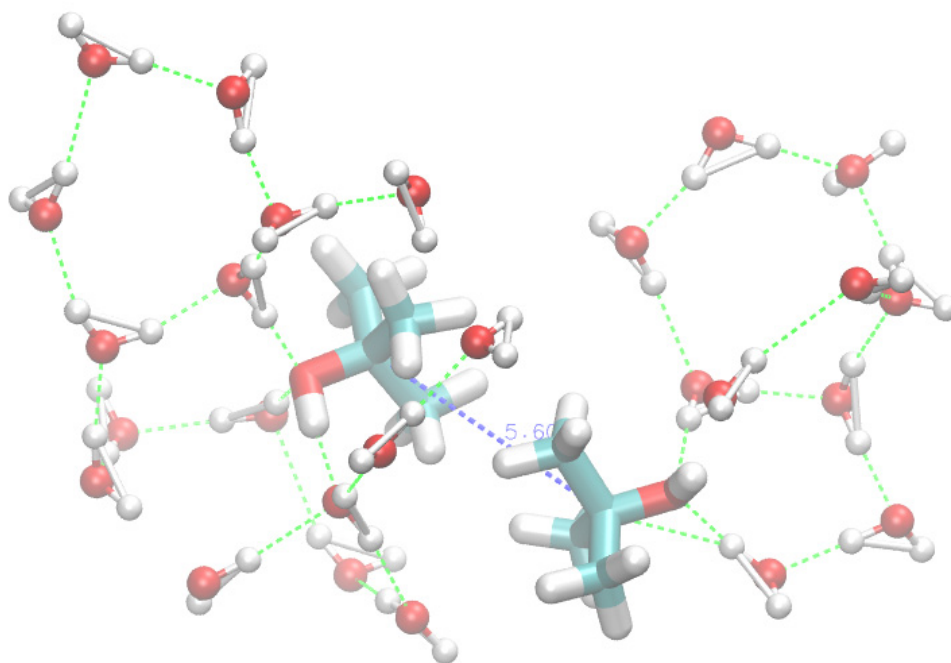
exhibit a secondary peak at a distance of about 8 Å, whose magnitude decreases on increasing TBA concentration. Bowron *et al.* further explain that at low TBA concentrations (0.06 mole fraction TBA) solute-solute interactions are obtained through methyl group contacts, evidencing a significant association between TBA molecules. This association is spontaneous and persists for tens of picoseconds. This association occurs until the intermolecular solute-solute interactions can no longer be accommodated through the nonpolar methyl-group interactions. As the TBA concentration is further increased, beyond 0.16 mole fraction TBA, the interactions between the TBA molecules resemble those in pure TBA.

The RDFs between the oxygen atoms of TBA are shown in Figure 2.19. As stated earlier, the first peak in pure TBA corresponds to strong hydrogen bonds between TBA molecules, which disappears when in aqueous solutions. Thus it is seen that in pure TBA the hydroxyl groups are hydrogen bonded with themselves, whereas in aqueous solution, the hydroxyl groups of TBA hydrogen bond with water. This correlates with the behaviour of the activity coefficient of water, discussed in Section 2.5.

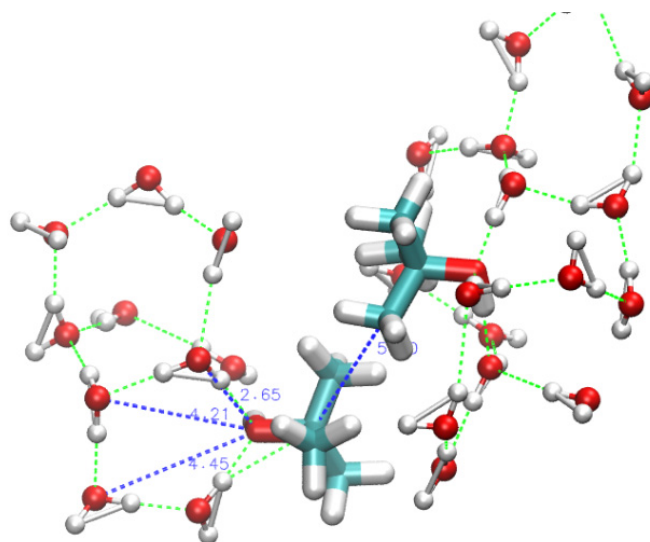
Snapshots from MD simulations in aqueous TBA solutions, shown in Figure 2.20, facilitate in the interpretation of the RDFs. Figure 2.20 a) shows a snapshot from molecular simulations, indicating a dimer of TBA with van der Waals interactions between its methyl groups, surrounded by a hydrogen-bonded polygonal (either pentagonal or hexagonal) network between TBA-water and water-water molecules. The main peak at ~ 6 Å, as seen in Figure 2.17, corresponds to the distance between central C-atoms of TBA, which form a dimer. The secondary peak

at $\sim 8 \text{ \AA}$ corresponds to a distance between the central C-atoms in TBA which may be trimerized. The water molecules form a structure around TBA molecules, with the hydroxyl group of the TBA molecules forming one of the vertices of a polygon.

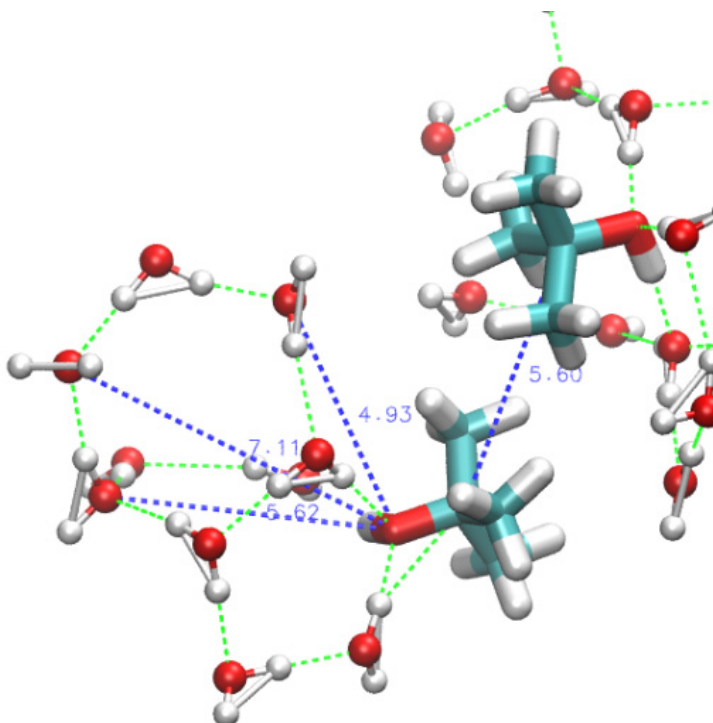
Figure 2.20 (see below). Snapshots from molecular dynamics simulations of 0.038 mole fraction aqueous TBA solutions obtained by using the TIP4ICE model at 285 K, simulated for 100 ns. (Taken from [83].)



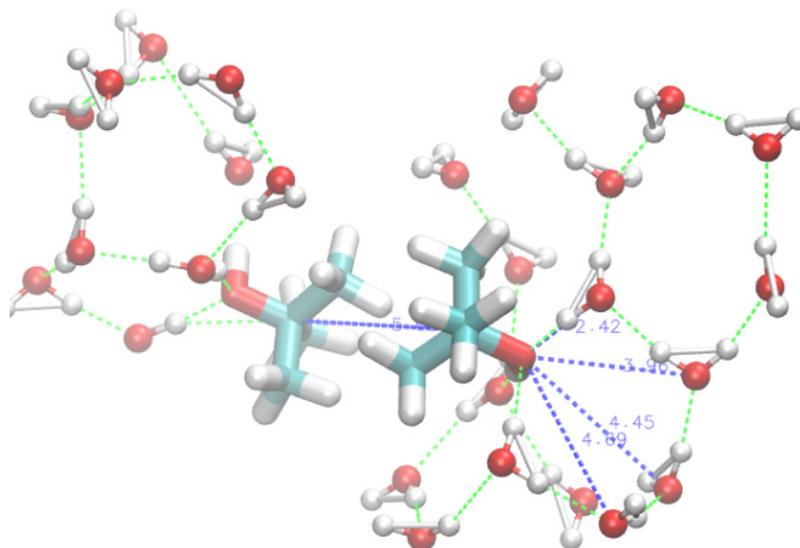
a.) Snapshots showing water structure around two coordinated TBA molecules. The distance between the central carbon of TBA is 5.6 \AA . Hydrogen bonds are shown by dashed green lines.



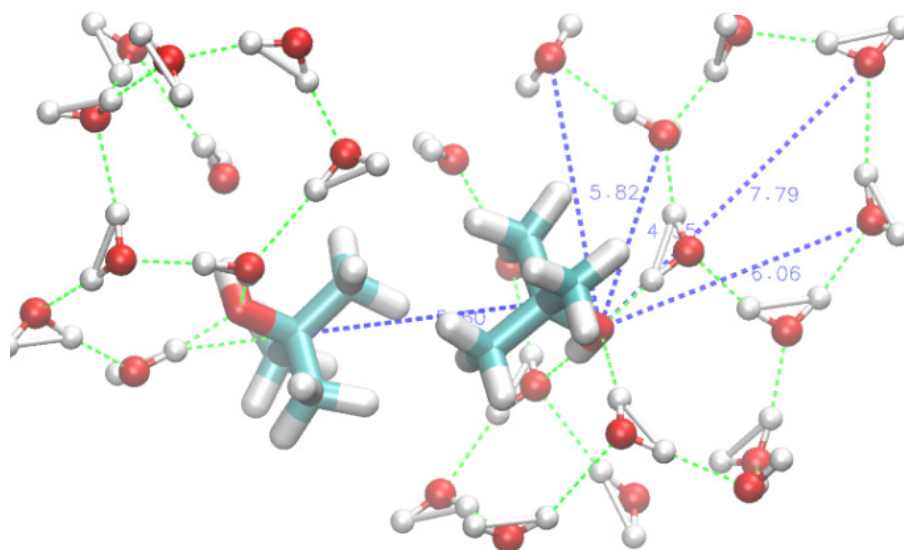
b.) Snapshots highlighting the primary and secondary peaks seen in RDF's from a water pentagon.



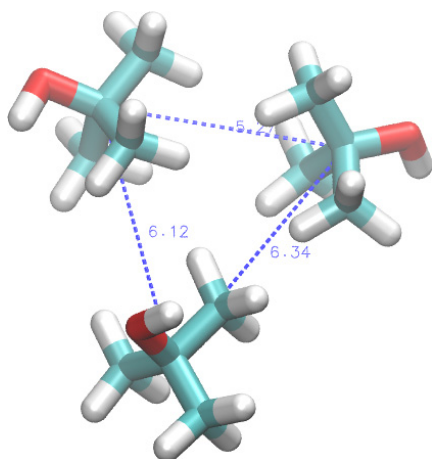
c.) Snapshot highlighting the tertiary peaks and beyond as seen in the RDF's.



d.) Snapshot highlighting a water hexagon.



e.) Snapshot highlighting the tertiary peaks and beyond as seen in the RDF's.



f.) Common triangular clustering of TBA in water.

Figure 2.21 shows the RDFs between the oxygen on TBA and water. The main peak at ~ 2.7 Å in Figure 2.21 corresponds to hydrogen bonds between TBA and immediately neighboring water. This distance is closer by 0.2 Å than in pure TBA and indicates that the hydrogen bonds between water and TBA molecules are stronger than hydrogen bonds between TBA molecules [83]. The secondary peaks at ~ 4.4 Å and the tertiary peak at ~ 5.6 Å in Figure 2.21 corresponds to larger distances between the vertices in hexagon and pentagon ring of water. The water clustering immediately neighboring a TBA molecule consists of ~ 3 water molecules, which come from the first peak in the RDF shown in Figure 2.21. The secondary and the tertiary peaks correspond to additional $\sim 17 - 21$ surrounding water molecules. This leads to an effective “micelle” radius of 7.5 Å with the first water shell and 10.5 Å including the surrounding shells of water. These bonds between TBA and water molecules appear to be transient, with an estimated life-time of the order of 10 – 50 ps.

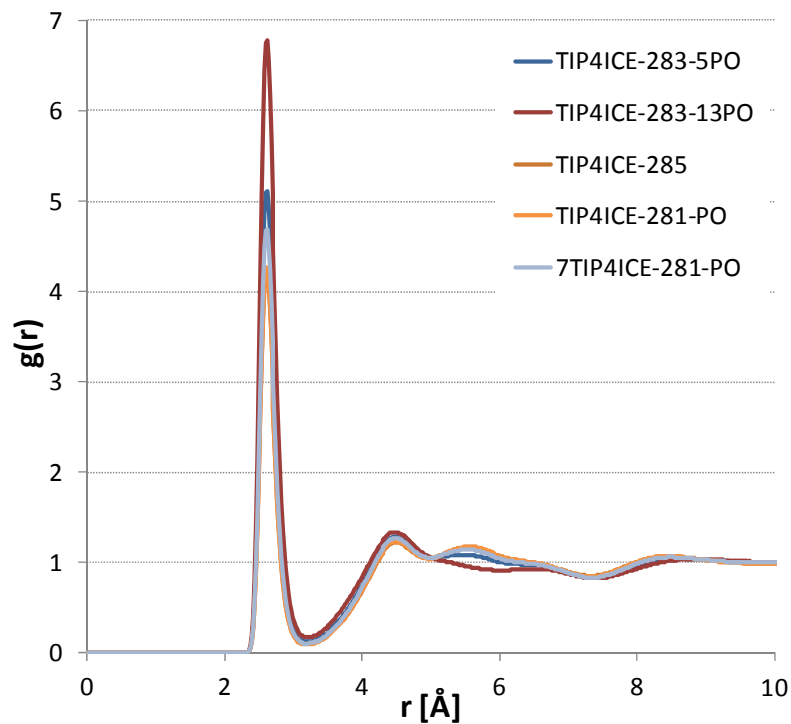


Figure 2.21. Radial distribution function between the oxygen on TBA and water obtained by using the TIP4P-ICE model. The composition of the various components, temperature, and time taken for simulations are shown in Table 2.1

(Taken from [83].)

Clusters of TBA molecules, larger than 3, can also form in aqueous TBA solutions. A cluster of 6 TBA molecules in aqueous solution is shown in Figure 2.22. Part of these molecules is in one-plane, while the rest correspond to a secondary shell of TBA.

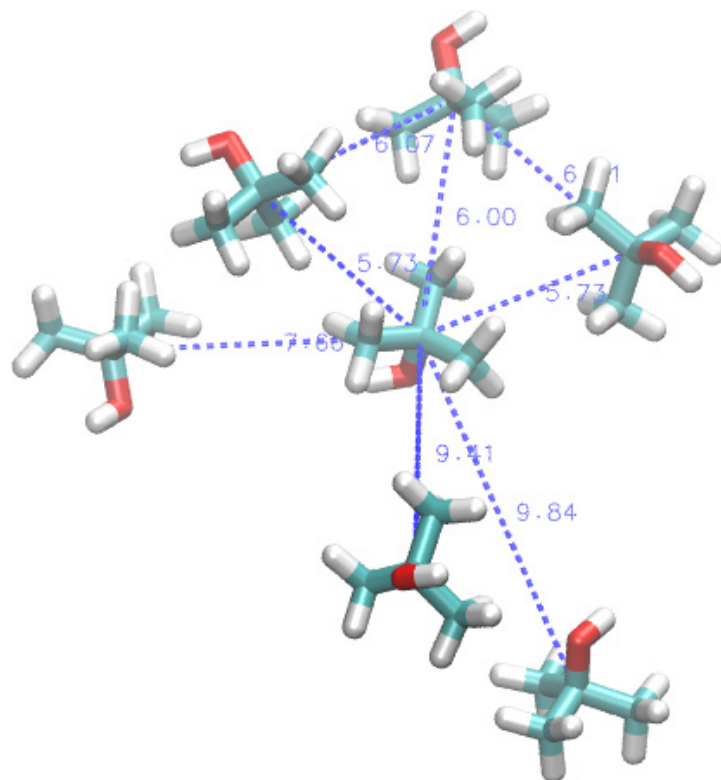


Figure 2.22. Large clustering of neighboring TBA in the same plane and second shell

TBA (TIP4ICE-285). (Taken from [83].)

Chapter 3: Mesoscale inhomogeneities in aqueous TBA solutions

In the previous chapter, macroscopic thermodynamics and molecular properties of aqueous TBA solutions were presented. Results from small-angle scattering measurements and molecular dynamics simulations were also discussed. In this chapter, mesoscopic properties of aqueous TBA solutions are discussed. First, a literature review of light-scattering results from aqueous TBA solutions is presented, followed by the discussion of a detailed light-scattering study performed in this work. The procedure for light-scattering experiments and results from an investigation of the effects of temperature, concentration, scattering angle, and source of the solutes are discussed.

3.1 Controversies surrounding the mesoscopic properties of aqueous TBA solutions – Review of light-scattering investigations

The physical chemistry of aqueous TBA solutions has been studied for a long time. In addition to evidence on clustering of TBA molecules in solution, occurring on the order of few nanometers [23-44], as seen in the previous chapter, investigations from light scattering have shown the presence of mesoscopic aggregates of the order of 100 nm [85-88].

The spectrum of views and explanations on the interpretation of the observed phenomena in aqueous TBA solutions is extremely broad: from structural “phase transitions” [85] to alleged artifacts [86], from genuine equilibrium or long-lived micro-phase separation, to clathrate precipitation, from micellar-like structural fluctuations to concentration fluctuations [87,88].

Light-scattering investigations in aqueous TBA solutions were first reported by Vuks and Shurupova in 1972 [85]. They observed anomalous light scattering in an aqueous solution of TBA at about 0.03 mole fraction of TBA in water. They attributed this phenomenon to some kind of a “phase transition” in the liquid phase between a clathrate-like structure and a less ordered structure.

Two years later more detailed light-scattering experiments on this system were carried out by Beer, Jr. and Jolly [86]. They noticed that the effects reported by Vuks and Shurupova are dependent on the purity and the prehistory of the sample and attributed those results to the formation of droplets of insoluble impurities.

Soon after this, isobaric heat-capacity measurements in the same system were carried out by Anisimov *et al.* [68], as shown in Figure 2.6 and 2.7, who observed a line of heat-capacity maxima between 0.01 and 0.1 mole fractions TBA in water. The greatest effect was observed at about 0.074 mole fraction TBA at a temperature of about 0 °C. As discussed in chapter 2, Anisimov *et al.* attributed this heat-capacity anomaly to a nanoscale structural transformation in the liquid phase, but, at the same time, pointed out that this transformation could not cause the anomalous light scattering observed by Vuks and Shurupova. They further suggested that a sudden decrease in solubility of liquid impurities or gases near the line of these structural

transformations could produce nanosize droplets or bubbles, which might cause anomalous light scattering.

Further light-scattering experiments by Iwasaki and Fujiyama in 1977 showed a strong Rayleigh scattering for various concentrations of aqueous TBA solutions [87]. They observed that for concentrations below 0.05 mole fraction TBA, the Rayleigh scattering increases on decreasing the temperature, while beyond 0.05 mole fraction TBA, the Rayleigh scattering increases on increasing temperature [88]. They interpreted the observed phenomenon as due to presence of concentration fluctuations of clathrate hydrate structures forming in aqueous TBA solutions.

Later experiments carried out by Euliss and Sorensen in 1984 showed that in an aqueous TBA solution, at a concentration of 0.07 mole fraction TBA, stable submicron particles (about 100 nm size) appeared below room temperature [89]. These particles disappeared upon heating to room temperature. Even after double distilling the TBA and redistilling the water in quartz still, these particles persisted. These observations led Euliss and Sorensen to speculate that the effect “*might be related to some stable solid clathrate of tert-butanol in water perhaps involving a trace help gas to promote stability*”.

Subsequent light-scattering studies in aqueous TBA solutions were also carried out by Bender and Pecora, but their experiments did not show any anomalous light scattering [90]. On the other hand, Bender and Pecora did observe mysterious submicron particles in aqueous solutions of 2-butoxyethanol (2BE) below 0.02 mole fraction 2BE [91]. However, the phenomenon was strongly dependent on the source of 2BE, forcing Bender and Pecora to conclude that small amounts of undetectable

impurities might be responsible for the anomaly. Another system, which shows similar behavior, is the aqueous solution of tetrahydrofuran (THF) [92].

Motivated by these controversies regarding the mesoscopic properties of aqueous TBA solutions as observed by light scattering, a comprehensive static and dynamic light scattering study of aqueous TBA solutions has been carried out in this work [55]. Results from light scattering have been supplemented by results from confocal microscopy and gas chromatography, which help elucidate the mesoscopic properties of aqueous TBA solutions.

The details of the experimental procedure and results thereof are discussed below.

3.2 Experimental techniques and procedures

Light scattering technique

The light-scattering experiments in aqueous TBA solutions were carried out with a setup consisting of a single He-Ne laser, a single photomultiplier, and an automatic goniometer. The set-up and its schematic are shown in Figure 3.1.

The optical cell with the aqueous TBA sample was submerged in a liquid (silicone oil with a refractive index of 1.498 that closely matches the refractive index of the optical cell) to obtain a uniform temperature around the sample and to avoid any stray light. The sample was subjected to various temperatures ranging from 8 °C to 50 °C, with a temperature control of about ± 0.1 °C. The thermostat consists of an

electric heater and a water cooler, which are part of the Photocor light-scattering setup. The heating rate was about 8 °C/hr, while the cooling rate was about 5 °C/hr.

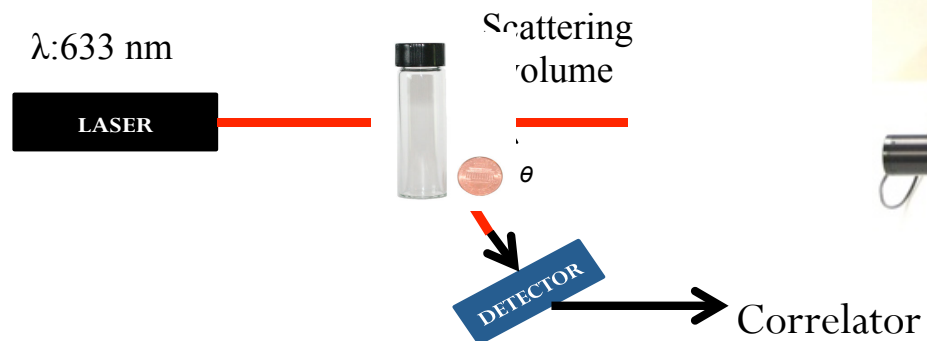
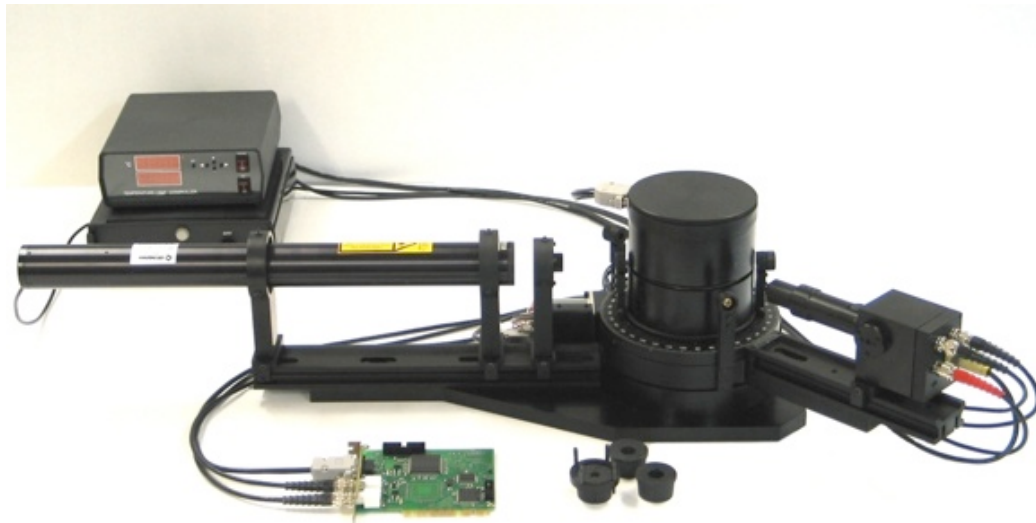


Figure 3.1. Experimental set-up (and schematic) used for static and dynamic light scattering experiments.

At each temperature, the sample was allowed to equilibrate for about 2 hr before taking a reading. The time-dependent auto-correlation function in the homodyne

mode was obtained by using a Photocor correlator. An option in the Photocor software control was used to eliminate the effect of occasional spikes seen in the intensity caused by large ($> 10 \mu\text{m}$) aggregates. In this software the total accumulation time is broken down into small segments [of the order of (30 to 60) s]. After all segments of the correlation function are collected, the program disregards any segments during which the scattering intensity spiked beyond a preset limit and then computes the correlation function based on the remaining segments.

For dynamic light-scattering experiments, the time-dependent auto-correlation function in the homodyne mode, $g_2(t)$ for a single-exponential mode (Eq. 3.1), or a two-exponential relaxation mode (Eq. 3.2), is given by [93]:

$$g_2(t) - 1 = \left[A \exp\left(-\frac{t}{\tau}\right) \right]^2, \quad (3.1)$$

$$g_2(t) - 1 = \left[A_1 \exp\left(-\frac{t}{\tau_1}\right) + A_2 \exp\left(-\frac{t}{\tau_2}\right) \right]^2, \quad (3.2)$$

where A_i are the amplitudes, t is the lag time, and τ_i are the relaxation times of the fluctuations. If the relaxation time is associated with diffusion of molecules or particles, then the decay rate, $\Gamma = 1/\tau$, is:

$$\Gamma = Dq^2, \quad (3.3)$$

where $q = (4\pi n / \lambda) \sin(\theta/2)$ is the wave number (n is the refractive index of the scattering medium, λ is the wavelength of the laser beam, and θ is the scattering angle) and D is the translational diffusion coefficient. For Brownian monodisperse

spherical non-interacting particles, the diffusion coefficient can be related to the hydrodynamic radius, R , of the particles as [93]:

$$D = \frac{k_B T}{6\pi\eta R} \quad , \quad (3.4)$$

where k_B is Boltzmann's constant, T is the temperature, and η is the shear viscosity of the medium.

Sample preparation for light-scattering experiments

For the light-scattering experiments, aqueous TBA solutions are prepared from two sources of TBA: one from Sigma Aldrich with purity > 0.997 mass fraction and another one from Alfa Aesar with purity > 0.998 mass fraction. One sample with 0.083 mole fraction TBA is prepared by using the TBA from Sigma Aldrich. Other aqueous samples with 0.010, 0.040, 0.073, 0.087, and 0.110 mole fraction TBA are prepared by using TBA from Alfa Aesar. The optical cells are first washed and rinsed with dust-free water and ethanol/isopropanol, and then dried with dust-free nitrogen gas. The dust-free nitrogen gas is of high-purity (HP) grade, purchased from Airgas. Water (from a Millipore setup) and TBA are initially filtered 2-3 times with a 200 nm nylon filter. Each sample is first checked visually for the presence of any dust particles in the propagating laser beam. Additional filtrations are carried out until no sudden spikes are detected the scattered intensity. All the samples, with the exceptions of those with 0.040, 0.073, and 0.087 mole fraction TBA, are covered with a Teflon tape (previously washed with dust-free water, ethanol and dried using HP

nitrogen gas) and sealed with polyethylene glue. The remaining samples with 0.040, 0.073, and 0.087 mole fraction TBA are flame sealed.

Confocal microscopy

Confocal microscopy experiments are carried out in a Leica CTR 6500 instrument at the Department of Physics, Georgetown University. The confocal microscopy unit and the sample holder cell are maintained at cold temperatures by the use of ice. While the system is at low temperatures (about 10 °C), a drop of 0.083 mole fraction TBA solution is transferred from the optical glass vial into the sample holder.

Gas chromatography

Gas chromatography experiments are carried out in Agilent instrument at the Department of Chemistry and Biochemistry, University of Maryland, College Park. The sample under study is dissolved in methanol, which is used as a solvent. The mixture is then subjected to a temperature ramp from 70 to 200 °C. The different components evaporate at different times, and the time at which a component reaches a detector, known as retention time, is proportional to the boiling point of that component. The area under the recorded chromatograph is proportional to the concentration of that component. Aqueous TBA solutions with 0.083 mole fraction TBA (TBA procured from Sigma Aldrich) and 0.073 mole fraction TBA (TBA

procured from Alfa Aesar) are tested in the gas chromatograph to determine the composition of impurities in TBA.

3.3 *Experimental results*

On analyzing the correlation function from a 0.083 mole fraction TBA aqueous solution, (TBA procured from Sigma Aldrich) at room temperature (22.8 °C), two dynamic modes are detected – the molecular diffusion mode and a mesoscale relaxation mode, as seen from Figure 3.2. The molecular diffusion mode is of the order of 10 μ s at $\theta = 30^\circ$, corresponding to a correlation length (or hydrodynamic radius from Eq. 3.4) of ~ 0.5 nm, matching with previously published results [89]. The mesoscale relaxation mode is of the order of a millisecond at $\theta = 30^\circ$, corresponding to a correlation length of about 300 nm. The refractive index and viscosity of aqueous TBA solutions needed for determining the above parameters were taken from the literature [87-89]. In addition, the correlation function also shows a contribution from much slower inhomogeneities with a decay time of the order of seconds, similarly to what was observed in 3MP solutions. It has been confirmed that these inhomogeneities are associated with sharp spikes in the light-scattering intensity previously reported by Kostko *et al.* [54]. By using the Photocor “dust cut-off” software the contribution from the intensity spikes are reduced or completely eliminated, such that the long-time tail of the correlation function would practically disappear.

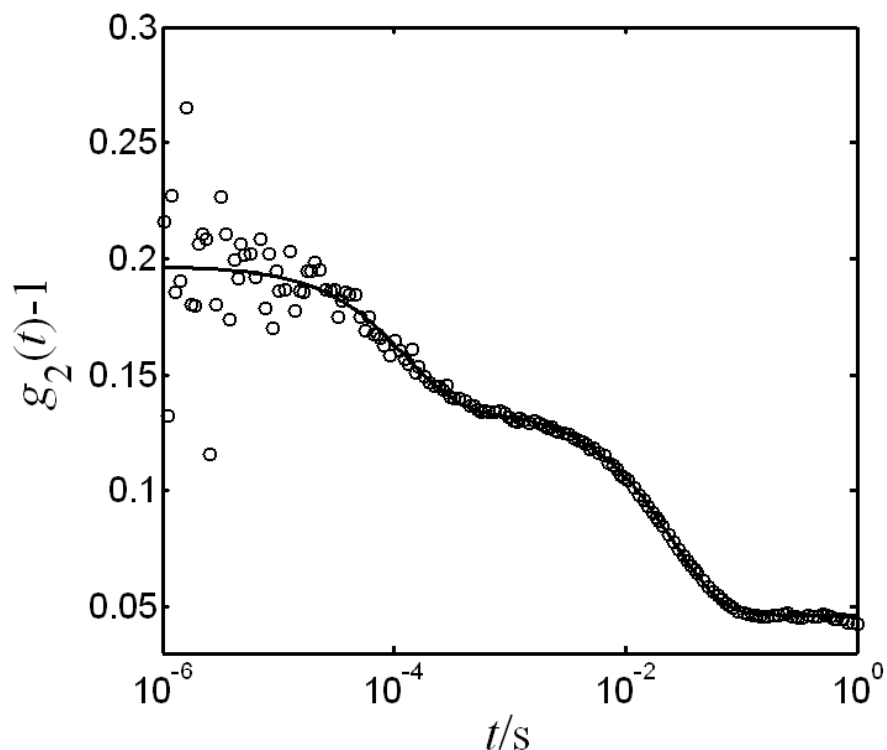


Figure 3.2. Time-dependent intensity auto-correlation function (open circles) for the 0.083 mole fraction TBA aqueous solution at a scattering angle $\theta = 30^\circ$ obtained at $T = 22.8^\circ\text{C}$. The solid curve represents a fit of the data to two exponential decays with two decay times corresponding to molecular diffusion and mesoscale diffusion, respectively. An additional long-time tail of the dynamic correlation function is assumed to be a background contribution [55].

Upon cooling below room temperature, a significant increase in intensity was observed. The intensity increased by an order of magnitude, as seen in Figure 3.3. The sample was heated from 8°C up to 50°C , and then cooled back to 8°C . This cycle was repeated several times. On cooling, an increase of the light-scattering

intensity, an increase of the amplitude of the mesoscale mode, and on heating a virtual disappearance of this effect was observed.

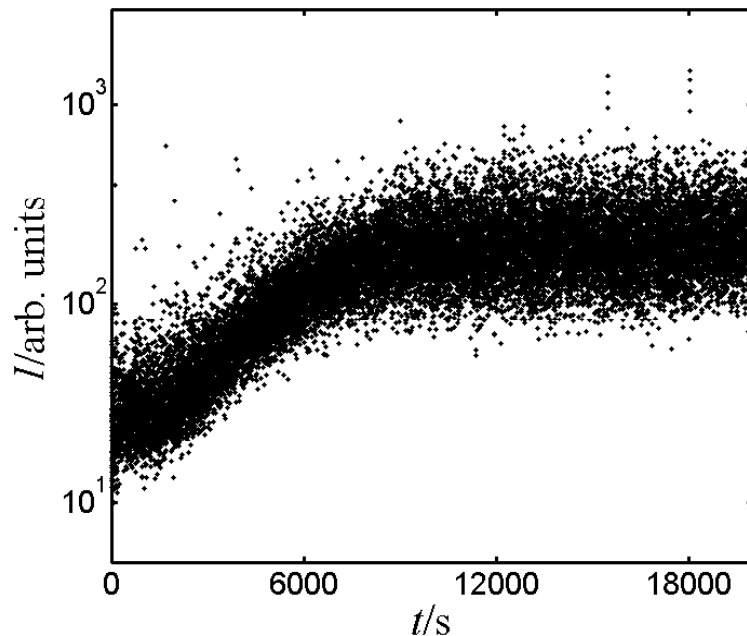


Figure 3.3. Time evolution of the light-scattering intensity upon cooling from 50 °C to 8 °C for the 0.087 mole fraction TBA aqueous solution at a scattering angle $\theta = 45^\circ$ [55].

This cycle was also repeated after filtering the sample with a 200 nm filter at room temperature. This filtration did not have any significant effect on the observed anomaly. The sample was also analyzed after leaving it undisturbed for five days at 15°C. During this period the light-scattering intensity remained relatively stable.

The correlation function, obtained for the sample with 0.083 mole fraction TBA at $\theta = 60^\circ$ and 8.5 °C, is shown in Figure 3.4. The fit of the correlation function to a single exponential decay corresponds to a pronounced mesoscale mode.

Contributions from the molecular scattering and from large ($>10 \mu\text{m}$) inhomogeneities become insignificant.

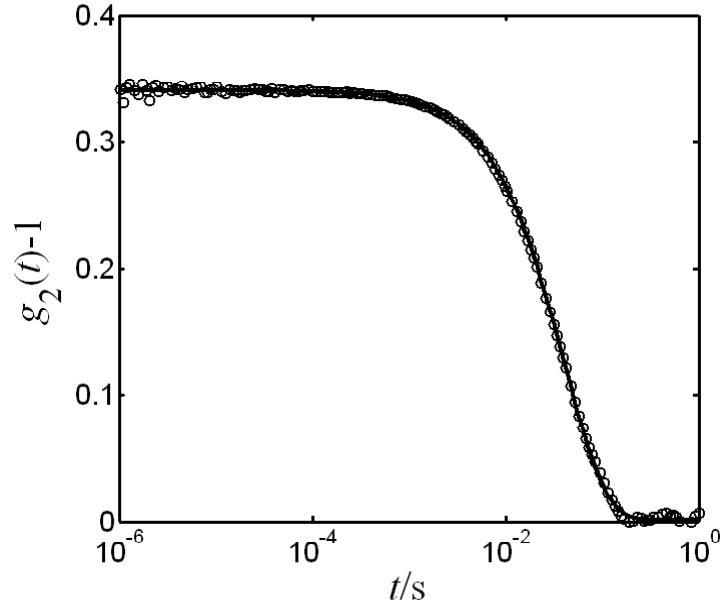


Figure 3.4. Time-dependent intensity auto-correlation function (open circles) for the 0.083 mole fraction TBA aqueous solution at $T = 8.5 \text{ }^\circ\text{C}$ and a scattering angle $\theta = 60^\circ$. The solid curve represents the fit to a single exponential decay. This fit approximates the mesoscale mode as being associated with Brownian diffusion ($D = 4.2 \times 10^{-9} \text{ cm}^2/\text{s}$) of monodisperse particles, which actually display some polydispersity [55].

The decay rate of the mesoscale mode at $8.5 \text{ }^\circ\text{C}$ has also been measured at various scattering angles. As seen from Figure 3.5, the mesoscale mode in the TBA solutions obeys, within the experimental errors, simple diffusion dynamics described by Eq. 3.3. Hence, the mesoscale mode can be referred to as mesoscale diffusion.

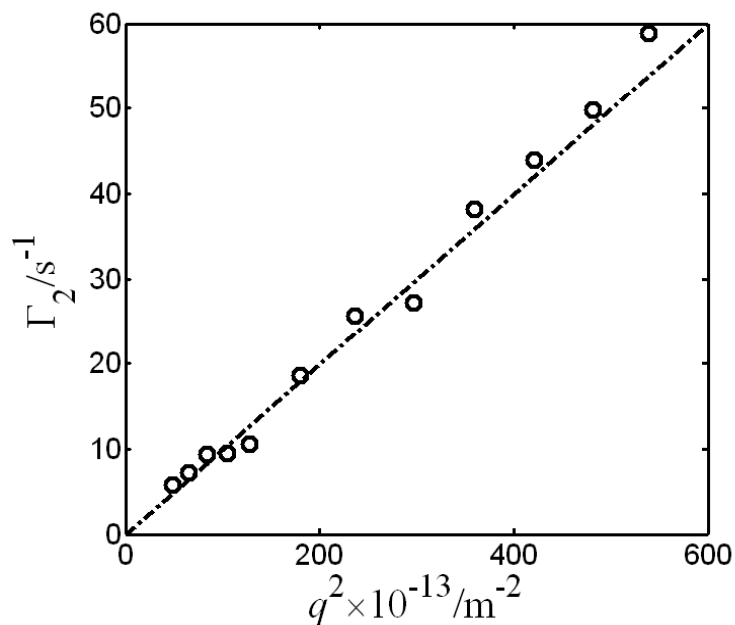


Figure 3.5. Wave-number dependence of the decay rate Γ_2 of the mesoscale mode in the 0.083 mole fraction TBA aqueous solution at $T = 20.8^\circ\text{C}$. The slope of the linear

dependence yields the average effective diffusion

coefficient ($D \approx 1 \times 10^{-9} \text{ cm}^2/\text{s}$) [55].

An average hydrodynamic radius associated with the mesoscale diffusion for the 0.073 mole fraction TBA aqueous solution is calculated by using Eq. 3.4. The average size of the observed particles as a function of temperature and at various scattering angles is shown in Figure 3.6. From this figure, it is seen that the average size varies from about 300 nm at 21°C to about 800 nm at about 8°C . If these particles were monodisperse, one would expect that the particle size, at a particular temperature, should remain constant when probed from different angles. However, it is seen from Figure 3.6 that there is a certain discrepancy in the particle size measured at different angles at a given temperature. Thus we conclude that these particles are

generally polydisperse. The polydispersity increases upon cooling. This conclusion is supported by the fact that at 8 °C the effective particle sizes obtained for small angles ($\theta = 20^\circ$ and $\theta = 30^\circ$) are largest, because larger particles scatter more light at smaller angles [94,95].

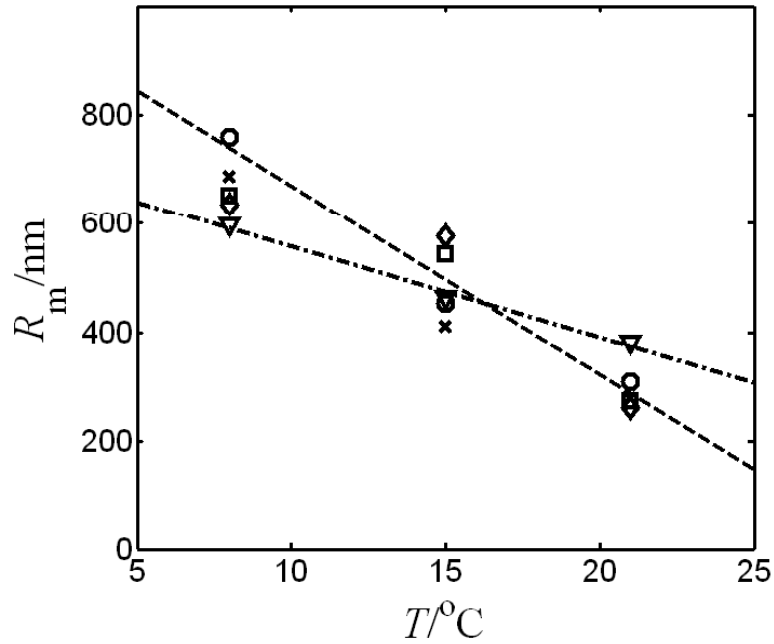


Figure 3.6. Effective hydrodynamic radius R_m of the mesoscale particles as a function of temperature for the 0.083 mole fraction TBA aqueous solution. Open circles: $\theta = 20^\circ$; crosses: $\theta = 30^\circ$; open squares: $\theta = 45^\circ$; open diamonds: $\theta = 60^\circ$; open triangles: $\theta = 90^\circ$. The dashed line shows the trend of the temperature dependence of the particles size obtained from scattering at $\theta = 20^\circ$ and the dotted-dashed line the trend of the particles size obtained from scattering at $\theta = 90^\circ$. The steeper slope is attributed to particle polydispersity [55].

The overall static light-scattering intensity at various scattering angles ranging from 20° to 135° has also been measured. For Brownian, monodisperse particles, the inverse intensity, I^{-1} follows a linear q^2 dependence [93] according to the equation:

$$I^{-1} = K \left[1 + \frac{1}{3} R_g^2 q^2 \right] \quad , \quad (3.5)$$

where R_g is the radius of gyration of the particle and K is a constant.

As shown in Figure 3.7, the wave-number distribution of the inverse intensity follows a linear q^2 dependence, however, the deviation from linearity becomes pronounced at low temperatures. These results are consistent with the results obtained from the analysis of the dynamic-correlation-function (Figure 3.6).

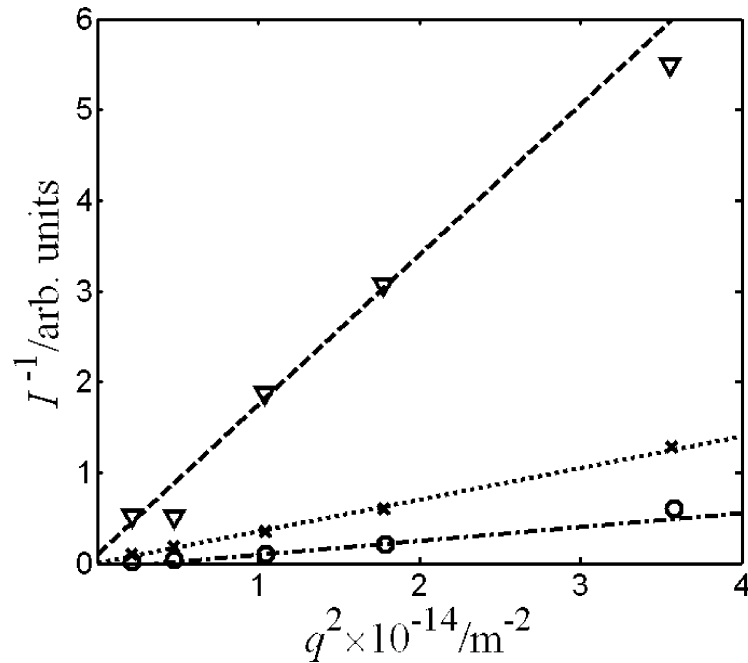


Figure 3.7. Wave-number dependence of the inverse light-scattering intensity for the 0.073 mole fraction TBA aqueous solution. Open circles: $T = 8.5^\circ\text{C}$; crosses: $T = 21^\circ\text{C}$; open triangles: $T = 50^\circ\text{C}$ [55].

The scattered-intensity depolarization ratio at 90° angle is measured. This ratio is very close to zero. We thus conclude that the shape of the particles associated with the mesoscale mode is nearly spherical, as the anisotropic contribution in the light-scattering intensity is negligible [94].

In addition, confocal microscopy experiments are also performed on this sample. The mesoscale Brownian particles are clearly seen under the confocal microscope, Figure 3.8. These particles are stable only at low temperatures: as the temperature is raised they disappear. The confocal nature of these images tells us that these particles are not of uniform size, but they range in size from a hundred nanometers to about a micron. These observations are consistent with what is observed from light-scattering experiments.

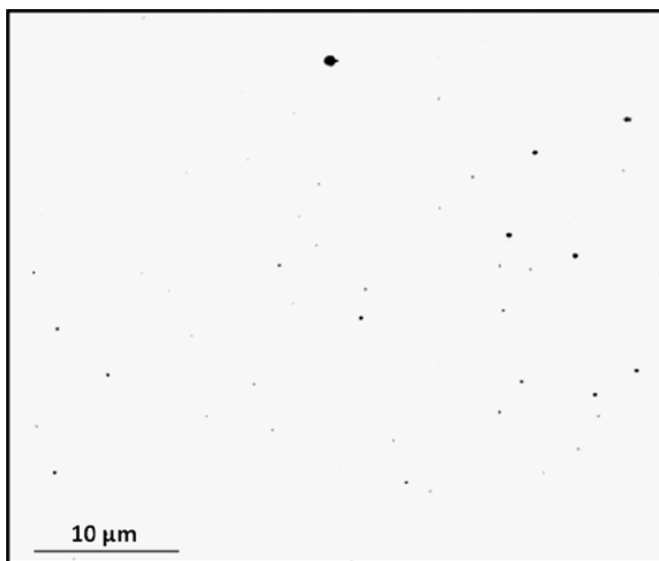


Figure 3.8. Confocal microscopy image of the 0.083 mole fraction TBA aqueous solution at about 10°C . The particles are polydisperse and range in size from a few hundred nanometers to a micrometer [55].

Similar experiments are performed on TBA aqueous solutions, with TBA being procured from Alfa Aesar. Samples with concentration from 0.01 to 0.11 mole fraction TBA are tested. A maximum in the light-scattering intensity is observed for the 0.073 mole fraction TBA solution at 8.5 °C, as shown in Figure 3.8. This concentration corresponds to where a maximum in the heat-capacity anomaly is observed, as was shown in Figure 2.7. At all concentrations studied the molecular diffusion mode is detected, along with the mesoscale mode that becomes pronounced at low temperatures. The average size of the observed mesoscale particles, for various concentrations at 8.5 °C, varies between 150 nm to 400 nm. Therefore, the mesoscale particles are equally formed in solutions prepared from different sources of TBA, although the average size and absolute intensity under the same conditions is not exactly the same.

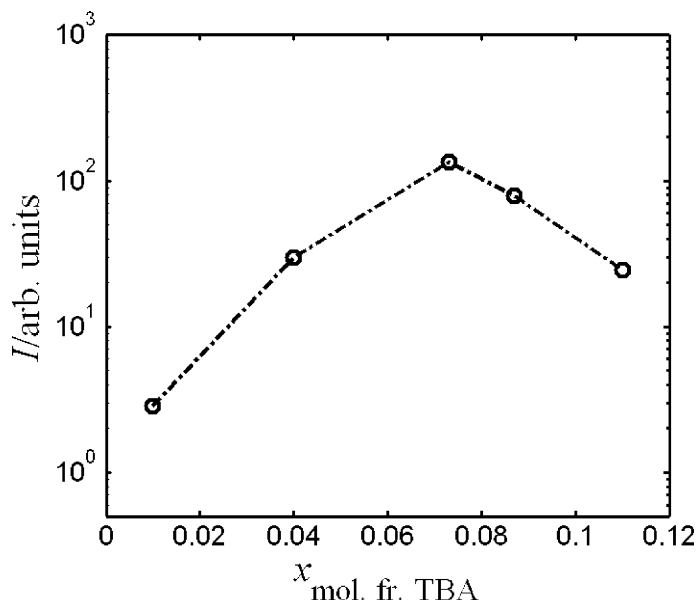


Figure 3.9. Light-scattering intensity in the aqueous TBA solutions as a function of TBA concentration, at a scattering angle $\theta = 45^\circ$ and at $T = 8.5^\circ\text{C}$ [55].

The effect of ultrasonication in a 0.073 mole fraction aqueous TBA solution at 8.5 °C is studied. The sample is ultrasonically agitated for about 10 minutes at a frequency of 60 Hz. On comparing the sample before and after ultrasonication, it is seen that the observed light-scattering intensity and the dynamic correlation function remains unchanged.

Furthermore, the 0.073 mole fraction aqueous TBA solution is centrifuged in a traditional centrifuge (Fisher-Scientific Centrifuge Model 225), with an angular velocity of 320 radians/second, for about 30 minutes. The centrifuge is maintained at temperatures below 10 °C by using dry ice. Separating the “precipitant” and “supernatant” parts of the sample, and then observing them separately under the laser, led to no significant change in intensity or the dynamic correlation function, compared to samples before centrifugation. This result indicates that the density of the particles is very close to the density of the solution.

3.4 Origin of mesoscale inhomogeneities

In the quest for understanding the behavior of aqueous solutions of small molecules, the origin of the slow mode is a primary question. To answer this, aqueous solutions of TBA are analyzed in further detail. Experiments are carried out by continuously filtering 0.073 mole fraction TBA solution through a 20 nm Anopore filter with the help of a recirculating pump. The filtration is carried out in a clean glove-box, which is maintained at a temperature below 10 °C by using dry ice. After filtration, it is observed that the intensity dramatically reduced to levels typical for ordinary binary fluids, and did not rise again when monitored for about a week. As

seen from Figure 3.10, the mesoscale diffusion mode is hardly detectable. The refractive index of the solution after the cold filtration step remains unchanged, so the filtration does not significantly change the TBA concentration.

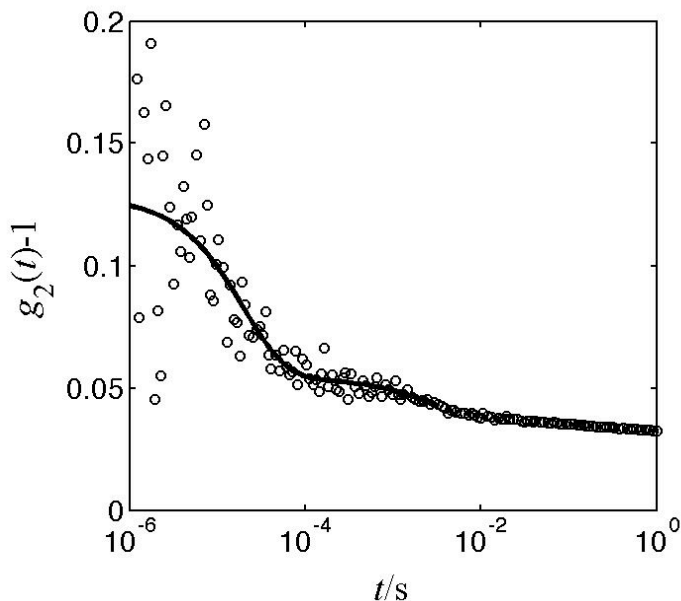


Figure 3.10. Time-dependent intensity auto-correlation function (circles) for a 0.073 mole fraction TBA aqueous solution after repeated cold filtrations by using a 20 nm Anopore filter at a scattering angle $\theta = 45^\circ$ and at $T = 8.5^\circ\text{C}$. The solid curve represents the fit to two-exponential decays according to Eq. 3.3 [98].

Next, to regenerate the slow mode, controlled amount of impurities are added to the cold-filtered aqueous TBA solution. Two microliters of an amphiphilic nonionic impurity, namely propylene oxide (PO), is added to 10 mL of a cold filtered 0.073 mole fraction TBA solution under cold conditions, with the help of a micropipette.

PO is selected because it is obtained as a co-product in the synthesis of TBA [96] and is also known as a clathrate former [97]. Thus PO is a candidate impurity that may be present in commercial TBA samples and it may induce the formation of clathrate-like structures in TBA aqueous solution, as suggested by other research groups [76,98].

After adding PO, and allowing the sample to “equilibrate” for about 24 hours, it is observed that at 8.5 °C the intensity rose almost four times compared to before the addition of PO. The dynamic correlation function shows the presence of “particles” with a relaxation time of about a few milliseconds as seen at a scattering angle of 60° (Figure 3.11). This corresponds to a hydrodynamic radius of about 200 nm in size.

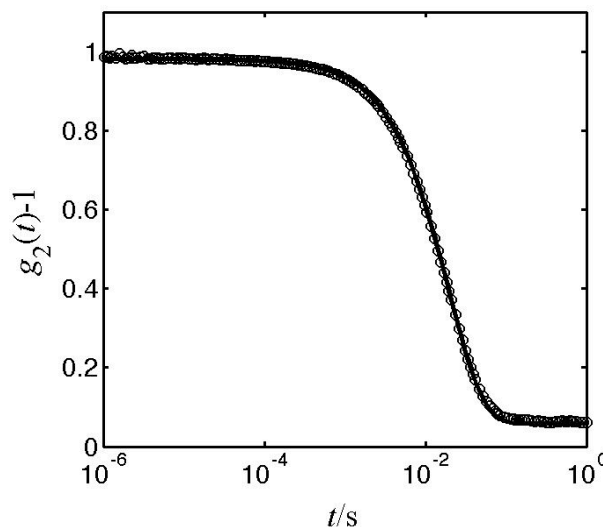


Figure 3.11. Time-dependent intensity auto-correlation function (open circles) for 0.073 mole fraction TBA aqueous solution, after cold filtering and doping with 10^{-5} mole fraction of PO, at a scattering angle of 60 ° and $T = 8.5$ °C. The black curve represents fit of the data to a single exponential [98].

Experiments are also repeated by adding controlled amounts of other impurities, such as 4 μL of isopropanol, 4 μL of isobutanol, and 2 μL of cyclohexane, to 10 mL of cold filtered 0.073 mole fraction TBA solution in the same manner as when PO is added. Although isopropanol and isobutanol dissolved in the aqueous TBA solution, cyclohexane did not, and was observed to have phase separated. Trace amounts of PO (4 μL) are also added to a 10 mL cold filtered aqueous isopropanol system and 10 mL of pure injection-grade water. All these systems are studied by light scattering at about 8.5 $^{\circ}\text{C}$ and angle 45 $^{\circ}$. However, none of these systems show any dramatic results in the dynamic auto-correlation function as is seen on the addition of PO to a cold-filtered aqueous TBA solution.

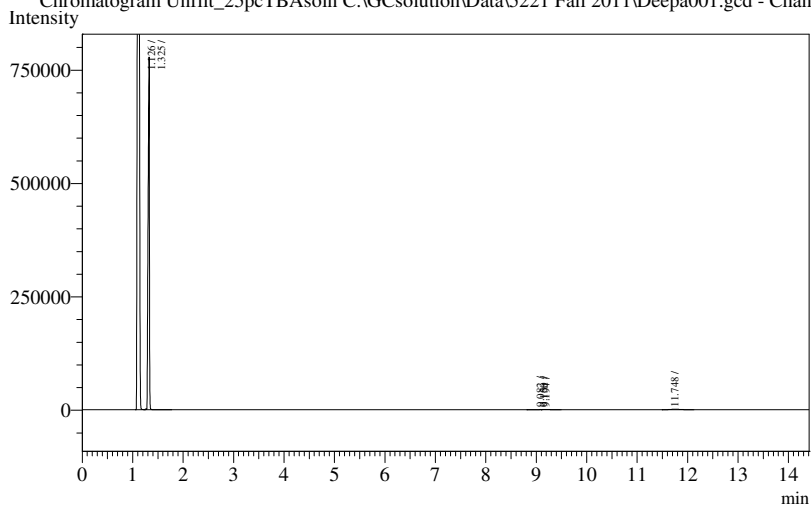
Gas chromatography of commercial TBA samples is carried out. Impurities, of the order of 0.001 mass fraction is detected in the TBA procured from Sigma Aldrich. No impurities, within the tolerance of the instrument, are detected from the TBA procured from Alfa Aesar. These observations are consistent with the declared purities of the samples.

To further verify that the origin of the mesoscopic inhomogeneities in aqueous TBA solutions are due to the presence of trace amounts of a third component, gas chromatography between unfiltered and cold-filtered aqueous TBA solutions is carried out. TBA, with purity > 0.99 mass fraction was procured from Alfa Aesar and 0.073 mole fraction TBA aqueous solutions was prepared from this sample. Strong mesoscopic inhomogeneities are seen from this aqueous TBA solution. One of the samples is then cold filtered, with the help of a recirculating pump by using 20 nm Anopore filter. Results from gas-chromatography experiments carried out in both

these samples are shown in Figure 3.12 a) and b), respectively. From this figure it is seen that cold filtration eliminates the trace impurities present in aqueous TBA solutions.

Figure 3.12 (see below). Gas chromatogram of a 0.073 mole fraction aqueous TBA solution before and after cold-filtration. It is seen from the following figures that cold filtration eliminates trace impurities present in TBA aqueous solution.

a.) Un-filtered sample

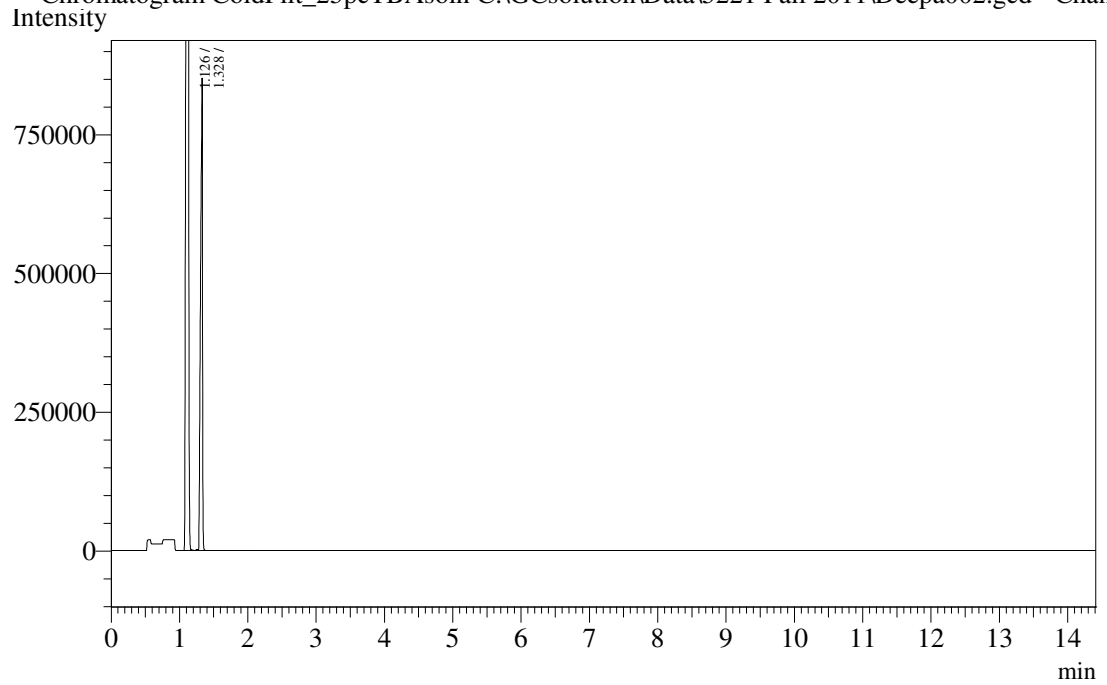


The area under the curve (values given below) is proportional to the composition of the components.

Peak Table - Channel 1

Peak#	Ret.Time	Area	Height	Name
1	1.126	3749051	1119877	
2	1.325	1380267	735582	
3	9.082	2076	263	
4	9.150	1183	313	
5	9.194	3026	351	
6	11.748	14008	987	
Total		5149611	1857373	

b.) After cold filtration



The area under the curve (values given below) is proportional to the composition of the components.

Peak Table - Channel 1

Peak#	Ret.Time	Area	Height	Name
1	1.126	3585470	1120272	
2	1.328	1672445	816250	
Total		5257915	1936522	

To characterize these mesoscale particles further, the 0.073 mole fraction TBA solution with 2 μL of PO is fast cooled (3 $^{\circ}\text{C}/\text{min}$) from 50 $^{\circ}\text{C}$ to 8.5 $^{\circ}\text{C}$, as compared to previous cooling rates of 5 $^{\circ}\text{C}/\text{hr}$. The sample is then left to “equilibrate” for about 24 hours. As seen in Figure 3.13, the correlation function is accurately fit to a single exponential, without any significant polydispersity. Moreover, the particle size obtained is much smaller (about 120 nm). The correlation function is monitored for about 2 weeks and no significant change of this size upon time is observed. This reflects the high stability of these particles.

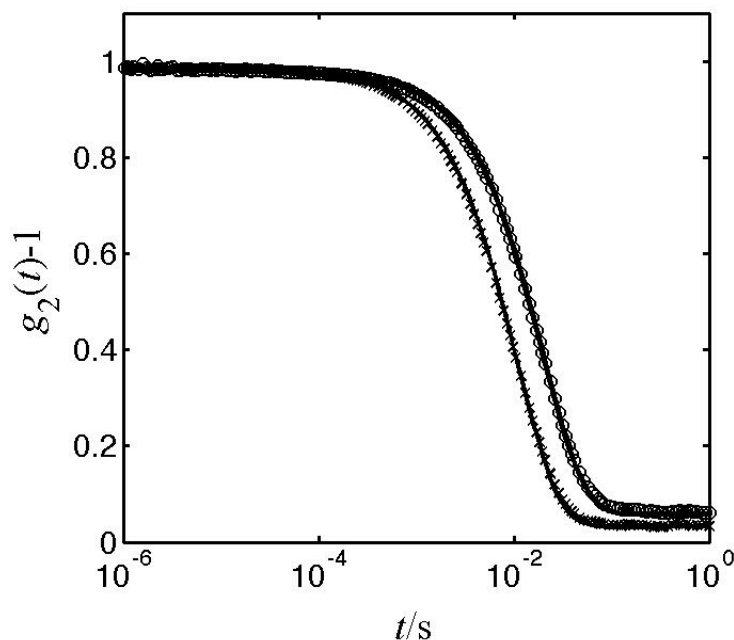


Figure 3.13. Time-dependent intensity auto-correlation function for a 0.073 mole fraction TBA aqueous solution, after cold filtering and doping 10^{-5} mole fraction of PO, at a scattering angle of 60° , $T = 8.5^{\circ}\text{C}$, and two different cooling rates. Open circles = 8.5 $^{\circ}\text{C}/\text{hr}$. Crosses = 3 $^{\circ}\text{C}/\text{min}$. The black curve represents fit of the data to a single exponentials [98].

Next, we investigated whether the observed mesoscopic inhomogeneities could be gaseous nanobubbles stabilized by adsorption of small organic molecules on the gas-liquid interface. Light-scattering experiments are carried out by forcefully injecting the clathrate-forming methane gas (commercial purity grade) in 10 mL of cold filtered 0.073 mole fraction TBA solution, for about 10 minutes, while maintaining the sample below 5°C. After injecting methane, it was observed that the intensity did not increase much. However, the intensity seemed to be oscillating irregularly, with occasional large spikes, two or three times greater in magnitude than the average intensity, as seen in Figure 3.14.

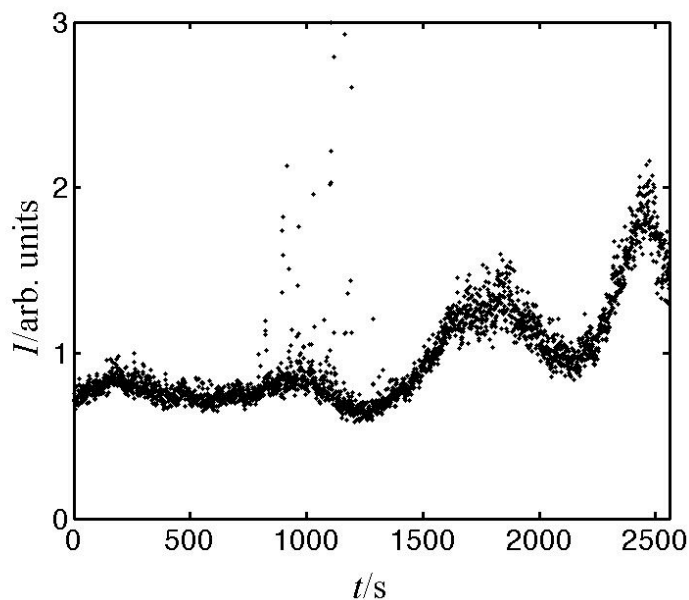


Figure 3.14. Light-scattering intensity for a 0.073 mole fraction TBA aqueous solution, after cold filtering and saturating with methane gas, at $\theta = 45^\circ$ and $T = 8.5^\circ\text{C}$.

The angular distribution of the intensity was highly asymmetric, showing large intensities at small angles ($\theta = 30^\circ$ and 45°). The dynamic correlation function is shown in Figure 3.15. The molecular diffusion mode in aqueous TBA solutions is detected. In addition, it is observed that the system is polydisperse, with various sizes ranging from about 70 nm to about 2500 nm detected by using the distribution analysis of the Photocor Software.

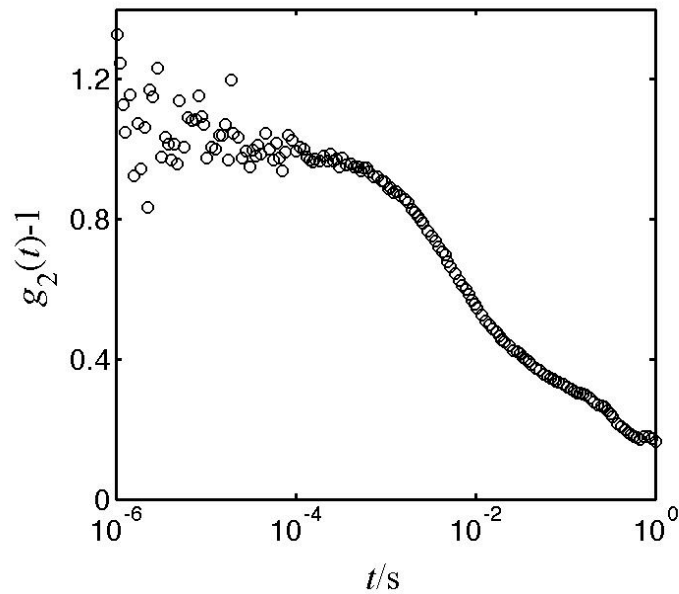


Figure 3.15. Time-dependent intensity auto-correlation function (open circles) for a 0.073 mole fraction TBA aqueous solution, after cold filtering and saturating with methane gas, at a scattering angle of 60° and $T = 8.5^\circ\text{C}$ [98].

From the above experiments, we answer an important question, namely, the origin of the mesoscale particles. We conclude that the mesoscopic inhomogeneities observed in aqueous TBA solutions are due to the presence of trace amounts of an impurity, such as PO. They are not an inherent part of binary TBA-water solution, because if it were so, then the particles should re-emerge after cold filtration of aqueous TBA solution, but this does not happen. It can be further confirmed that the observed inhomogeneities are genuine mesoscopic particles, not gaseous nanobubbles. It is possible to eliminate these particles by cold filtration and regenerate their formation by controlled addition of specific dopants. It is also possible to control the size and the polydispersity of these particles by controlling the rate of cooling.

To answer the next question, about the role of these particles in the thermodynamic stability of the system and to understand as to what is the nature of these inhomogeneities, a comprehensive study of the ternary system TBA-water-PO is carried out. In addition to TBA-water-PO system, analyses of isopropanol-water-PO, TBA-water-isobutanol, and TBA-water-cyclohexane systems have been carried out. The thermodynamic phase behavior and mesoscale characterization of these systems is discussed in the following chapter.

Chapter 4: Macro and mesophases of aqueous solutions of hydrotropes

As shown in the previous chapter, mesoscale inhomogeneities are observed in aqueous TBA solutions only in the presence of a third component. Based on this observation and on the discussion of the molecular properties of aqueous TBA solutions in Chapter 2, it can be inferred that TBA is a non-ionic hydrotrope, which shows short-ranged, short-lived micelle-like structural fluctuations in an aqueous medium, but forms mesoscopic aggregates upon the addition of a solubilizate.

Our next goal is to understand the role of these mesoscopic aggregates in the thermodynamic stability of the system. To answer this question, various ternary systems such as TBA-water-PO, isopropanol-water-PO, TBA-water-cyclohexane, and TBA-water-isobutanol systems have been studied. Phase behavior and results from light scattering are discussed below.

4.1 TBA-water-propylene oxide system

Before proceeding to the TBA-water-PO ternary system, we will first discuss each of the binary systems. The TBA-water binary system was discussed in Section 2.1 and the thermodynamic phase diagram at ambient pressure was shown in Figure 2.1. From this figure, it is seen that at ambient conditions TBA and water are completely miscible with each other. The other binary system PO-water has also been well studied in the literature [99]. The PO-water phase diagram at ambient pressure is shown in Figure 4.1. It is seen from this figure that PO exhibits a miscibility gap with

water under ambient conditions. This miscibility gap depends weakly on temperature. Experiments on the third binary system, namely TBA-PO, carried out in this work, show that this system is completely miscible under ambient conditions.

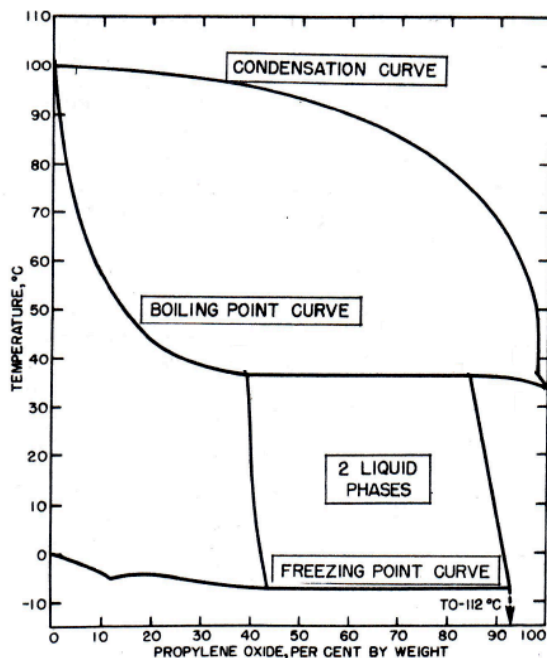


Figure 4.1. Thermodynamic phase diagram of propylene oxide – water binary system at ambient pressure. (Taken from [94].)

The thermodynamic phase diagram of the ternary system TBA-water-PO is then investigated and shown in Figure 4.2. TBA, with purity > 0.998 mass fraction, procured from Alfa Aesar; PO, with purity > 0.995 mass fraction, procured from Sigma Aldrich; and Millipore water are used for these experiments. The procedure to develop the phase diagram is adapted from ref. [100]. Various samples of PO-water, whose compositions lie within the miscibility gap, are prepared and incremental amounts of TBA are added to it until the macroscopic one-phase region is observed.

The accuracy of temperature of the thermostatic bath used to observe the phase separation in TBA-water-PO system was about ± 0.3 °C.

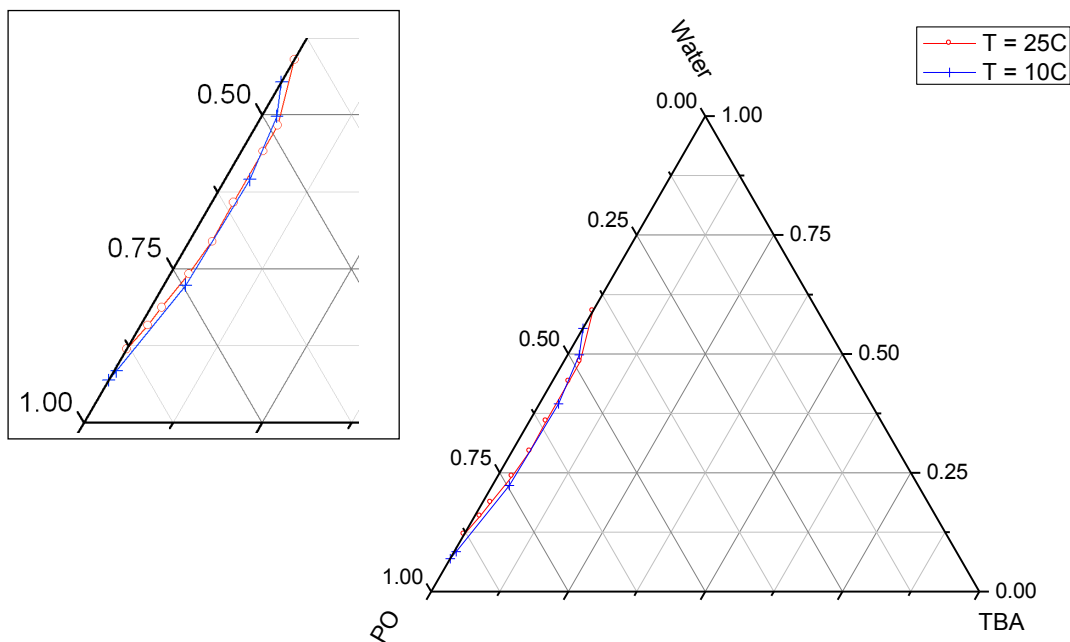


Figure 4.2. Thermodynamic phase diagram of tertiary butyl alcohol – water – propylene oxide ternary system at $T = 25$ °C and $T = 10$ °C, and at ambient pressure.

The phase diagram (also known as mutual solubility curves, equilibrium curves, or binodal) for the ternary system, TBA-water-PO, at 25 °C and 10 °C is shown in Figure 4.2. The region inside the binodal curves is the two-phase region, while the region outside it is the one-phase region. As seen from this figure, the mutual solubility curves are weakly dependent on temperature within the range of temperatures studied, similar to the PO-water binary system [97]. It is also seen that

the binodal curve is almost flat, making it quite difficult to accurately locate the critical point of this system.

To understand the role of the mesoscopic inhomogeneities in the thermodynamic stability of the system, the entire ternary system is studied by light scattering. Analyses of static light-scattering intensity are carried out across various samples and the part of the ternary system where strong mesoscopic inhomogeneities are observed is shown in Figure 4.3. The light-scattering intensity in this region is at least an order of magnitude higher than the intensity observed for the corresponding binary systems. In addition, the dynamic auto-correlation functions for samples within this region show the presence of a slow relaxation mode, corresponding to mesoscopic inhomogeneities or “particles” having a hydrodynamic radius of about 200 nm. We interpret this region as a micro-emulsion-like phase or micro phase separation.

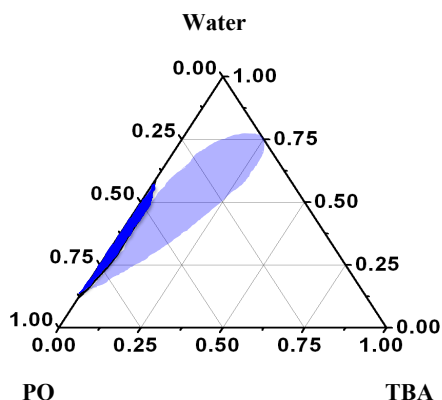


Figure 4.3. Composition of micro-emulsion-like phase in TBA-water-PO ternary system at $T = 25\text{ }^{\circ}\text{C}$, as characterized by static light scattering at a scattering angle 45 ° . Light blue = micro-emulsion-like region. Dark blue = Macroscopic two-phase region.

To characterize the behavior of this region in more detail, static and dynamic light-scattering analyses of many samples are carried out. The compositions of four characteristic samples are shown in Figure 4.4. Each of the samples is prepared by first cold filtering the aqueous TBA solution, by repeated filtrations with 20 nm Anopore filter, so as to remove all existing mesoscopic inhomogeneities, and then adding (unfiltered) PO to it. Since PO is extremely volatile, samples are always prepared under cold conditions. The samples are let to “equilibrate” for at least 4 hours and light-scattering readings are then taken within a few hours (less than 48) of their preparation.

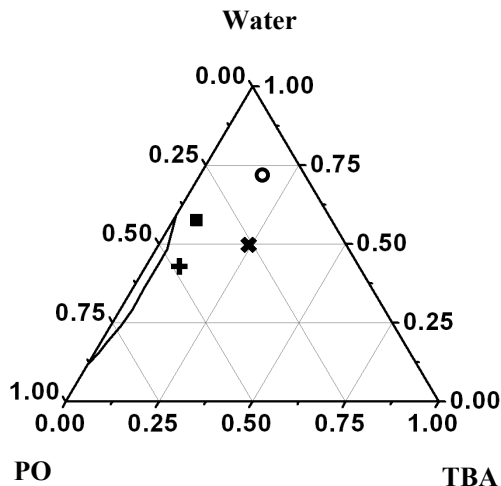


Figure 4.4. Representation of characteristic samples studied in the TBA –water –PO system on the ternary phase diagram. Compositions in mass fractions are : Open circles = 0.12 PO, 0.20 TBA; Crosses = 0.26 PO, 0.25 TBA; Filled squares = 0.38 PO, 0.05 TBA; Pluses = 0.48 PO, 0.08 TBA.

Samples within this micro-emulsion-like phase are studied at two different temperatures, 25 °C and 10 °C, and at various scattering angles ranging from 30° to 150°. The dynamic auto-correlation functions for four characteristic samples at $T = 10$ °C and $\theta = 45^\circ$ are shown in Figure 4.5. Each of these correlation functions is fit with a single exponential, as discussed earlier in Eq. 3.1. The relaxation times (at $\theta = 45^\circ$), are about a few milliseconds. They correspond to “particles” with a hydrodynamic radius of about 200 nm. The refractive-index data needed to determine the wave number is measured with an Abbe refractometer. The kinematic viscosity of these samples is measured with an Ubbelohde viscometer purchased from Cannon instruments. The dynamic viscosity needed to determine the hydrodynamic radius is then calculated from the kinematic viscosity and the average molar density. The compositions, refractive indices, viscosities, relaxation times (at scattering angle 45°), and the corresponding hydrodynamic radii are displayed in Tables 4.1 and 4.2. From Table 4.2, it is clear that for various compositions of the ternary system, the “size” of the inhomogeneities is not strongly dependent on the composition of the constituents. However, as discussed in Section 3.4, the “size” may depend on the method of sample preparation, such as rate of cooling.

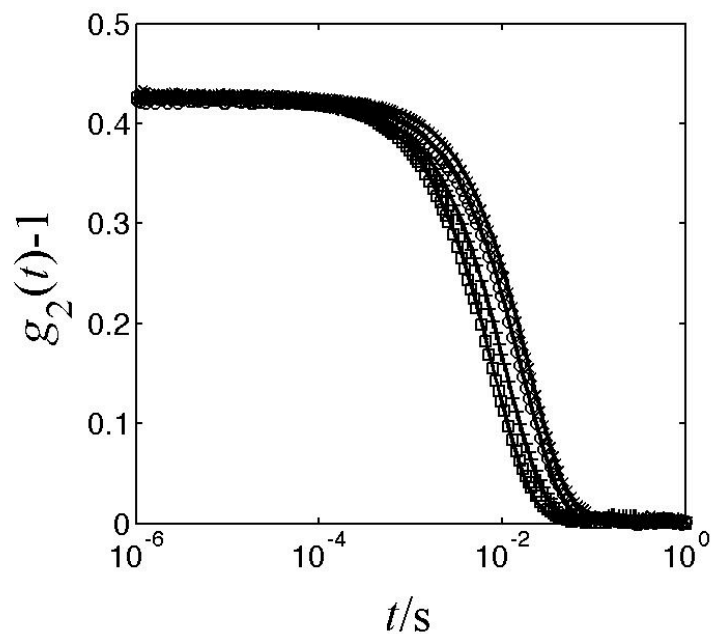


Figure 4.5. Time-dependent intensity auto-correlation functions of four characteristic TBA-water-PO samples at $T = 10\text{ }^{\circ}\text{C}$ and at a scattering angle $\theta = 45^{\circ}$. The compositions of the four samples correspond to the ones shown in Figure 4.4. Open circles = 0.12 PO, 0.20 TBA; Crosses = 0.26 PO, 0.25 TBA; Filled squares = 0.0.38 PO, 0.05 TBA; Pluses = 0.48 PO, 0.08 TBA. The black curves are a fit to single exponential decays.

Table 4.1. Compositions (in mass fraction and mole fractions), refractive indices, and viscosities of samples analyzed by light scattering in TBA-water-PO ternary system

#	TBA (mass fr.)	Water (mass fr.)	PO (mass fr.)		TBA (mole fr.)	Water (mole fr.)	PO (mole fr.)
A1	0.20	0.68	0.12		0.06	0.89	0.05
A2	0.25	0.49	0.26		0.10	0.78	0.13
A3	0.05	0.57	0.38		0.02	0.81	0.17
A4	0.08	0.44	0.48		0.03	0.72	0.25

#	R.I.	Kinematic viscosity at 25 °C ($\times 10^{-6} \text{ m}^2/\text{s}$)	Kinematic viscosity at 10 °C ($\times 10^{-6} \text{ m}^2/\text{s}$)
A1	1.3593	2.330	3.965
A2	1.3649	2.286	3.696
A3	1.3601	1.529	2.314
A4	1.3635	1.394	2.022

Table 4.2. Relaxation times (at scattering angle 45°) and corresponding hydrodynamic radii for various samples in TBA-water-PO ternary system at $T = 10^\circ\text{C}$.

#	Relaxation times (ms)	Hydrodynamic radius (nm)
A1	31.9	192
A2	38.3	256
A3	15.5	162
A4	21.0	257

The wave-number dependence (q^2 dependence) of the rate of relaxation of fluctuations is investigated next. Figure 4.6 shows the q^2 dependence of the decay rate, at 10°C , for sample # A4. Fit of Eq. 3.3 for these data shows that at small angles (low- q) the system exhibits diffusive behavior. However, at larger angles (larger- q), the rate does not follow the q^2 dependence in accordance with Eq. 3.3.

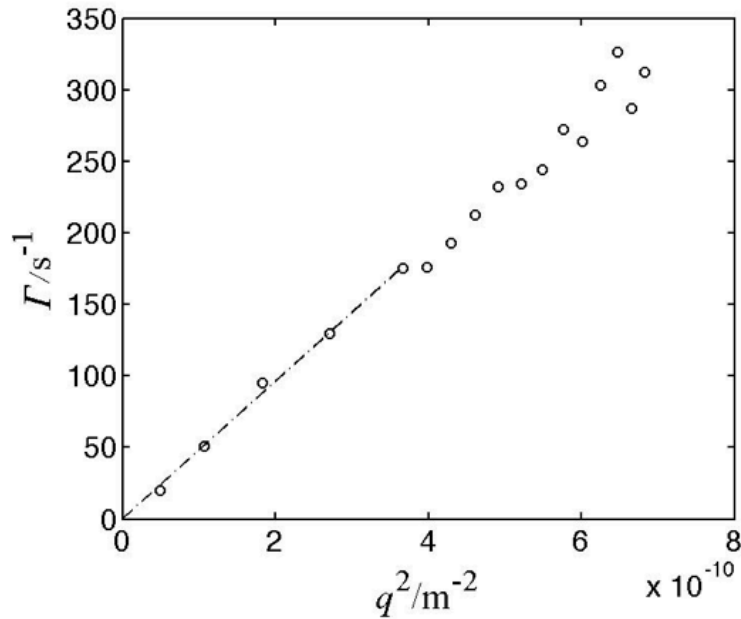


Figure 4.6 Wave-number dependence of relaxation rate of TBA – water-PO sample at $T = 10\text{ }^\circ\text{C}$. The composition of the sample is 0.48 mass fraction PO, 0.08 mass fraction TBA. The dashed black line is fit to Eq. 3.3.

Figure 4.7 shows the wave-number dependence of the inverse intensity (normalized to the light-scattering intensity at scattering angle 90°), at $10\text{ }^\circ\text{C}$, for sample A4. It is seen that the inverse intensity does not follow a linear q^2 dependence, as it would be expected for a dilute solution of non-interacting Brownian submicron particles [93]. On comparing the light-scattering intensities of the various samples shown in Table 4.1, it is seen that as the amount of PO increases the intensity of the sample increases, but seems nearly independent of the TBA concentration.

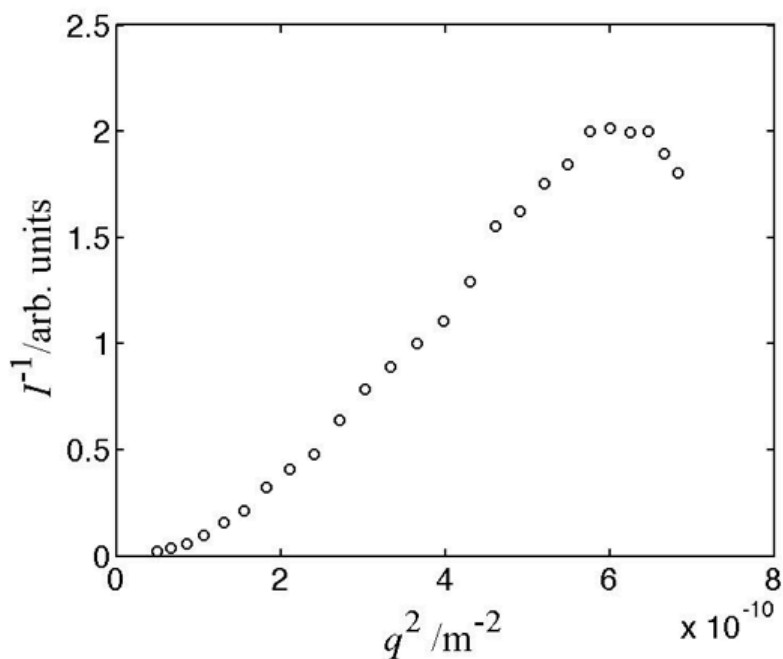


Figure 4.7. Wave-number dependence of inverse intensity of TBA – water-PO sample at $T = 10\text{ }^{\circ}\text{C}$. The composition of the sample is 0.48 mass fraction PO, 0.08 mass fraction TBA.

Intensity auto-correlation functions are determined at $25\text{ }^{\circ}\text{C}$ and $10\text{ }^{\circ}\text{C}$, shown in Figure 4.8, to study the effect of temperature on the micro-emulsion-like phase. Analyses of q^2 dependence of the decay rate and q^2 dependence of the inverse intensity for samples at $25\text{ }^{\circ}\text{C}$ show a trend similar to what is observed at $10\text{ }^{\circ}\text{C}$, although the values of the static light-scattering intensity are lower at $25\text{ }^{\circ}\text{C}$ as compared to those at $10\text{ }^{\circ}\text{C}$.

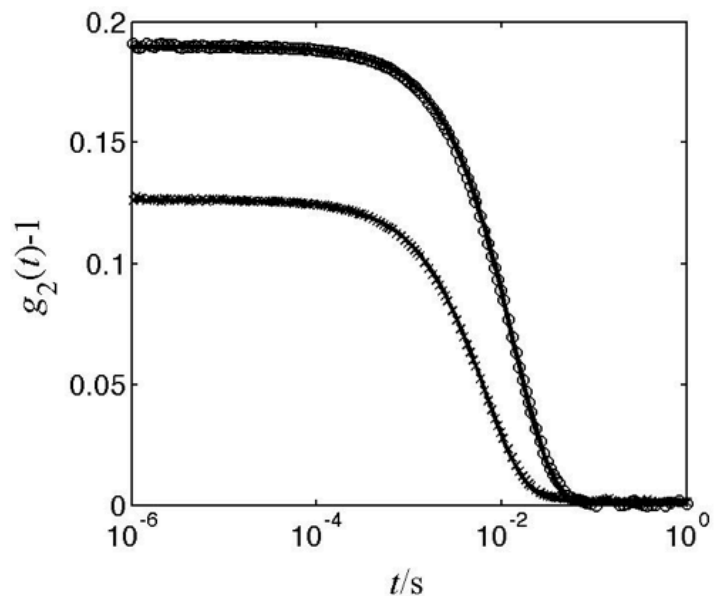


Figure 4.8. Effect of temperature on the properties of micro-emulsion-like phase in a TBA-water-PO sample. The composition of the sample is 0.48 mass fraction PO, 0.08 mass fraction TBA. Circles = 10 °C; Crosses = 25 °C.

In order to determine the stability of these inhomogeneities, two characteristic samples are monitored over time. The compositions of these samples are shown in Table 4.3 and they are displayed in the phase diagram shown in Figure 4.9 (a). Both of these samples are prepared from the same source of PO, but the TBA is from different bottles. Although both the TBA bottles have a stated purity of > 0.998 mass fraction and are procured from Alfa Aesar company, the TBA used for the first sample (# A5) shows the presence of inhomogeneities, while the TBA used for the second sample (# A6) does not show the presence of any inhomogeneities. As discussed earlier, the observation of these inhomogeneities in aqueous TBA solutions depends on the source of the solutes and is triggered by trace amounts of an impurity

in TBA, so it seems that the TBA used to prepare #A5 contains some unknown impurities, while the TBA used to prepare #A6 does not contain any detectable impurities. This agrees well with observations and results presented earlier in Chapter 3.

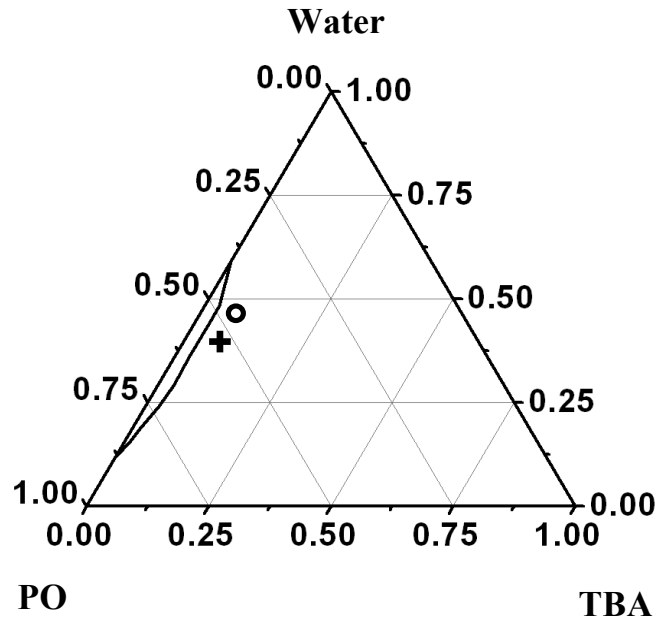


Figure 4.9. a) Representation of characteristic samples in TBA-water-PO system to determine its kinetic behavior.

For Figures 4.9 a), b), and c), the compositions in mass fractions are:

Open circle (sample # A5 from Table 4.3) = 0.04 TBA, 0.53 PO at $T = 10\text{ }^{\circ}\text{C}$;

Cross (sample # A6 from Table 4.3) = 0.04 TBA, 0.48 PO at $T = 25\text{ }^{\circ}\text{C}$.

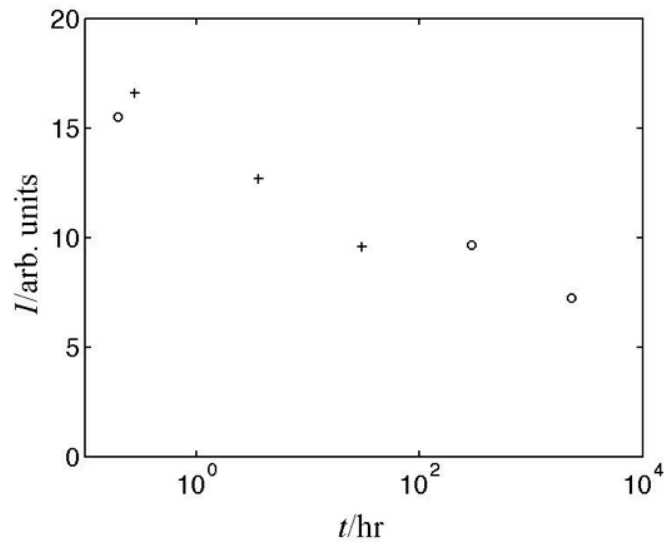


Figure 4.9. b) Kinetic behavior of light-scattering intensity in TBA-water-PO samples, at $\theta = 45^\circ$.

Open circles (sample # A5) at $T = 10^\circ\text{C}$; Crosses (sample # A6) = at $T = 25^\circ\text{C}$.

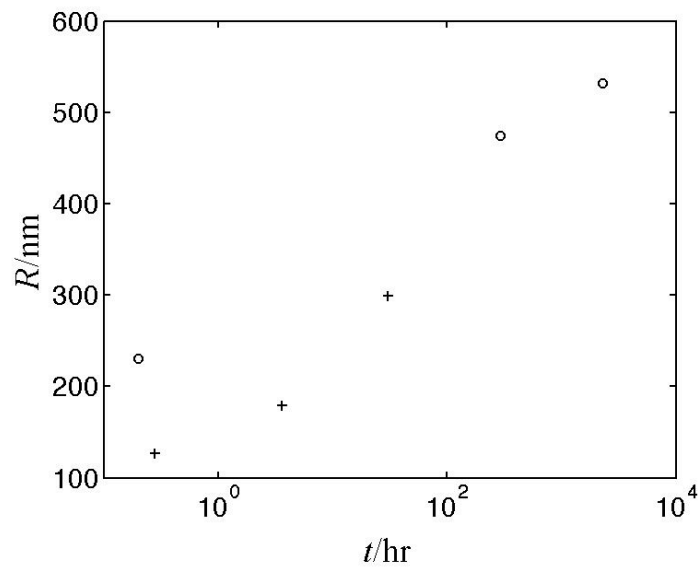


Figure 4.9. c) Kinetic behavior of hydrodynamic radius in TBA-water-PO samples, at $\theta = 45^\circ$.

Open circles (sample # A5) at $T = 10^\circ\text{C}$; Crosses (sample # A6) = at $T = 25^\circ\text{C}$.

Table 4.3. Compositions of TBA-water-PO samples, whose kinetic stability has been analyzed.

#	TBA	Water	PO	Comments
A5	Mass fr. = 0.04 Mole fr. = 0.02	Mass fr. = 0.43 Mole fr. = 0.71	Mass fr. = 0.53 Mole fr. = 0.27	Commercial TBA shows presence of mesoscopic inhomogeneities in aqueous solution
A6	Mass fr. = 0.04 Mole fr. = 0.02	Mass fr. = 0.48 Mole fr. = 0.75	Mass fr. = 0.48 Mole fr. = 0.23	Commercial TBA DOES NOT show presence of mesoscopic inhomogeneities in aqueous solution

To study the effect of adding a controlled impurity, namely PO, the aqueous TBA solutions are always cold-filtered multiple times by using a 20 nm Anopore filter, to remove all existing mesoscopic inhomogeneities. However, it is impossible to remove 100 % of the inhomogeneities by cold filtration. As a result, some inhomogeneities, originating from impurities present in TBA, may still be present in cold-filtered aqueous TBA solutions. These inhomogeneities come to the forefront when PO is added to this system. Long-time monitoring of these samples, shows that the mesoscopic inhomogeneities in the sample prepared from “dirty” TBA (# A5) become weaker within a few months, while mesoscopic inhomogeneities in the

sample prepared from “new clean” TBA (# A6) almost disappear within a month. The trends in the light-scattering data are such that the light-scattering intensity decreases over time, as seen in Figure 4.9 (b) and the “size” of the inhomogeneities increases over time, as seen from Figure 4.9 (c). It is also observed that the intensity auto-correlation function develops a “tail”, which corresponds to “spikes” in the intensity, maybe due to larger ($> 10 \mu\text{m}$) aggregates as discussed by Kostko *et al.* [54].

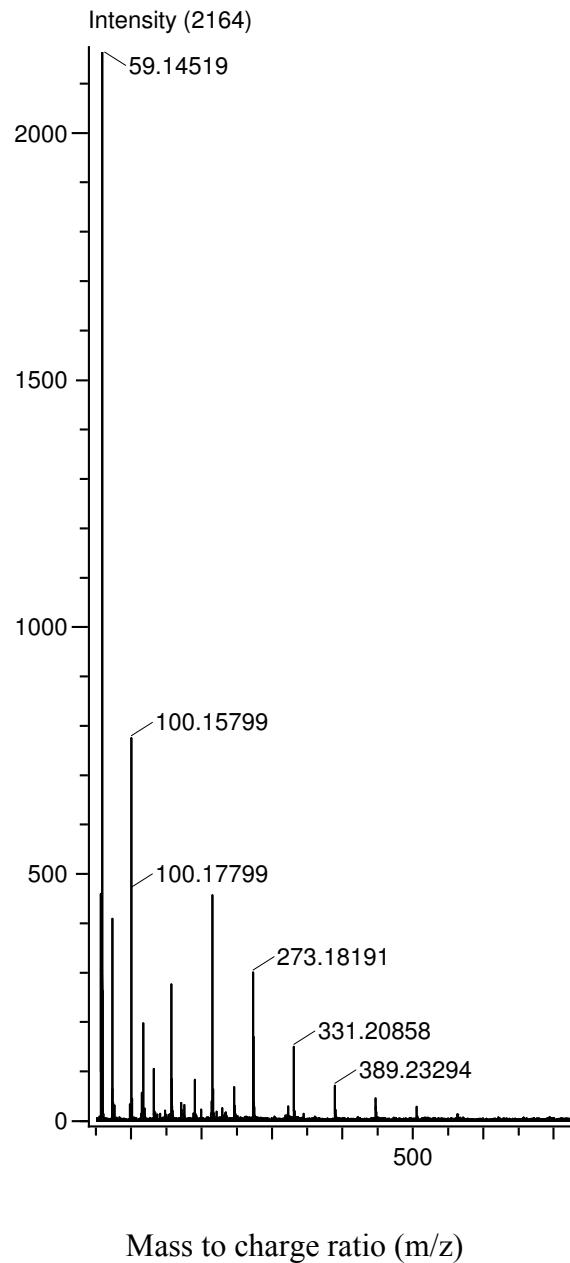
The last experiment shows that there are two events occurring in TBA-water-PO solutions. The first event is the presence of mesoscopic inhomogeneities in aqueous TBA solutions, which are triggered by trace amounts of a third component. The second event is due to some specific interactions between TBA, water, and PO, which lead to slow kinetics of solubilization. This may explain the reason why in “new clean” TBA solutions, the ternary system shows initial strong scattering from mesoscopic inhomogeneities, but then this scattering virtually disappears within a month. Additionally, concentration fluctuations, which diverge close to the critical point, may also play a role in the slow kinetics.

Another feature with aqueous solutions containing PO is the possibility of polymerization of PO to polypropylene oxide (PPO) in aqueous media. To investigate this possibility, mass spectrometry experiments are carried out in samples containing various amounts of PO. Mass spectrometry experiments in pure PO and TBA-water-PO systems (source of TBA was the “dirty” TBA as used for experiments described above) were carried out. Mass spectrometry results are shown in Figure 4.10. From this figure, it is seen that PO polymerizes to form oligomers of dimers, trimers, or tetramers, with peaks at a repeating distance of $\sim 58 \text{ m/z}$ (molecular weight of PO).

However, no large molecular weight polymer, up to 80,000 m/z (mass to charge ratio) of polymer, is observed. The oligomers of PO alone are too small to cause strong light scattering.

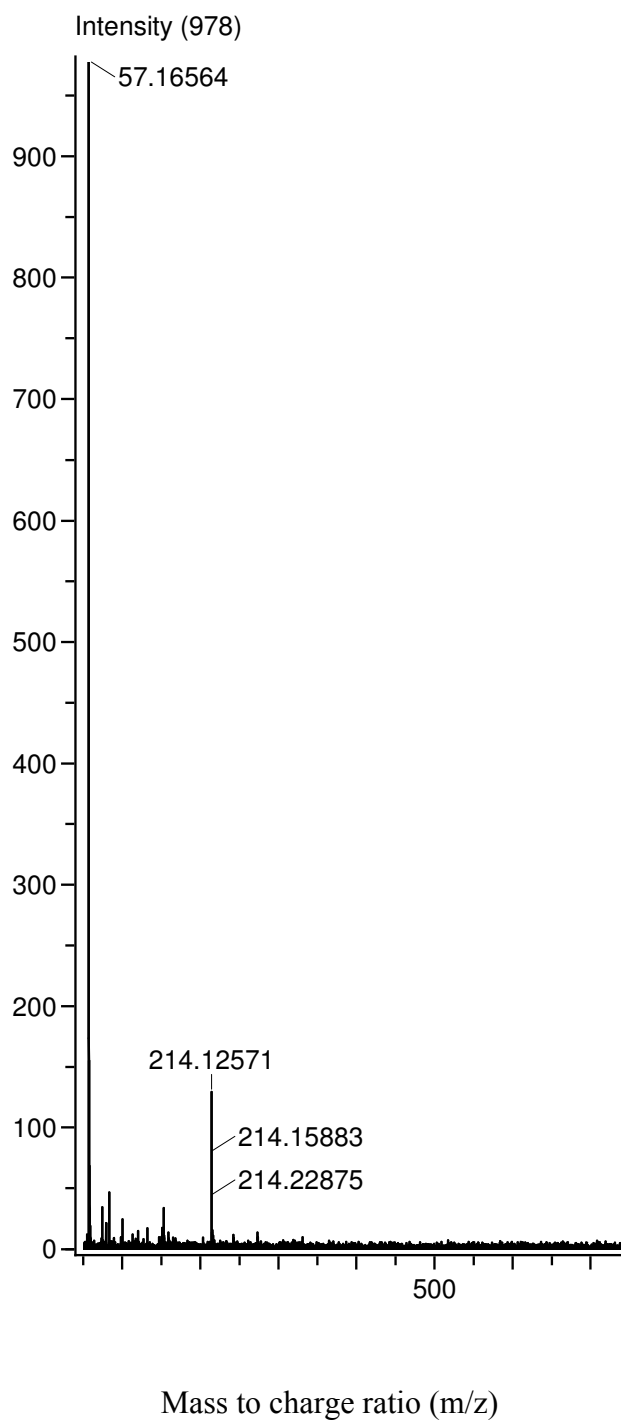
Figure 4.10 (see below) Results from mass spectrometer

a) Pure PO system

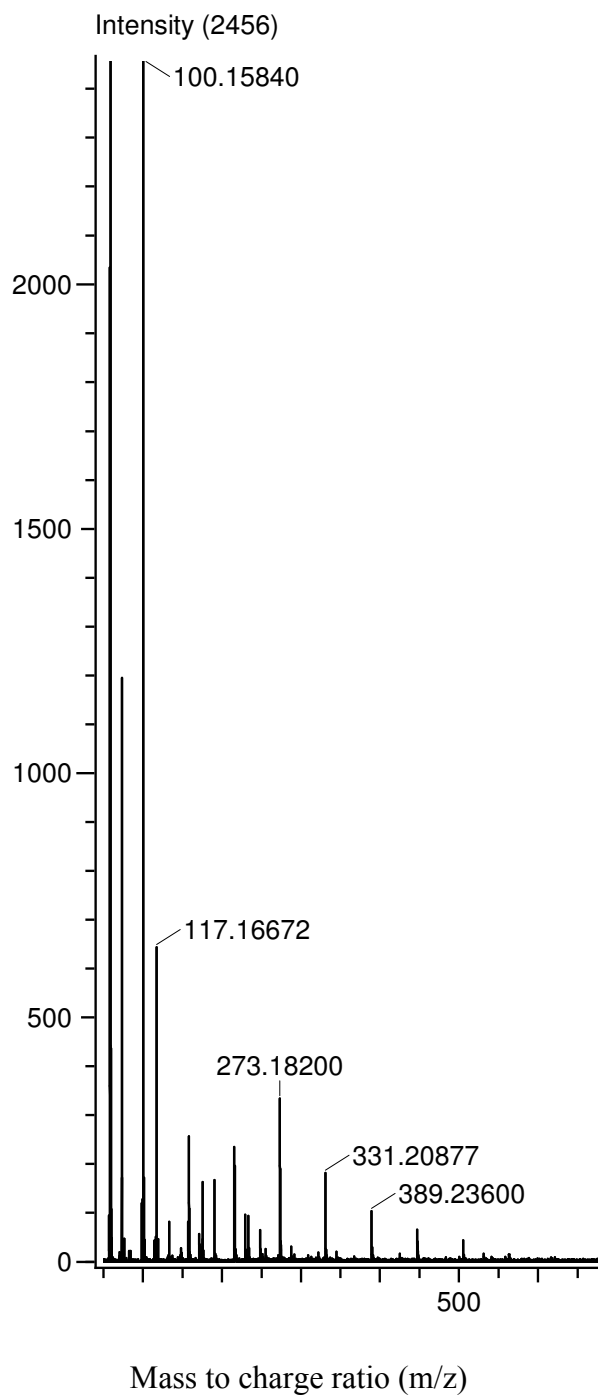


b) TBA-water-PO ternary system.

Mass fractions: TBA = 0.25, PO = 0.01



c) TBA-water-PO ternary system. Mass fractions: TBA = 0.25, PO = 0.12



In order to further understand the nature of the mesoscopic inhomogeneities, another ternary system with PO, namely isopropanol-water-PO is investigated. A static light-scattering study of this ternary system revealed also the presence of a micro-emulsion-like phase; however, not as pronounced as in TBA-water-PO systems.

In the next section, the behavior of other “impurities” in aqueous TBA solutions is discussed.

4.2 TBA-water-cyclohexane ternary system

Species in binary systems TBA-water (as shown in the phase diagram of Figure 2.1 [22]) and TBA-cyclohexane (as determined in this work) are completely miscible at ambient conditions. However, cyclohexane and water are almost completely immiscible under ambient conditions [101].

A part of the thermodynamic phase diagram of the ternary system TBA-water-cyclohexane is determined at $\sim 21^\circ\text{C}$ and shown in Figure 4.11. TBA, with purity > 0.998 mass fraction, procured from Alfa Aesar; cyclohexane, with purity > 0.990 mass fraction, procured from E. M. Science (a division of Merck); and Millipore water are used for these experiments. Various samples of TBA-cyclohexane are prepared and incremental amounts of water are added to it until phase separation or droplet formation is seen. The accuracy of the temperature of the thermostatic bath used to measure this phase diagram is about $\pm 0.5^\circ\text{C}$.

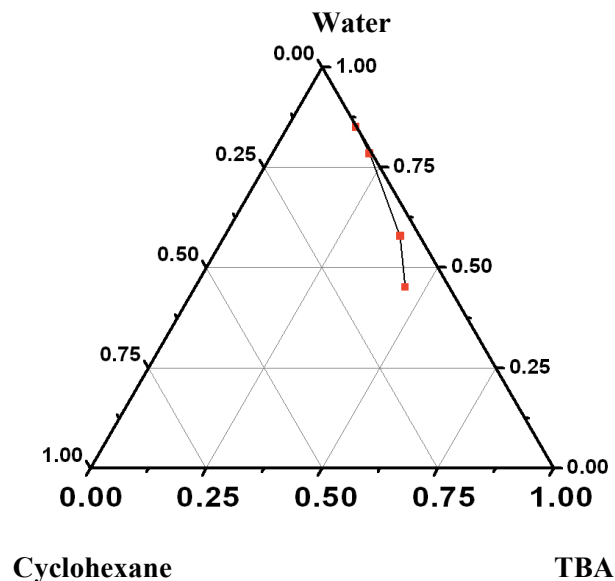


Figure 4.11. Phase diagram of TBA-water-cyclohexane system at ambient conditions,
 $T \sim 21\text{ }^{\circ}\text{C}$.

The TBA-water-cyclohexane phase behavior is similar to that of the TBA-water-PO system, discussed in Section 4.1; however, the miscibility gap in this system is much larger. In addition, cyclohexane is completely immiscible with water, as opposed to PO, which shows significant partial miscibility with water. This makes cyclohexane, an almost perfect solubilizate, whose “solubility” in aqueous phase gets enhanced on the addition of non-ionic hydrotrope TBA.

Light-scattering analyses of certain characteristic ternary samples in the one-phase region of the ternary system are carried out. The compositions of some of the samples studied are listed in Table 4.4.

Table 4.4. Compositions of TBA-water-cyclohexane system as studied by light scattering

#	TBA	Water	CHX	TBA	Water	CHX
	Mass %			Mole %		
B1	25.70 %	74.20 %	0.11 %	7.80 %	92.12 %	0.03 %
B2	25.90 %	74.00 %	0.10 %	7.87 %	92.10 %	0.03 %

As discussed previously, the addition of 2 μL of cyclohexane to 10 mL of cold-filtered aqueous TBA solution led to cyclohexane phase separating from the solution. Thus a certain change in the procedure of sample preparation is adopted for the light-scattering experiments in the TBA-water-cyclohexane ternary system. The samples prepared for the light-scattering study of this ternary system is from the “new clean” TBA, purity > 0.998 mass fraction, procured from Alfa Aesar. Cyclohexane and TBA, each filtered separately with 200 nm Nylon filters, are first thoroughly mixed and then Millipore water, also filtered with 200 nm Nylon filters, is added. The ternary system is then mixed thoroughly and the sample is let to “equilibrate”.

The intensity auto-correlation function of sample # B1 from Table 4.4, measured after 24 hours of preparation, at $T = 25\text{ }^{\circ}\text{C}$ and $\theta = 45^{\circ}$, is shown in Figure 4.12. Figure 4.12 shows the presence of two relaxation modes - a fast mode, with a relaxation time of $\sim 50\text{ }\mu\text{s}$ (at $\theta = 45^{\circ}$) and a slow mode with a relaxation time of $\sim 20\text{ ms}$ (at $\theta = 45^{\circ}$). In addition it also shows a (non-exponential) “tail” of long-time relaxation processes, which could be due to presence of few large-size ($> 10\text{ }\mu\text{m}$) inhomogeneities in the system. This correlation function is very similar to the

correlation function seen in Figure 3.2, for aqueous “dirty” TBA solutions, as discussed in Chapter 3.

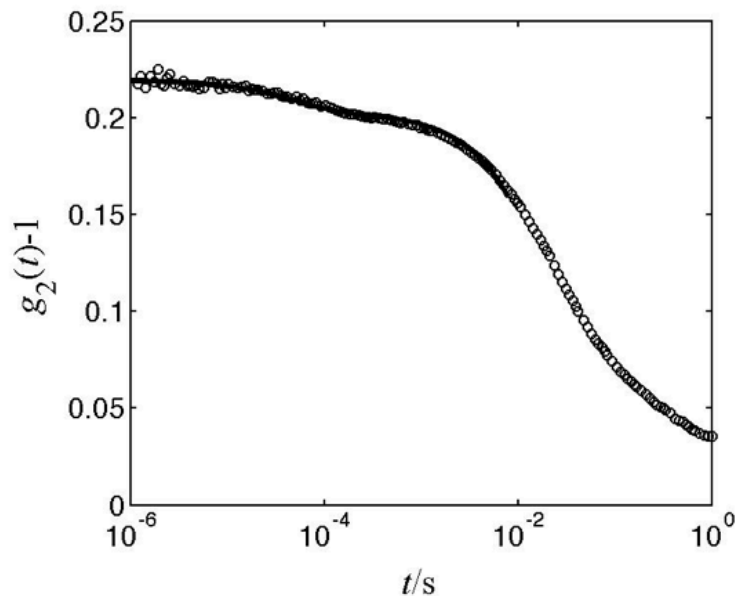


Figure 4.12. Intensity auto-correlation function from a characteristic sample of TBA-water-cyclohexane ternary system, at $T = 25$ °C and $\theta = 45^\circ$. The black line is a fit to two-exponential decay, as shown in Eq. 3.2.

In order to understand the time evolution of the mesoscopic inhomogeneities, samples # B1 and # B2 are compared within a few hours of preparation and after a few days of preparation. Both these samples are identical in composition (as seen in Table 4.4), prepared by using the same source of TBA and cyclohexane, and by using the procedure described above. The dynamic auto-correlation function for sample # S1, determined at $T = 25$ °C and $\theta = 45^\circ$, obtained from a “freshly” prepared sample is shown in Figure 4.12. As discussed above, this sample shows the presence of mesoscopic inhomogeneities soon after preparation. On the other hand, mesoscopic

inhomogeneities are not seen in sample # S2 soon after preparation, but are seen only after a few days of preparation. Thus we conclude that kinetics or presence of local energy barriers, not fully understood, plays an important role in the observation of mesoscopic inhomogeneities - sometimes the inhomogeneities appear instantly after sample preparation, as for sample # B1, while sometimes they appear only after few days of sample preparation, as for sample # B2. One additional sample, with composition same as for sample # B2 was prepared and analyzed. This sample showed the presence of mesoscopic inhomogeneities similar to sample # B1, thus reinforcing the presence of local energy barriers in the formation of these inhomogeneities.

The q^2 dependence of the rate of relaxation of fluctuations at 25 °C, for sample # B1, is shown in Figure 4.13. From this figure, it is seen that a simple fit of Eq. 3.3 for these data shows that at small angles (low q) the system exhibits diffusive behavior. However, at larger angles (larger q), the rate does not follow the q^2 dependence as given by Eq. 3.3.

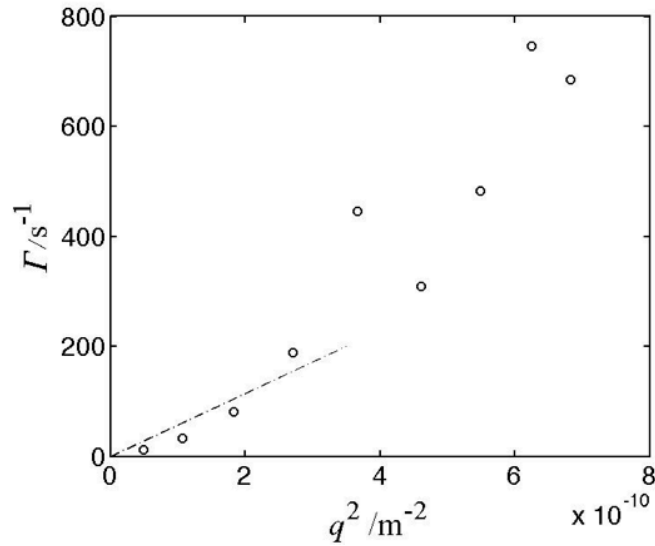


Figure 4.13. Wave-number dependence of relaxation rate of TBA – water-cyclohexane sample at $T = 25 \text{ }^\circ\text{C}$. The composition of the sample is 0.0011 mass fraction cyclohexane, 0.257 mass fraction TBA. The dashed black line is fit to Eq. 3.3.

The average hydrodynamic radius corresponding to these inhomogeneities is calculated by using Eqs. 3.3 and 3.4. The angular dependence of this “size” is shown in Figure 4.14. From this figure, it is seen that the system is highly polydisperse with larger inhomogeneities seen at smaller angles.

The wave-number dependence of the inverse light-scattering intensity (normalized to the light-scattering intensity at angle 90°), at $25 \text{ }^\circ\text{C}$, for sample # B1, is shown in Figure 4.15. It is seen that the intensity exhibits a strong asymmetry and the inverse intensity does not follow a linear q^2 dependence.

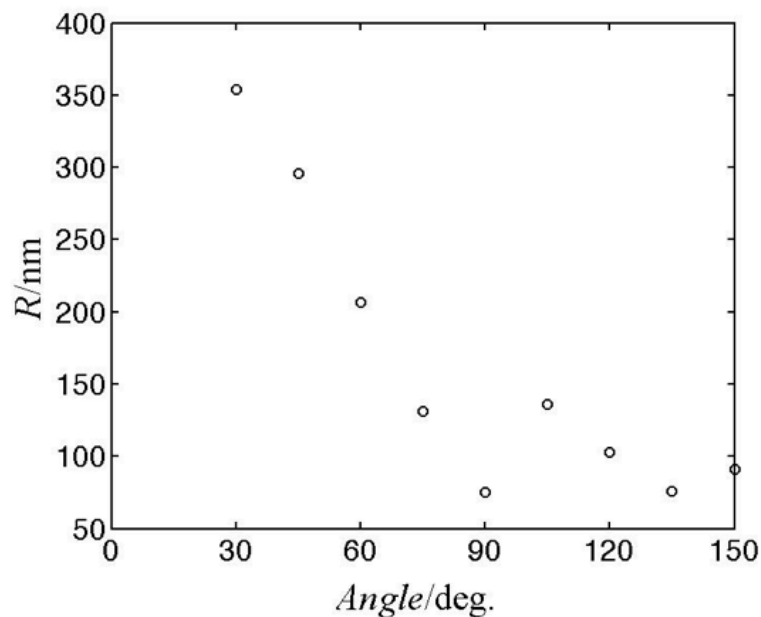


Figure 4.14. Angular dependence of the hydrodynamic radius of TBA – water-cyclohexane sample at $T = 25$ °C. The composition of the sample is 0.0011 mass fraction cyclohexane, 0.257 mass fraction TBA.

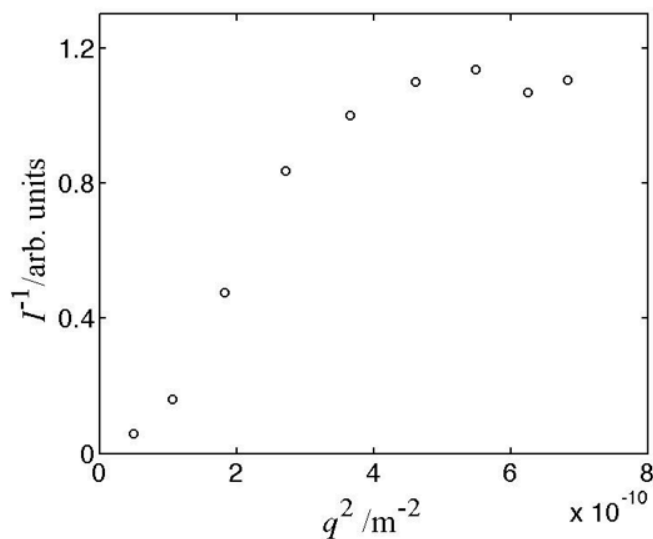


Figure 4.15. Wave-number dependence of inverse intensity of TBA – water-cyclohexane sample at $T = 25$ °C. The composition of the sample is 0.0011 mass fraction cyclohexane, 0.257 mass fraction TBA.

The refractive indices and viscosities used for the above investigation were taken from the literature for aqueous TBA solutions [87-89].

The micro-emulsion-like phase of the one-phase region is then studied to determine the effect of temperature. Sample # B2 is heated from 25 °C to 50 °C and then cooled from 50 °C to 10 °C and then warmed up again to 25 °C. On heating it is observed that the light-scattering intensity decreased; however, on cooling down to temperatures below room temperature, the light-scattering intensity increased significantly. The intensity auto-correlation functions for sample # B2, at 25°C (initial), 50°C, and 10°C, are shown in Figure 4.16. The corresponding average “size” of the inhomogeneities remains almost independent of temperature, while the “number” of inhomogeneities decreases with an increase of temperature, as evidenced by the light-scattering intensity. Thus the inhomogeneities seem to be favored at low temperature. This is again consistent with what was observed and discussed in Chapter 3.

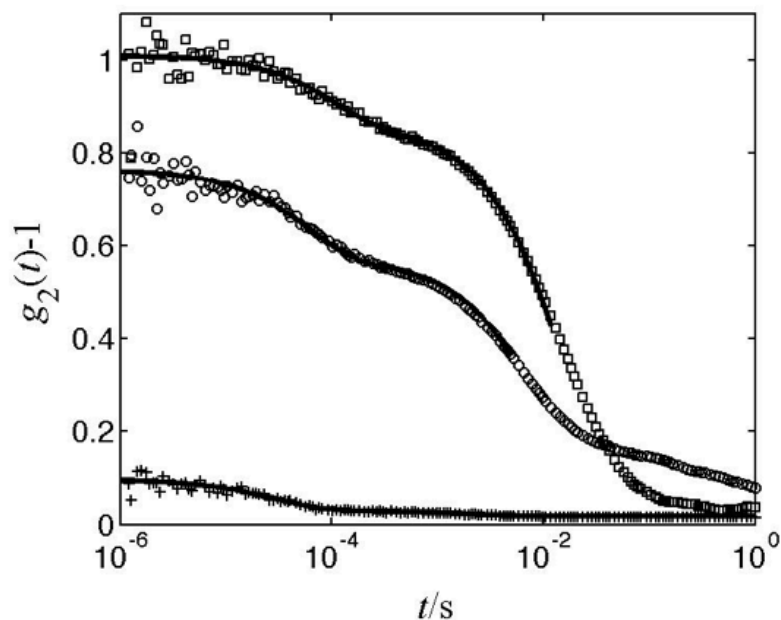


Figure 4.16. Intensity autocorrelation functions for TBA – water- cyclohexane system at $\theta = 45^\circ$, at three different temperatures. The composition of the sample is 0.001 mass fraction cyclohexane, 0.259 mass fraction TBA. Crosses: $T = 10^\circ\text{C}$; Open circles: $T = 25^\circ\text{C}$; Open squares: $T = 50^\circ\text{C}$. The continuous lines are fits to two-exponential decays as given by Eqs. 3.2.

Cold filtration of the ternary sample containing cyclohexane is also carried out. The intensity auto-correlation functions before and after cold-filtration are shown in Figure 4.17. It is seen that after cold filtration, the slow mode corresponding to mesoscale inhomogeneities is completely eliminated and does not re-appear when monitored for about 1 week.

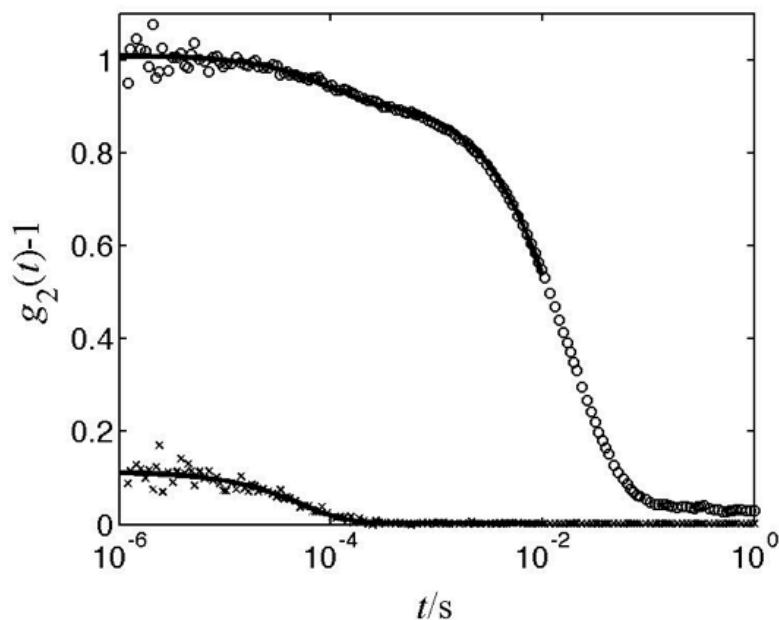


Figure 4.17. Intensity auto-correlation functions for TBA – water- cyclohexane system at $\theta = 45^\circ$, before (open circles) and after (crosses) cold filtration. The composition of the sample is 0.001 mass fraction cyclohexane, 0.259 mass fraction TBA. The continuous lines are fits to two-exponential and single exponential decays as given by Eqs. 3.1 and 3.2, respectively.

To better understand the nature of the inhomogeneities in the micro-emulsion-like phase of the ternary system, a comparison with the inhomogeneities in the two-phase region is carried out. A characteristic sample in the two-phase region, whose composition (in mass fractions) is TBA=0.13, cyclohexane=0.29, is prepared and let to “equilibrate” for about 2 days. Each of the two layers is studied by light scattering and the correlation functions are shown in Figure 4.18. It is seen that the water-rich region shows a correlation function with a mesoscopic mode, while the correlation function from the organic-rich layer shows no mesoscopic mode. Thus it can be

concluded that the inhomogeneities prefer the aqueous-rich phase to the organic-rich phase.

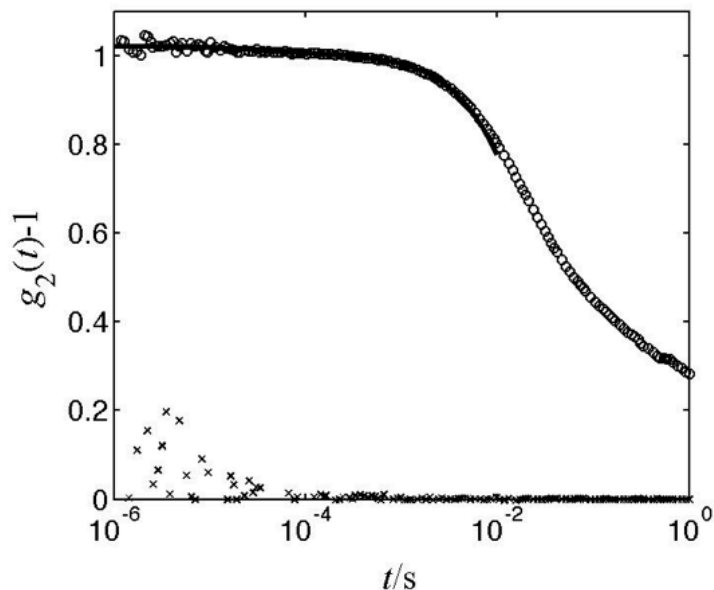


Figure 4.18. Intensity auto-correlation functions from aqueous (open circles) and organic (crosses) layers of a TBA – water- cyclohexane sample in the two-phase region. $T = 25\text{ }^\circ\text{C}$, $\theta = 45^\circ$. The composition of the sample is 0.29 mass fraction cyclohexane, 0.13 mass fraction TBA. The continuous line is a fit to two-exponential decay as given by Eqs. 3.2.

The stability of these mesoscopic inhomogeneities, in sample # B2, has been monitored over time. It is seen that as time progresses, the “size” of these inhomogeneities changes very slowly, as evidenced from Figure 4.19 a). The static light-scattering intensity also increases very slowly with time, as seen in Figure 4.19 b).

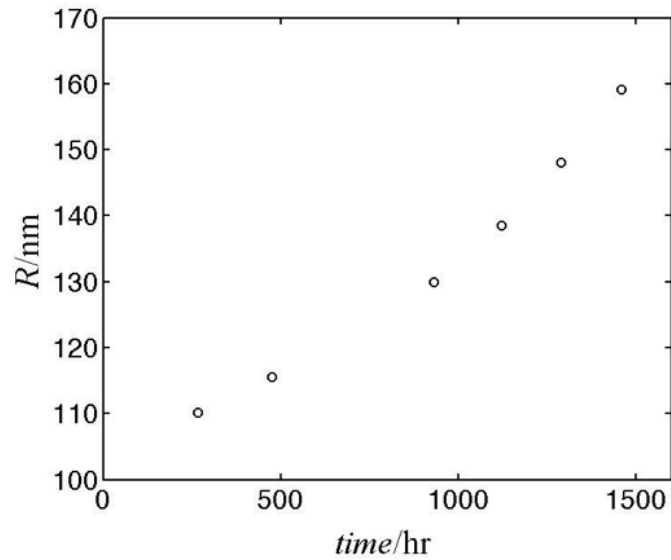


Figure 4.19 a). Time dependence of the average hydrodynamic radius of inhomogeneities in TBA – water- cyclohexane sample at $T = 25\text{ }^{\circ}\text{C}$ and determined at $\theta = 45^{\circ}$. The composition of the sample is 0.001 mass fraction cyclohexane, 0.259 mass fraction TBA.

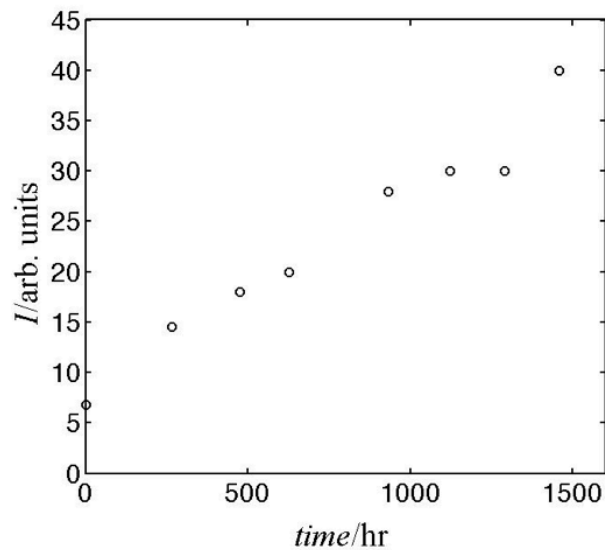


Figure 4.19 b). Time dependence of static light-scattering intensity in TBA – water- cyclohexane sample, at $T = 25\text{ }^{\circ}\text{C}$ and determined at $\theta = 45^{\circ}$. The composition of the sample is 0.001 mass fraction cyclohexane, 0.259 mass fraction TBA.

4.3 TBA-water-isobutyl alcohol ternary system

In order to understand properties of the micro-emulsion-like phase formed in aqueous TBA solutions on the addition of a “solubilizate”, isobutyl alcohol (IBA) is added to TBA – water systems and the TBA-water-IBA ternary system is investigated.

The IBA-water phase behaviour is well studied in the literature. Under ambient conditions, IBA exhibits a miscibility gap with water [102]. This miscibility gap is smaller than in cyclohexane-water systems, but larger than in PO-water systems. In addition, the hydroxyl groups of IBA can form hydrogen bonds with water, which PO and cyclohexane could not. Moreover, IBA is an isomer of TBA and, hence, forms an almost ideal solution with it [60]. Thus IBA could play a possible dual role of acting as a hydrotrope similar to TBA or as a hydrophobic component that exhibits demixing behavior with water.

The thermodynamic phase diagram of the ternary system TBA-water-IBA is determined and is shown in Figure 4.20. TBA, with purity > 0.998 mass fraction, procured from Alfa Aesar (corresponding to “dirty” TBA from above discussions); IBA with purity > 0.999 mass fraction, procured from J. T. Baker; and Millipore water are used for these experiments. Various samples of TBA-water are prepared and incremental amounts of IBA are added to it until phase separation is seen. The accuracy of temperature of the thermostatic bath used to observe the phase separation is about ± 0.1 °C.

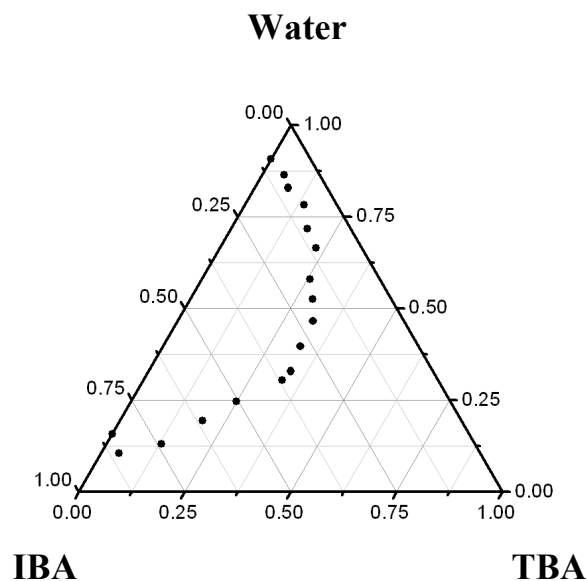


Figure 4.20. Ternary phase diagram of TBA-water-IBA system at 25 °C.

The TBA-water-IBA phase diagram, as seen in Figure 4.20, is similar to the TBA-water-PO and TBA-water-cyclohexane systems, discussed in Sections 4.1 and 4.2 respectively; however, the miscibility gap in this system is between those of the above two ternary systems.

In order to investigate the possibility of a micro-emulsion-like phase in the TBA-water-IBA ternary system, three samples in the one-phase region are studied by static and dynamic light scattering. Samples prepared for the light-scattering studies of this ternary system are from the “clean” TBA discussed in Section 4.1. Ternary samples are prepared as per the procedure described in Section 4.1, but without cold filtering the aqueous TBA solution. The samples are let to “equilibrate” for at least 2 hours and then light-scattering readings are taken. The compositions of the various samples studied are shown in Table 4.5 and represented in the ternary diagram shown in Figure 4.21.

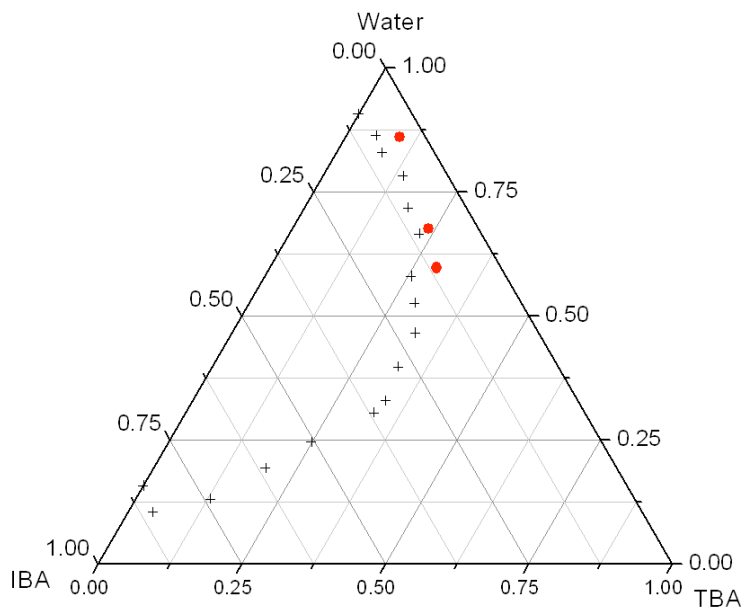


Figure 4.21. Ternary phase diagram of TBA-water-IBA system at 25 °C showing compositions of the three samples investigated by light scattering.

Table 4.5. Compositions, refractive indices and viscosities of TBA-water-IBA system

#	TBA	Water	IBA		TBA	Water	IBA
	Mass Fractions				Mole Fractions		
C1	0.26	0.65	0.09		0.09	0.88	0.03
C2	0.29	0.60	0.11		0.10	0.86	0.04
C3	0.10	0.86	0.04		0.03	0.96	0.01

#	R.I.	Kinematic viscosity at 25 °C ($\times 10^{-6} \text{ m}^2/\text{s}$)	Kinematic viscosity at 10 °C ($\times 10^{-6} \text{ m}^2/\text{s}$)
C1	1.3650	3.39	6.36
C2	1.3691	3.99	7.60
C3	1.3559	1.78	2.96

The intensity auto-correlation functions for ternary sample # C1 at two different temperatures, 25 °C and 10 °C, and at scattering angle, $\theta = 45^\circ$, are shown in Figure 4.22. The correlation functions show the presence of a single exponential mode, with a relaxation time of the order of tens of microseconds. No mesoscopic mode, with a relaxation time of the order of milliseconds, is seen in this sample.

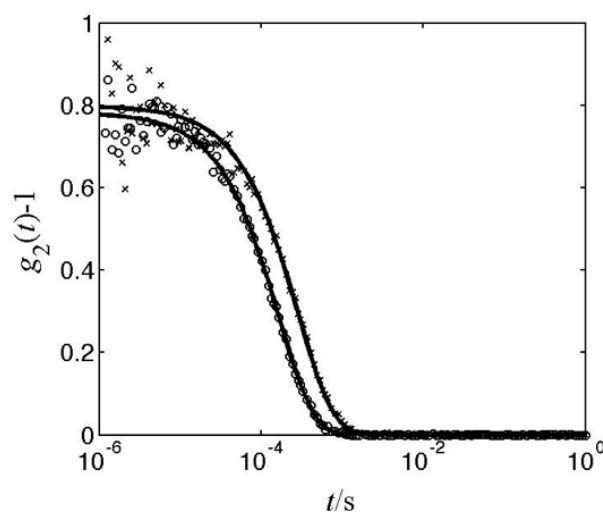


Figure 4.22. Intensity auto-correlation functions for a ternary TBA-water-IBA sample (composition in mass fractions: TBA = 0.26; IBA = 0.09), at scattering angle $\theta = 45^\circ$, and two different temperatures. Open circles = 25 °C; Crosses = 10 °C. The black curves are fits to single exponential decays according to Eq. 3.1.

The wave-number dependence of the relaxation rate for sample # C1, at 25 °C and 10 °C, are shown in Figure 4.23. From this figure, it is seen that the relaxation rate follows a linear q^2 dependence in accordance with Eq. 3.3, thus obeying diffusion dynamics. In addition, it is also seen that as the temperature increases, the diffusion coefficient increases.

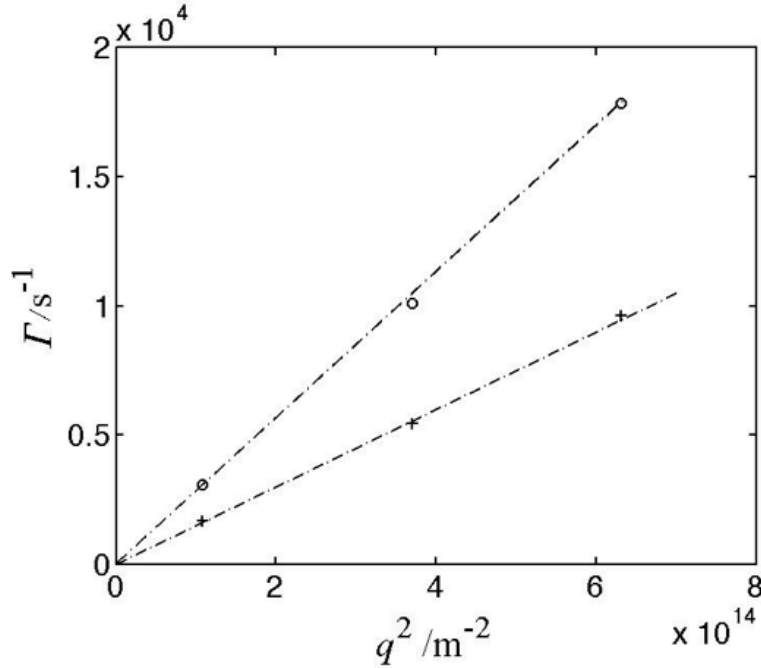


Figure 4.23. Wave-number dependence of the relaxation rate for a ternary TBA-water-IBA sample (composition in mass fractions: TBA = 0.26; IBA = 0.09). Open circles: $T = 25 \text{ }^\circ\text{C}$; Crosses: $T = 10 \text{ }^\circ\text{C}$. The dashed line is a fit to Eq. 3.3 with the slope giving the diffusion coefficient. $D_{25 \text{ }^\circ\text{C}} = 2.8 \times 10^{-11} \text{ m}^2/\text{s}$; $D_{10 \text{ }^\circ\text{C}} = 1.5 \times 10^{-11} \text{ m}^2/\text{s}$.

The hydrodynamic radii for sample # C1, at 25 °C and 10 °C, are computed by using Eq. 3.4. The angular dependence of the hydrodynamic radii for these systems, at two different temperatures, is shown in Figure 4.24. From this figure, it is seen that as the temperature increases the computed hydrodynamic radii also increase.

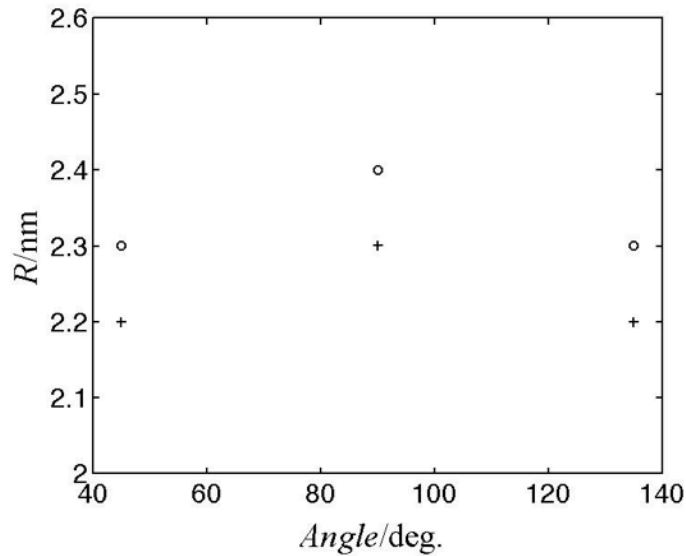


Figure 4.24. Angular dependence of hydrodynamic radii for a ternary TBA-water-IBA sample (composition in mass fractions: TBA = 0.26; IBA = 0.09). Open circles: $T = 25\text{ }^{\circ}\text{C}$; Crosses: $T = 10\text{ }^{\circ}\text{C}$.

The wave-number dependence of the inverse intensity for sample # C1, at 25 °C and 10 °C, is shown in Figure 4.25. It is seen that the intensity distribution is almost symmetric, with no angular dependence. This shows that there are no large (mesoscopic or submicron-sized) particles present in these samples.

The auto-correlation function for sample # C1 is compared with the correlation functions obtained for samples # C2 and # C3 at 10 °C, in Figure 4.26. From this figure, it is seen that sample # C2 behaves similarly to sample # C1, showing only molecular diffusion and no mesoscale diffusion. However sample # C3 shows the presence of a strong mesoscopic mode, with a relaxation time of the order of milliseconds. The molecular diffusion mode, corresponding to a relaxation time of microseconds, remains undetectable in this sample due to the strong scattering from

the mesoscopic mode. The hydrodynamic radius of the mesoscopic inhomogeneities, computed by using Eq. 3.4, indicates the presence of inhomogeneities with a radius of about 200 nm.

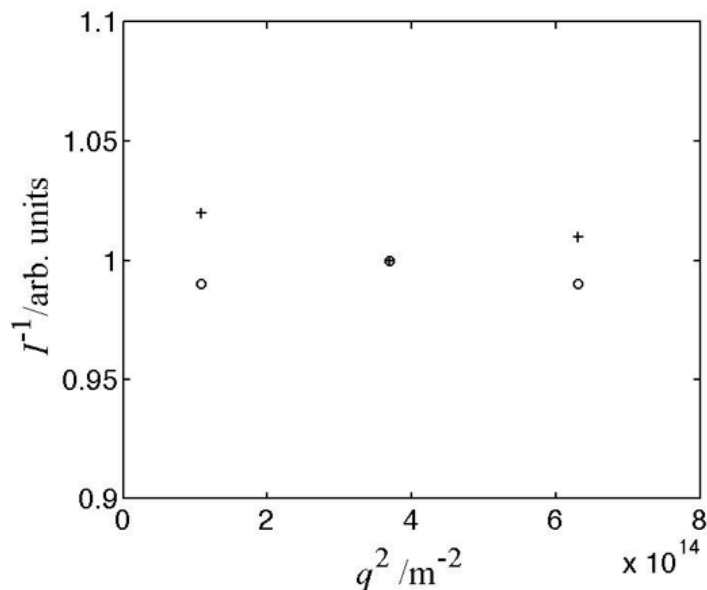


Figure 4.25. Wave-number dependence of inverse intensity for a ternary TBA-water-IBA sample (composition in mass fractions: TBA = 0.26; IBA = 0.09). Open circles:

$T = 25 \text{ }^\circ\text{C}$; Crosses: $T = 10 \text{ }^\circ\text{C}$.

Thus the above experimental results show that a micro-emulsion-like phase exists in TBA-water-IBA ternary system as well. The exact region of the micro-emulsion-like phase within this ternary system is different as compared to other ternary systems like TBA-water-PO and TBA-water-cyclohexane.

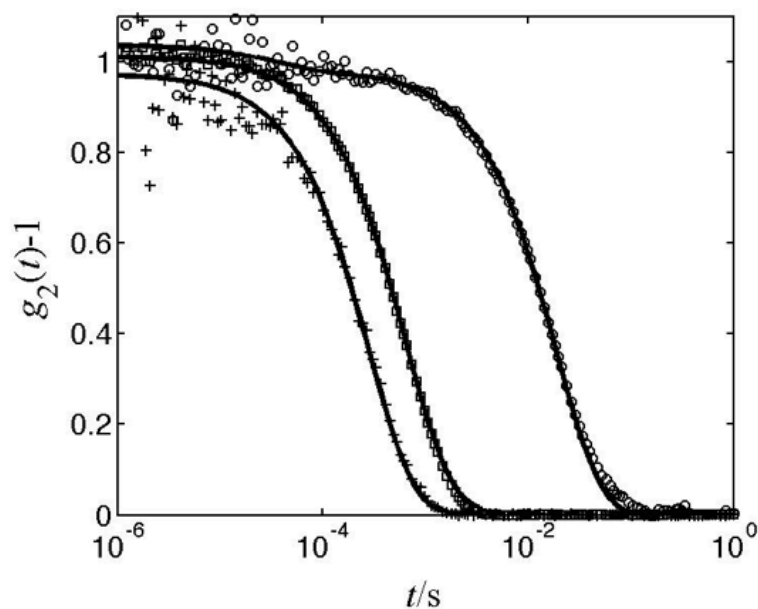


Figure 4.26. Intensity auto-correlation functions for various ternary samples of TBA-water-IBA system at $T = 10\text{ }^{\circ}\text{C}$ and $\theta = 45^{\circ}$. Compositions (in mass fractions) are:
 Open circles: TBA = 0.10, IBA = 0.04; Crosses: TBA = 0.26, IBA = 0.09; Open squares: TBA = 0.29, IBA = 0.11.

4.4 Results from molecular dynamics simulations [83]

Molecular dynamics simulations were carried out by our collaborator, Professor Klauda, to further investigate the nature of the mesoscopic inhomogeneities and to determine if there are any specific interactions or formation of structures on the molecular scales that lead to the formation of mesoscopic particles [83].

TBA-water-PO ternary system

Radial distribution functions obtained from molecular dynamics simulations in TBA-water-PO ternary systems (compositions shown in Table 2.1) are shown in Figures 2.17, 2.19, and 2.21. Snapshots from MD simulation are shown in Figure 4.27. These indicate that PO weakly associates with itself, but more strongly with TBA.

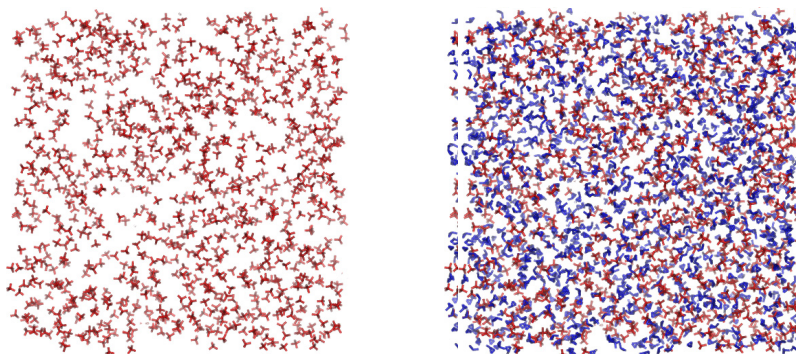


Figure 4.27. Snapshots from molecular dynamics simulations for a ternary TBA-water-PO system at $T = 10$ °C. Composition (in mole fractions) are:

TBA = 0.10, PO = 0.13. (Taken from [83].)

Red: TBA molecules; Blue: PO molecules.

TBA-water-cyclohexane ternary system

Radial distribution functions obtained from molecular dynamics simulations in a TBA-water-cyclohexane ternary system (composition – 0.0685 mole fraction TBA, 0.9305 mole fraction water, and 0.001 mole fraction cyclohexane, total number

of molecules = 2000, simulation time = 100 ns) are shown in Figures 4.28 and 4.29. Snapshots from the simulations are shown in Figures 4.30 and 4.31.

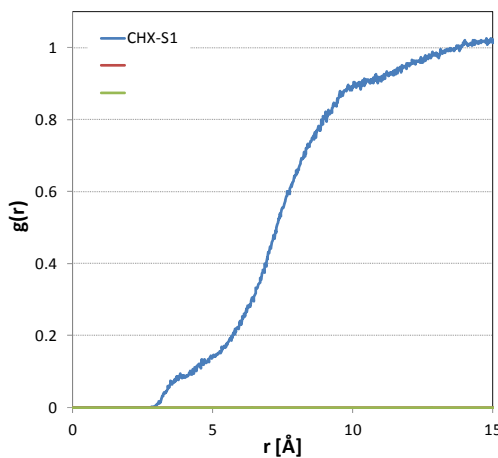


Figure 4.28. Radial distribution function between C1 on cyclohexane molecule and O on water molecule, for a ternary TBA-water-cyclohexane system at $T = 25$ °C. Composition (in mole fractions) are: TBA = 0.069, Cyclohexane = 0.001. (Taken from [83].)

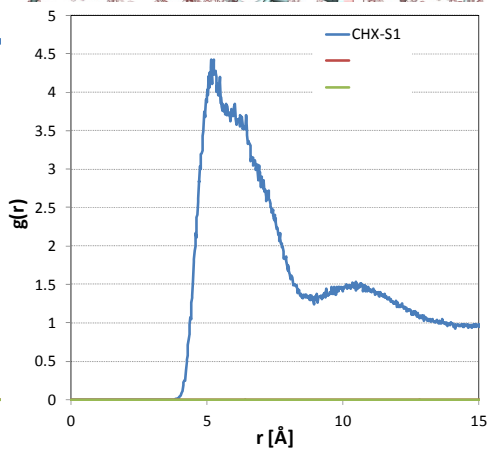
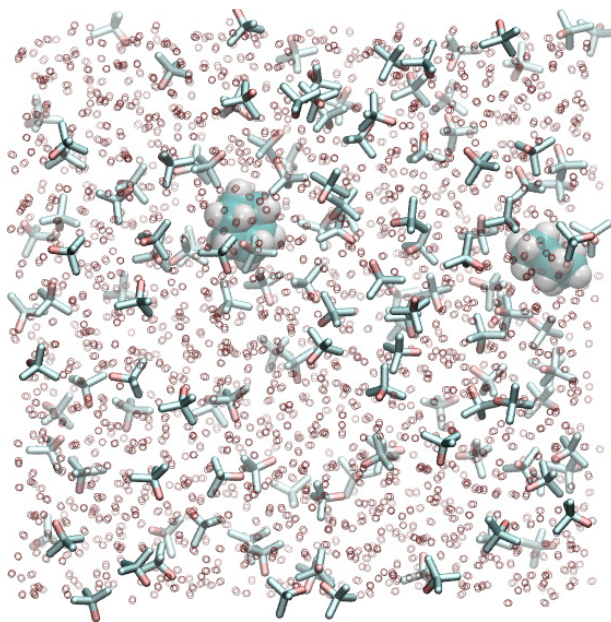


Figure 4.29. Radial distribution function between C1 on cyclohexane molecule and C on TBA molecule, for a ternary TBA-water-cyclohexane system at $T = 25$ °C. Composition (in mole fractions) are: TBA = 0.069, Cyclohexane = 0.001. (Taken from [83].)

Figure 4.30 shows snapshots wherein a single monomer of cyclohexane is considered. TBA molecules surround this single cyclohexane molecule in addition to surrounding a single small layer of water molecules, thus forming a cluster of TBA-water-cyclohexane molecules. As evidenced in this figure, the cluster has a size (diameter) of ~ 1.7 nm.

Figure 4.30. (see below) Snapshots from molecular dynamics simulations (~ 110 ns) for a ternary TBA-water-cyclohexane (with cyclohexane unimers) system at $T = 25$ °C. Composition (in mole fractions) are: TBA = 0.069, Cyclohexane = 0.001. (Taken from [83].)



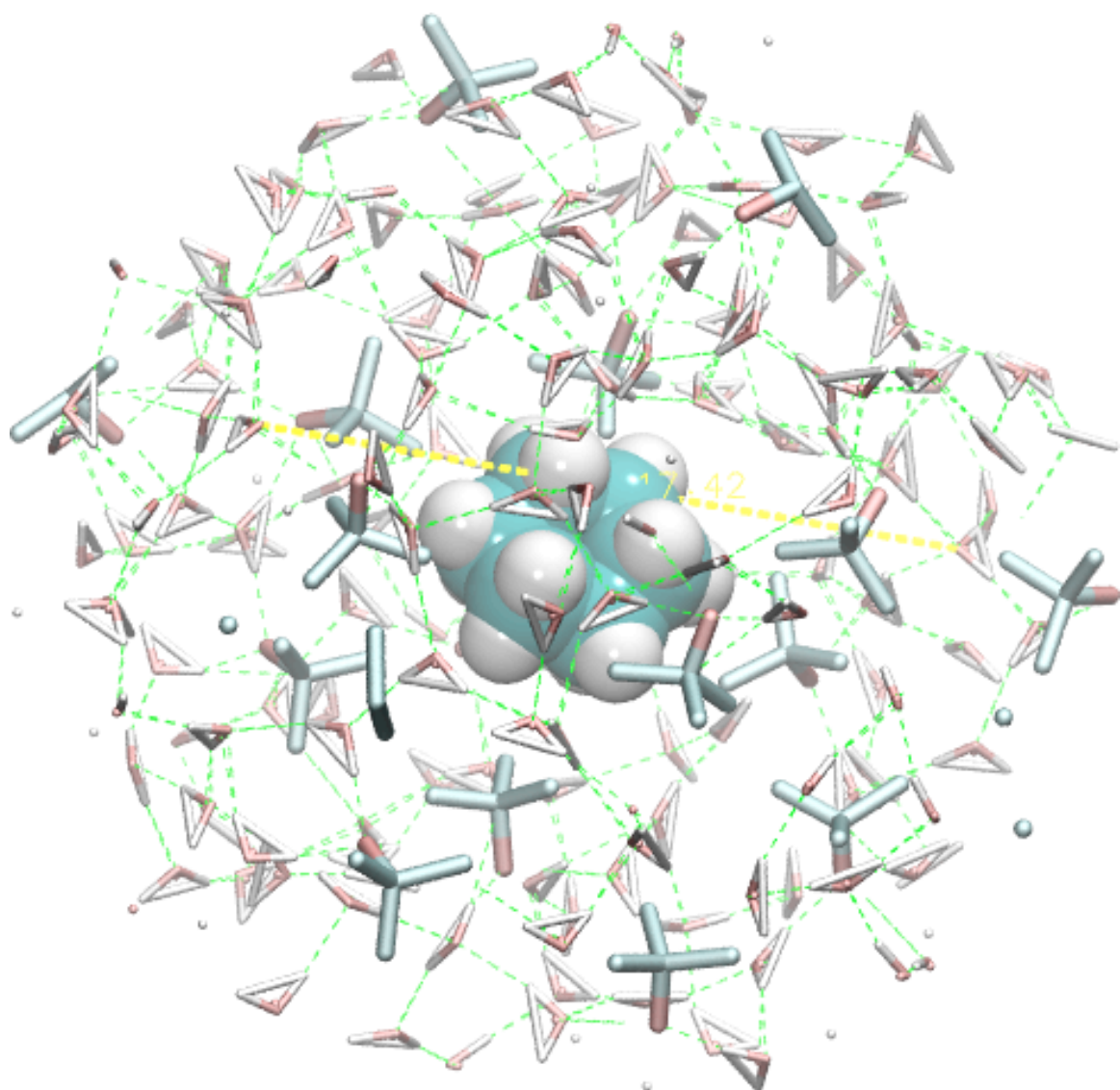
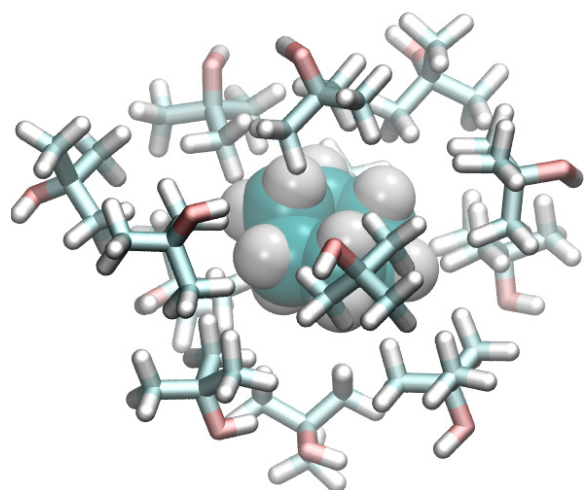
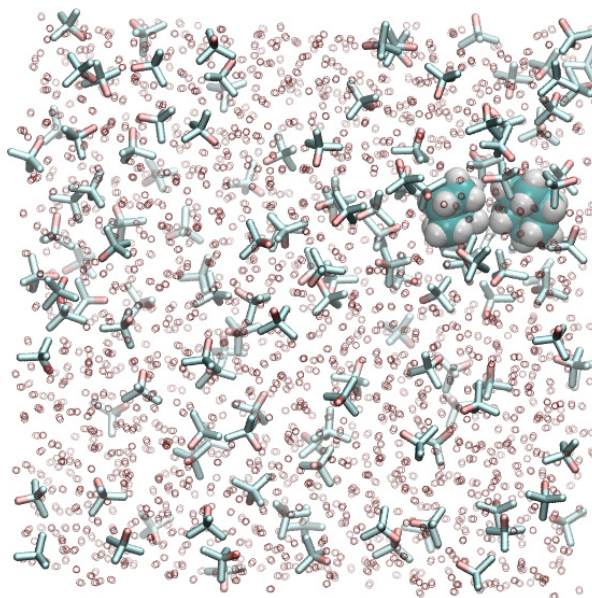
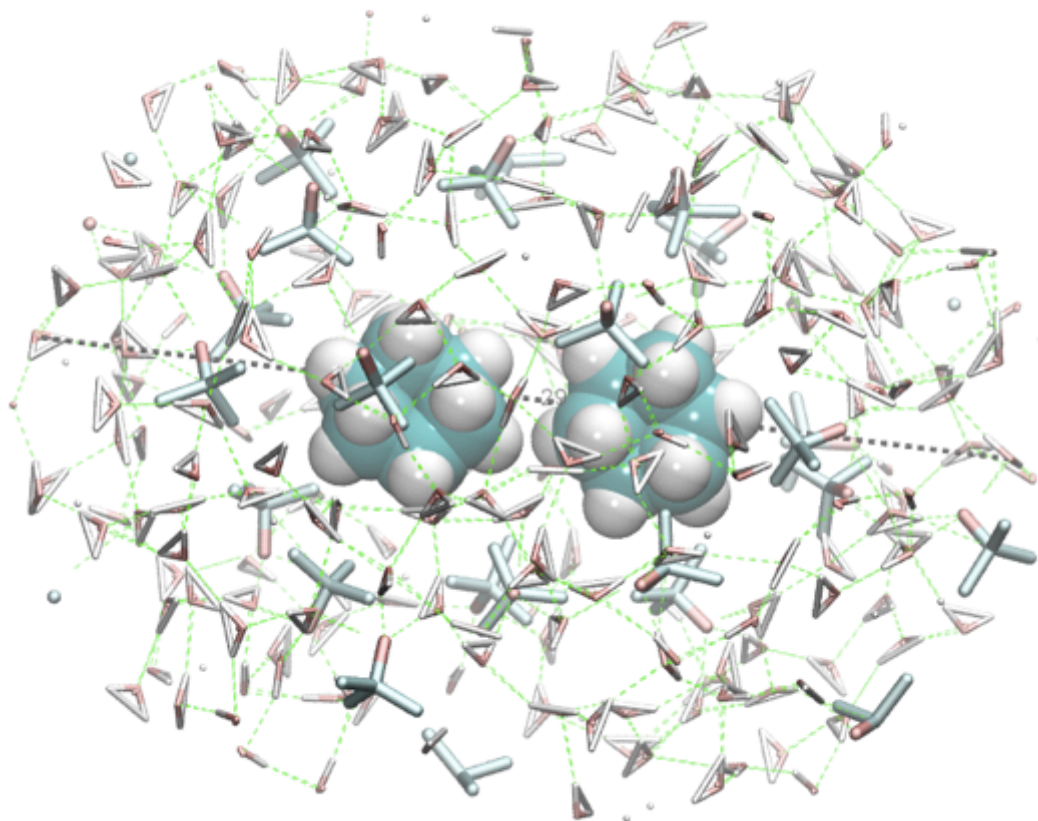
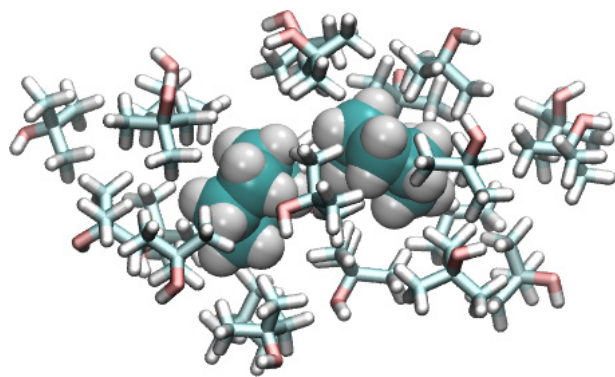


Figure 4.31 shows snapshots wherein a dimer of cyclohexane molecules is considered. Again, TBA molecules surround the cyclohexane dimer and a surrounding layer of water molecules. In this case the water shell is much larger consisting of $\sim 2 - 3$ layers of water molecules, with the resulting cluster having a size (diameter) of ~ 3 nm.

Figure 4.31. (see below) Snapshots from molecular dynamics simulations (~ 90 ns) for a ternary TBA-water-cyclohexane (with dimerized cyclohexane) system at $T = 25$ °C. Composition (in mole fractions) are: TBA = 0.069, Cyclohexane = 0.001.

(Taken from [83].)



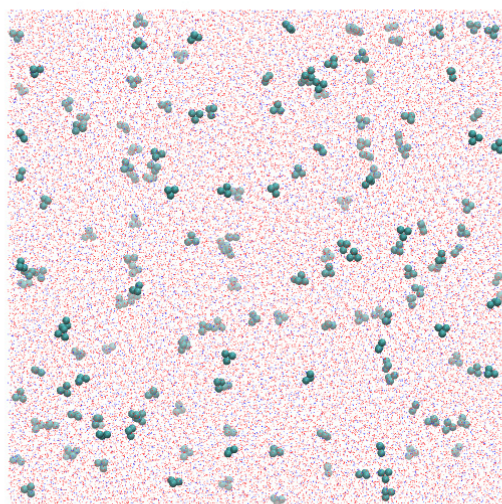


Coarse grained simulations of TBA-water-cyclohexane system are also carried out. The compositions of the ternary system are the same as above, but the total number of molecules is about 198,000. This system is simulated for 2700 ns at a temperature of 310 K. MARTINI-based coarse-grained force field is used; water molecules are modeled as a single bead while TBA molecules are modeled with propanol parameters, cyclohexane molecules are modeled with three beads. Snapshots from these simulations are shown in Figure 4.32.

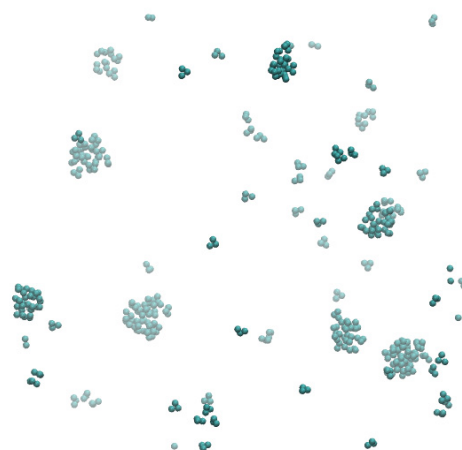
From Figure 4.32 it is seen that cyclohexane forms clusters with “TBA” and water, which grow from a few molecules to a final liquid droplet consisting of almost all cyclohexane molecules in the core. The size of the cyclohexane core is ~ 4 nm. This may indicate that the equilibrium state of the cyclohexane molecules is to aggregate, although may be slowly, to form larger structures which are in equilibrium with the ternary solution.

Figure 4.32. (see below) Snapshots from coarse grained simulations of “TBA”-water-cyclohexane system. TBA is modeled by using propanol parameters. The system consists of 198,000 molecules simulated for a period of 2700 ns. Composition (in mole fractions) are: TBA = 0.069, Cyclohexane = 0.001. (Taken from [83].)

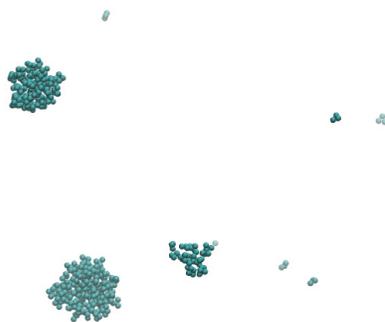
Initial configuration (water in blue, propanol in red, cyclohexane in green)



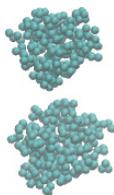
12.5 ns (water and propanol removed for clarity)



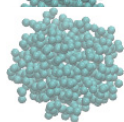
87.5 ns



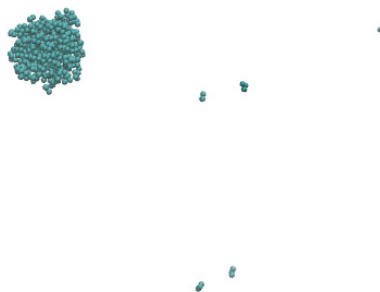
272.5 ns



301.25 ns



2628.75 ns



TBA-water-isobutanol ternary system

Radial distribution functions obtained from molecular dynamics simulations in TBA-water-isobutanol system are shown in Figures 4.33 and 4.34. The compositions and simulation details of these systems are shown in Table 4.6.

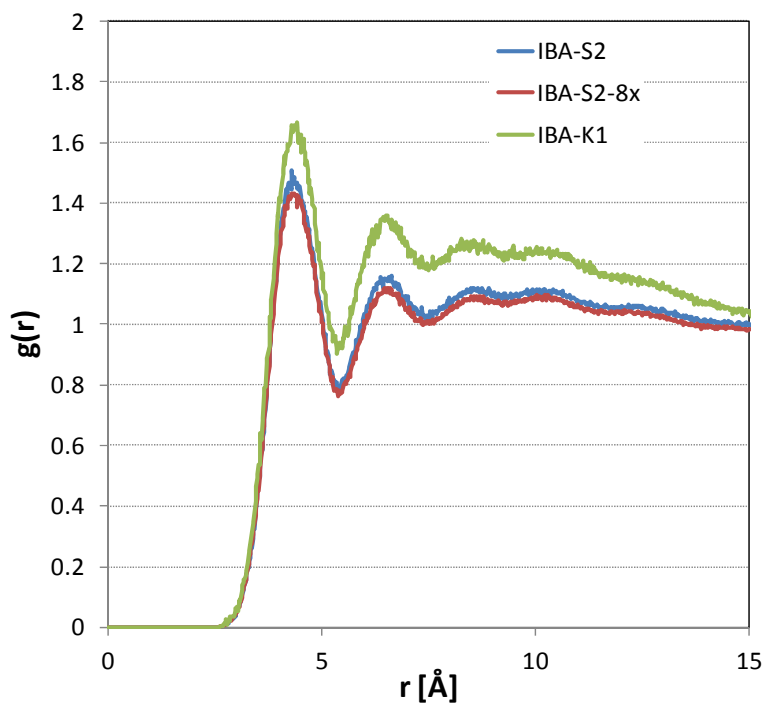


Figure 4.33. Radial distribution function between O-O on IBA molecules for a ternary TBA-water-IBA system at $T = 25$ °C. Composition (in mole fractions) for IBA-S2 are: TBA = 0.10, IBA = 0.04; for IBA-K1 are: TBA = 0.07, IBA = 0.03.

(Taken from [83].)

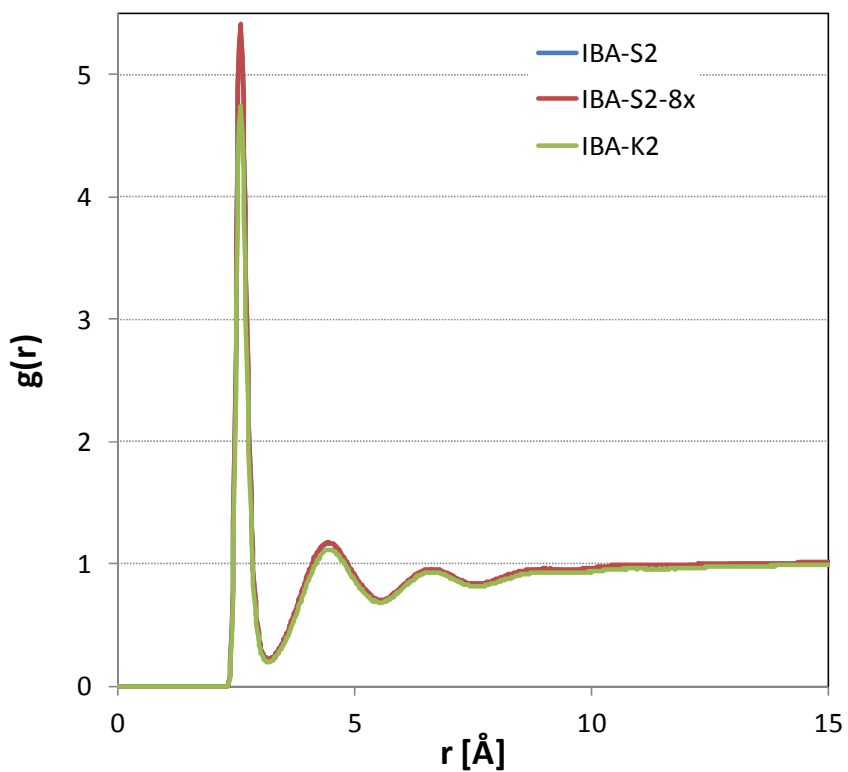


Figure 4.34. Radial distribution function between O on IBA and O on for a ternary TBA-water-IBA system at $T = 25$ °C. Composition (in mole fractions) for IBA-S2 are: TBA = 0.10, IBA = 0.04; for IBA-K1 are: TBA = 0.07, IBA = 0.03.

(Taken from [83].)

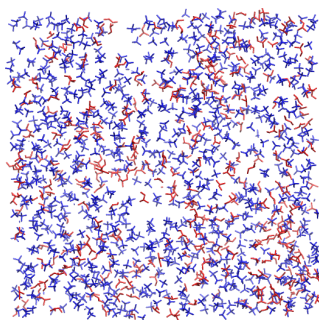
Table 4.6. Compositions and simulation details of TBA-water-IBA system

ID	T (K)	Total # of molecules	x_{TBA}	x_{water}	x_{IBA}	Time (ns)
IBA-S2	298	2000	0.102	0.859	0.039	200
IBA-S2-8x	298	16000	0.102	0.859	0.039	200
IBA-K1	298	2000	0.070	0.900	0.03	100

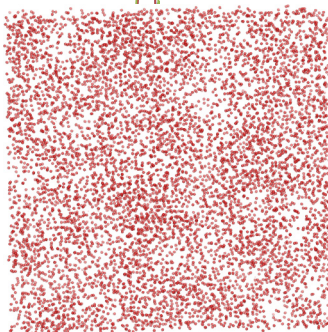
Snapshots from the simulations are shown in Figure 4.35. These indicate that TBA and IBA tend to associate into water-poor, organic-rich regions. The effective size (diameter) of these clusters is ~ 1.5 nm.

Figure 4.35. Snapshots from molecular dynamics simulations for a ternary TBA-water-IBA system at $T = 25$ °C. Composition (in mole fractions) are: TBA = 0.10, IBA = 0.04. (Taken from [83].)

Blue: TBA molecules, Red: IBA molecules



Red: Water molecules



Chapter 5: Nature of mesoscopic inhomogeneities in aqueous solutions of hydrotropes

5.1 Micro heterogeneities in aqueous TBA solutions

In this work, mesoscopic properties of aqueous solutions of TBA, a non-ionic hydrotrope, in the presence of various solubilizates, namely, propylene oxide, cyclohexane, and isobutanol, have been studied by static and dynamic light scattering. The phase diagrams of these systems have been also determined and results from molecular dynamic simulations have been discussed.

On studying the thermodynamics of the binary TBA-water system and on characterizing it through light-scattering studies and molecular dynamics simulations, we conclude that in dilute regions (TBA mole fraction between 0.035 and 0.1) TBA-water system exhibits short-lived, short-ranged structural fluctuations. These fluctuations are due to the formation of transient hydrogen bonds between TBA and water molecules. In this region, TBA molecules self-associate through van der Waals interactions between their methyl groups, while the hydroxyl groups of TBA molecules bond with surrounding water molecules to form hydrogen bonded shell structure, thus screening methyl groups of TBA molecules from water.

We want to emphasize an important point here - although these short-lived, short-ranged structures look similar to clathrate-hydrate-precursors, they are not. They are rather micelle-like fluctuations. The main distinguishing factor between

micelle-like fluctuations and clathrate-hydrate-precursors are that clathrate-hydrate-precursors, which would eventually form solid clathrate-hydrates, are mostly driven by geometric relations between the guest and the host molecules. In clathrate-hydrates the guest molecule does not interact with the host structure through the formation of hydrogen bonds. However, molecules forming a nonionic micelle interact with the solvent surrounding it mostly through hydrogen bonds. Thus, although the term “clathrate-like structure” is commonly used in the literature to describe TBA-water fluctuations, we instead envision these structures as micelle-like fluctuations.

Molecular dynamics simulations show that these fluctuations are short-lived (less than 100 ps) and they do not relax to the equilibrium state by diffusion. If such fluctuations are not accompanied by fluctuations of the refractive index, they cannot be seen by light scattering. However, molecular diffusion can be seen from light scattering. This is evidenced by the presence of the molecular diffusion mode in aqueous TBA solutions, as shown in Figure 3.2 and discussed in section 3.1. Molecular diffusion in aqueous TBA solutions corresponds to a hydrodynamic radius or a correlation length of concentration fluctuations of the order ~ 0.5 nm.

On comparing the thermodynamics of TBA-water solutions with the thermodynamic properties of other alcohols, namely C1-C4 alcohols, we see that alcohol-water solutions exhibit an anomaly in the water-rich region, which are most pronounced in TBA-water solutions. At low TBA concentrations, between TBA mole fraction 0.035 to 0.1, we see anomalies such as a maximum in the heat capacity at 0.07 mole fraction TBA at ~ 0 °C, a minimum in the excess molar volume at 0.05 mole fraction TBA at ~ 15 °C, a kink in the excess chemical potential of TBA at

0.045 mole fraction TBA at ~ 25 °C, a maximum in the sound velocity at 0.10 mole fraction TBA at ~ 25 °C, and a minimum in the isothermal compressibility at 0.035 mole fraction TBA at ~ 10 °C. As seen in Figure 2.14, the activity coefficient of water at low TBA concentrations is negative, and then becomes positive beyond 0.04 mole fraction TBA. The heat of mixing is negative at low TBA concentrations and then becomes positive above 0.06 mole fraction TBA. All these observations indicate that at low TBA concentrations, the solute-solvent interactions are energetically favored, leading to a negative heat of mixing, while at higher TBA concentrations the solute-solute interactions are preferred leading to a positive heat of mixing.

We believe that this mixing behavior is similar to the formation of micelle-like structures in aqueous TBA solutions, driven by hydrophobic hydration, as discussed by Bowron *et al.* [23]. As discussed in chapter 2, simulations of Bowron *et al.*, show that at low TBA concentrations (0.06 mole fraction TBA) solute-solute interactions are obtained through methyl group contacts, which are screened from water by TBA hydroxyls. At larger TBA concentrations (> 0.1 mole fraction TBA) the interactions between the TBA molecules resemble those in pure TBA with water molecules being screened from TBA methyl groups through TBA hydroxyls. These interactions lead to micro heterogeneities in solution. However these interactions are transient, short-lived with a lifetime of tens of picoseconds, thus not culminating into any stable micellar phase.

An older interpretation of the observed anomalous behavior in aqueous TBA solutions was based on the “iceberg” model of Frank and Evans [63]. According to this model, addition of non-polar solutes stabilizes the hydrogen-bonded network of

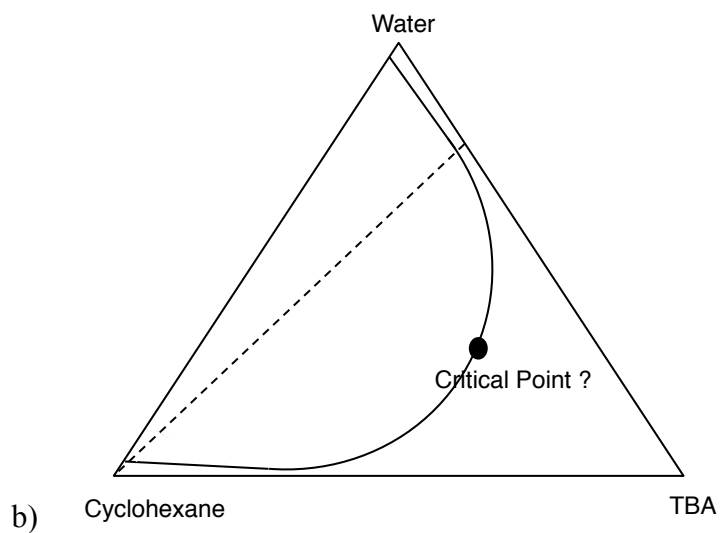
water by forming a shell of structured water around the solute. This model is essentially similar to the clathrate-hydrate hypothesis, which as discussed above, and does not adequately describe the molecular behaviour of aqueous TBA solutions.

Although these structural fluctuations cannot be seen from dynamic light scattering, the question arises, “what exactly is seen from dynamic and static light scattering?” We have clarified in Section 3.1 that mesoscopic inhomogeneities in aqueous TBA solutions are seen only when the binary solutions contains a third component, even if the third component is sometimes present in trace amounts. These mesoscopic inhomogeneities in TBA aqueous solutions, containing certain uncontrolled impurities, remain stable for long periods of time, as long as this study continued. To resolve this issue, we studied three systems with controlled amount the third component.

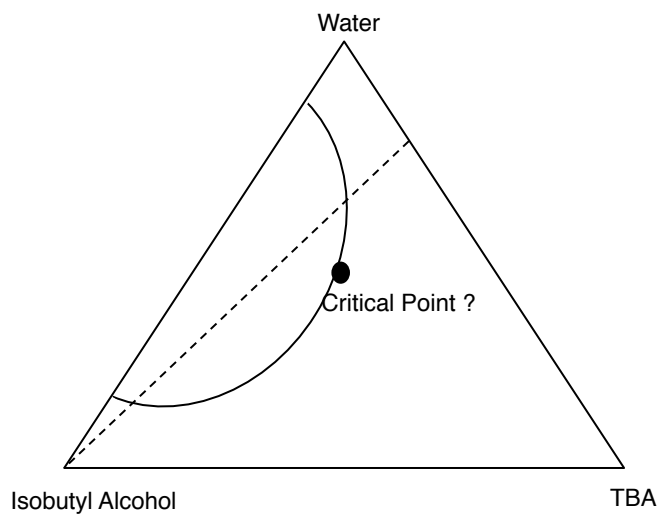
The three systems TBA-water-cyclohexane, TBA-water-IBA, and TBA-water-PO are similar in such a way that they all exhibit a liquid-liquid miscibility gap. However, these systems are distinguished in the following manner, as illustrated in Figure 5.1. The concentration line with a fixed ratio of TBA to water, which corresponds to the formation of micelle-like structures, either crosses the macroscopic liquid-liquid separation far away from the critical consolute point, as in TBA-water-cyclohexane and TBA-water-IBA systems, shown in Figure 5.1 (a) and (b) or passes through one-phase near critical region, as in TBA-water-PO systems, shown in Figure 5.1 (c).

Figure 5.1. (see below) Sketches of the ternary phase diagram in TBA-water-solubilizate systems. The solubilizates studied include: a) Cyclohexane; b) Isobutyl alcohol; c) Propylene oxide. The dashed line represents a constant molar ratio of TBA: water as 7:93.

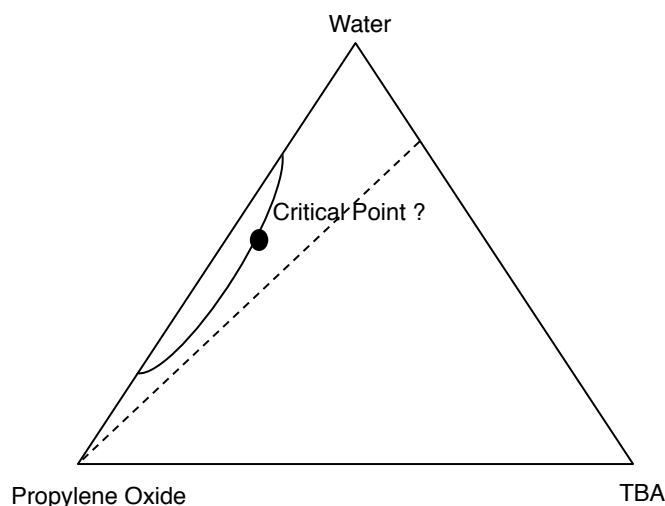
a) TBA-water-cyclohexane system



c) TBA-water-isobutanol system



c) TBA-water-propylene oxide system



The TBA-water-cyclohexane system shows the largest miscibility gap in comparison to the three systems studied, because cyclohexane is practically insoluble in water. This system is a well-defined example of how a hydrophobic cyclohexane, is “solubilized” by an aqueous solution of a nonionic hydrotrope. Snapshots from MD simulations show the formation of TBA-water layers around cyclohexane molecules. The critical composition of this system is far away from the domain of structural fluctuations in aqueous TBA solutions.

The next system, TBA-water-IBA, shows a smaller miscibility gap as compared to the TBA-water-cyclohexane system. This system shows mesoscopic inhomogeneities at a concentration range where the effective alcohol (TBA+IBA) concentration is similar to that in TBA-water-cyclohexane system. This concentration corresponds to the region where binary TBA-water solutions show micelle-like fluctuations. At higher effective alcohol content, TBA-water-IBA system exhibits

near-critical concentration fluctuations. It is possible that in this ternary system IBA may, at the same time, act as a co-solvent and a solubilize.

The third system, TBA-water-PO, exhibits the smallest miscibility gap as compared to the previous systems. In this system, the mesoscopic inhomogeneities could arise due to a balance between strong hydrogen bonding between TBA-water and a tendency for PO and water to demix near critical conditions. This system shows strong non-equilibrium mesoscopic inhomogeneities near the two-phase region, whose characteristics change over a few hours and which finally disappears within a few weeks. This event is reminiscent of near-critical behavior, as was seen by Kostko *et al.* in aqueous 3MP solutions on the addition of NaBr [54]. However, the details of this phenomenon in this system are difficult to interpret as they may be due to a combination of various factors such as coupling between micelle-like fluctuations in TBA-water and near-critical concentration fluctuations in the ternary system, or original impurities present in TBA and PO, or the ability of PO to partially polymerize in aqueous media.

5.2 Self-assembly in aqueous solutions of non-ionic hydrotropes

There are three distinct “phases” existing in TBA-water-solubilize systems. The first phase is water-rich. In addition to molecular clustering on a nanometer scale, this phase contains “particles” of order 100 nm. While the exact structure of these particles are not known, based on the latest simulations and SANS experiments on another hydrotrope, tetrahydrofuran [92], we speculate that the structure of these

particles maybe described as consisting of hydrophobic molecules in the core surrounded by layers of hydrogen bonded TBA and water molecules. The question now arises whether we can consider these particles as the second phase? This particle “phase” could be spread across the water-rich phase making a “microemulsion”. These particles could still represent a macroscopically separate phase, which is spread across the water-rich domain due to extremely small interfacial tension. This “microemulsion” may exhibit long-term stability. The third phase is the organic-rich phase (“oil” phase), which emerges at higher concentrations of the solubilizate.

In TBA-water-cyclohexane system, at the composition where two bulk phases, namely water-rich and organic-rich phases are observed; we noticed a small amount of another phase on the water-oil interface. We call it the mesophase. The mesophase is observed under similar conditions for various aqueous organic solutions, which exhibit phase separation [103]. An image of this mesophase in TBA-water-cyclohexane system is shown in Figure 5.2. The composition of this sample is: 0.16 TBA mass fraction, 0.39 cyclohexane mass fraction.

A speculative phase diagram, which may explain the formation of the mesophase on the water-oil interface, is shown in Figure 5.3. At a fixed TBA-water mole ratio of 7:93, upon addition of cyclohexane we first observe mesoscopic inhomogeneities in solution (region between WXNACW in Figure 5.3). Upon further addition of cyclohexane we enter the three-phase region (triangle ABC in Figure 5.3), for a point P in the three phase region, the compositions of the three co-existing



Figure 5.2. Image of 2-phase ternary system consisting of TBA-water-cyclohexane system. The composition (in mass fractions) is 0.16 TBA, 0.39 cyclohexane. The sample shows the presence of a mesophase at the interface of water-rich and oil-rich layers. (Vial outer diameter = 2.5 cm)

phases will be given by points A, B, and C, as shown in Figure 5.3. (The amount of phase A is proportional to the area of triangle CPB, the amount of phase C will be

proportional to area of triangle APB, and so on.) The amount of the mesophase could remain extremely small because on increasing the amount of cyclohexane, we may be sliding along the bottom of the triangle, which represents the three-phase equilibrium.

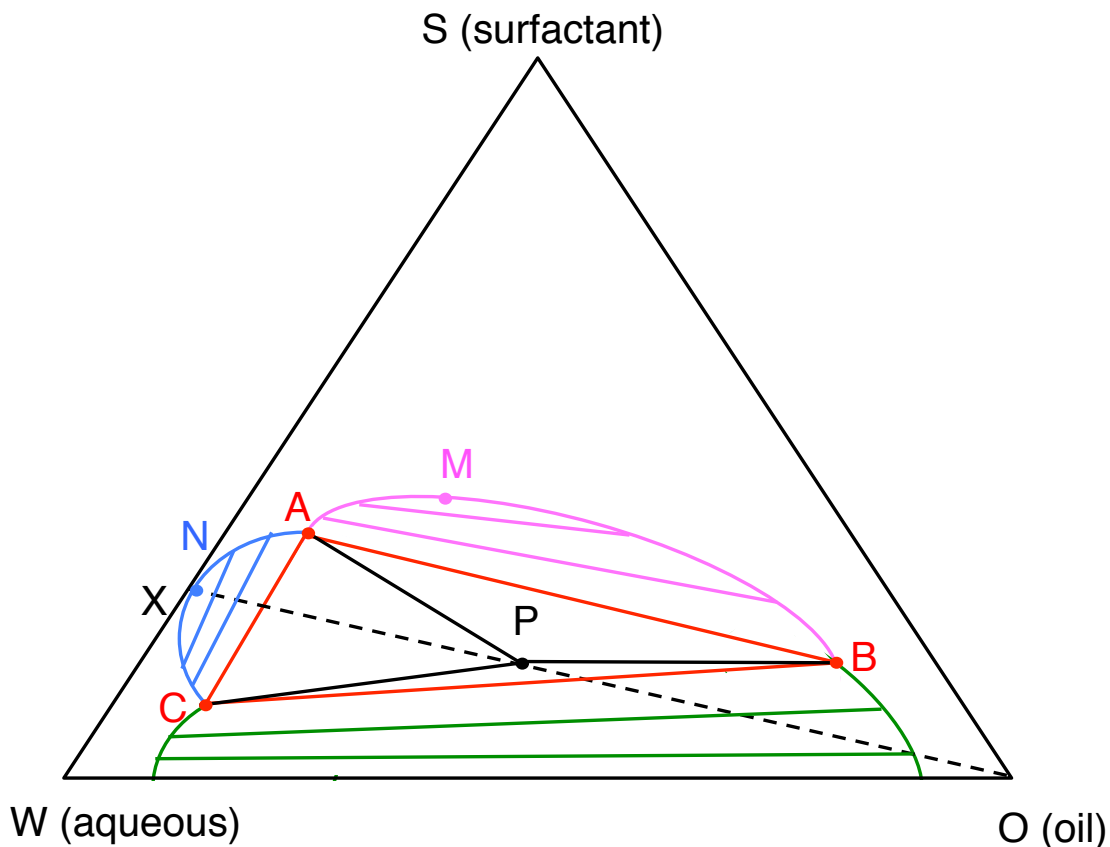


Figure 5.3. Hypothesized ternary phase diagram for water-oil-surfactant system. M represents the mesophase, while the triangle ABC represents the three-phase coexistence. Point P is any composition exhibiting three-phase coexistence. Line XO is composition with 7:93 TBA:Water mole ratio.

Unique features in the formation of the mesophases are the size of the mesoscopic inhomogeneities and their stability. The inhomogeneities that form in these ternary systems have a characteristic size, of the order of 100 nm. This size does not seem to depend on the type of solubilize in aqueous TBA solutions, nor does it seem to strongly depend on temperature. However, the number of these “particles” strongly increases as the temperature is lowered.

The characteristic size and the stability of these inhomogeneities depend on the interfacial tension between these inhomogeneities and the bulk of the solution. “Solubilization” by hydrotropes leads to a lower surface tension between the solubilize and the bulk solution.

Chapter 6: Outlook

This research work has elucidated two major phenomena – the first one being the “origin” and the second one being the “nature” of mesoscopic inhomogeneities in aqueous solutions of small organic molecules.

The work carried out in this dissertation and the results obtained are not unique to the systems studied. Mesoscopic inhomogeneities are seen in a wide variety of aqueous systems, such as in 3-methylpyridine [55], tetrahydrofuran [92], 2-butoxyethanol [91, 104-108], and others discussed in Chapter 1. Mesoscopic inhomogeneities occurring in aqueous 3MP solutions are strongly correlated with the source of the solute. Aqueous solutions of 2-butoxyethanol, as studied by Bender and Pecora, show similar mesoscopic behavior [91]. Very recently, Liu and co-workers have studied aqueous solutions of tetrahydrofuran (THF), by dynamic light scattering, UV-vis spectroscopy and small-angle neutron scattering. They observed that in the presence of trace amounts of a hydrophobic compound, namely butylhydroxytoluene (BHT), aqueous THF solutions show the presence of mesoscopic inhomogeneities [92]. The mesoscopic inhomogeneities thus formed in this system consist of a BHT-core surrounded by a shell of THF and water molecules. These results correlate well with what is observed in aqueous TBA solutions.

The binary aqueous solutions show short-lived, short-ranged structural fluctuations between the organic molecules and water molecules. The addition of the solubilize stabilizes this structure and leads to the formation of larger mesoscopic

aggregates. These mesoscopic structures are stable over long periods of time due to low interfacial tension between them and the bulk solution.

This goals attained in this research may have a wide range of applications. First and foremost, hydrotropic solutions are widely used in the “solubilization” of hydrophobic drugs into pharmaceutical formulations [13]. This is highly important because most pharmaceutical formulations are aqueous solutions and need to contain large amounts of drugs. The presence of a hydrotrope in the formulation will enhance the amount of drug that can be formulated into the product. Similarly, hydrotropes are also used in the formulations of soaps, detergents, cosmetics, *etc* [5]. Although this has been shown through many studies on traditional ionic hydrotropes, we show that similar effects can be achieved by non-traditional nonionic hydrotropes, such as short-chain alcohols.

Another property of such systems is their remarkable stability over long periods of time, practically rendering the system thermodynamically stable. This property leads to the formation of a new class of stable colloids, containing only small nonelectrolyte molecules.

Understanding the nature of interactions that lead to the formation of mesoscale structures in aqueous solutions of small organic molecules will help in elucidating the behavior of aqueous solutions of proteins, such as protein folding and unfolding

To answer the remaining fundamental questions on the nature of the mesoscopic inhomogeneities in aqueous solutions, the next steps would be to investigate the structure and dynamics of aqueous ternary systems, containing

hydrotropes and solubilizates through small-angle neutron scattering (SANS) and neutron spin echo (NSE) techniques. SANS will help probe the system at smaller length scales (about 0.1 nm to 100 nm), while NSE will help probe the system at faster time-scales (100 ps – 10 μ s). SANS experiments may provide an answer if clustering of molecules on a nanometer scale indeed occurs. NSE may elucidate the fast dynamics.

A comprehensive light-scattering study of aqueous ternary systems containing ionic hydrotropes, such as tetra butyl ammonium bromide and various solubilizates is also desirable. Detailed phase diagram, for ternary system with ionic hydrotropes and with nonionic hydrotropes, showing various mesoscopic phases should be determined and investigated.

Additional molecular dynamics simulations, with coarse-grained models, are needed to show the formation and development of mesoscale particles and the mesophase. Finally, a theoretical model, based on mesoscale thermodynamics, needs to be developed to explain the formation of the mesophase and its thermodynamic stability.

Bibliography

1. Neuberg, C. Hydrotropische erscheinungen. *Biochem. Z.* **1916**, *76*, 107-176.
2. Friberg, S. E.; Lochhead, R. V.; Blute, I.; Wörnheim, T. Hydrotropes – Performance chemicals. *J. Disp. Sci. Tech.* **2004**, *25*, 243-251.
3. Srinivas, V.; Rodley, G. A.; Ravikumar, K.; Robinson, W. T.; Turnbull, M. M.; Balasubramanian, D. Molecular organization in hydrotrope assemblies. *Langmuir* **1997**, *13*, 3235-3239.
4. Hogdgon, T. K.; Kaler, E. W. Hydrotropic solutions. *Curr. Opin. Coll. Int. Sci.* **2007**, *12*, 121-128.
5. Eastoe, J.; Hatzopoulos, M. H.; Dowding, P. J. Action of hydrotropes and alkyl-hydrotropes. *Soft Matt.* **2011**, *7*, 5917-5925.
6. Roy, B. K.; Moulik, S. P. Effect of hydrotropes on solution behavior of amphiphiles. *Curr. Sci.* **2003**, *85*, 1148-1155.
7. Ooya, T.; Huh, K. M.; Saitoh, M.; Tamiya, E.; Park, K. Self-assembly of cholesterol-hydrotropic dendrimer conjugates into micelle-like structure: Preparation and hydrotropic solubilization of paclitaxel. *Sci. Technol. Adv. Mater.* **2005**, *6*, 452-456.
8. Cheema, M. A.; Siddiq, M.; Barbosa, S.; Castro, E.; Egea, J. A.; Antelo, L. T.; Taboada, P.; Mosquera, V. Compressibility, isothermal titration, calorimetry, and dynamic light scattering analysis of the aggregation of the amphiphilic phenothiazine drug thioridazine hydrochloride in water/ethanol mixed solvent. *Chem. Phys.* **2007**, *336*, 157-164.

9. Cui, Y.; Xing, C.; Ran, Y. Molecular dynamics simulations of hydrotropic solubilization and self-aggregation of nicotinamide. *J Pharm. Sci.* **2010**, *99*, 3048-3060.
10. Saleh, A. M.; El-Khordagui, L. K. Hydrotropic agents: A new definition. *Int. J. Pharm.* **1985**, *24*, 231-238.
11. Srinivas, V.; Balasubramanian, D. When does the switch from hydrotropy to micellar behavior occur? *Langmuir* **1998**, *14*, 6658-6661.
12. Hatzopoulos, M. H.; Eastoe, J.; Dowding, P. J.; Rogers, S. E.; Heenan, R.; Dyer, R. Are hydrotropes distinct from surfactants? *Langmuir* **2011**, *27*, 12346–12353.
13. Kim, J. Y.; Kim, S.; Papp, M.; Park, K.; Pinal, R. Hydrotropic solubilization of poorly water-soluble drugs. *J. Pharm. Sci.* **2010**, *99*, 3953-3965.
14. Balasubramanian, D.; Srinivas, V.; Gaikar, V. G.; Sharma, M. M. Aggregation behavior of hydrotropic compounds in aqueous solution. *J. Phys. Chem.* **1989**, *93*, 3865-3870.
15. Booth, H. S.; Everson, H. E. Hydrotropic solubilities. *Ind. Eng. Chem.* **1948**, *40*, 1491–1493.
16. Da Silva, R.; Spitzer, M.; Da Silva, L. H. M.; Loh, W. Investigations on the mechanism of aqueous solubility increase caused by some hydrotropes. *Thermochim. Acta* **1999**, *328*, 161-167.
17. Friberg, S.; Hasinovic, H.; Yin, Q.; Zhang, Z.; Patel, R. The system water-ethanol-didodecyldimethylammonium bromide. Phase equilibria and vapor pressures. *Coll. Surf. A: Phys Eng. Aspects* **1999**, *156*, 145-156.

18. Mijaković, M.; Kežić, B.; Zoranić, L.; Sokolić, F.; Asenbaum, A.; Pruner, C. Ethanol-water mixtures: Ultrasonics, Brillouin scattering and molecular dynamics. *J. Mol. Liq.* **2011**, *164*, 66-73.
19. Roney, A. B.; Space, B.; Castner, E. W.; Napoleon, R. L.; Moore, P. B. A molecular dynamics study of the aggregation phenomena in aqueous *n*-propanol. *J. Phys. Chem. B* **2004**, *108*, 7389-7401.
20. Dempsey, G.; Molyneux, P. Solubility of the cosolutes 4-hydroxybenzoic acid and its alkyl esters ('alkylparabens') in aqueous urea: Evidence for 1:1 cosolute-urea association in solution and evaluation of the methylene group contribution to the free energy of association. *J. Chem. Soc. Faraday Trans.* **1992**, *88*, 971-977.
21. Srinivas, V.; Balasubramanian, D. Proline is a protein-compatible hydrotrope. *Langmuir* **1995**, *11*, 2830-2833.
22. Kasraian, K.; DeLuca, P.P. Thermal analysis of the tertiary butyl alcohol-water system and its implications on freeze-drying. *Pharm. Res.* **1995**, *12*, 484-490.
23. Finney, J. L.; Bowron, D. T.; Soper, A. K. The structure of aqueous solutions of tertiary butanol. *J. Phys.: Condens. Matter* **2000**, *12*, A123-A128.
24. Nishikawa, K.; Koder, Y.; Iijima, T. Fluctuations in the particle number and concentration and the Kirkwood-Buff parameters of *tert*-butyl alcohol and water mixtures studied by small-angle X-ray scattering. *J. Phys. Chem.* **1987**, *91*, 3694-3699.

25. Nishikawa, K.; Hayashi, H.; Iijima, T. Temperature dependence of the concentration fluctuation, the Kirkwood-Buff parameters, and the correlation length of *tert*-butyl alcohol and water mixtures studied by small-angle X-ray scattering. *J. Phys. Chem.* **1989**, *93*, 6559-6565.
26. Nishikawa, K.; Iijima, T. Structural study of *tert*-butyl alcohol and water mixtures by X-ray diffraction. *J. Phys. Chem.* **1990**, *94*, 6227-6231.
27. Hayashi, H.; Nishikawa, K.; Iijima, T. Small-angle X-ray scattering study of fluctuations in 1-propanol-water and 2-propanol-water systems. *J. Phys. Chem.* **1990**, *94*, 8334-8338.
28. Tanaka, H.; Nakanishi, K.; Nishikawa, K. Clathrate-like structure of water around some nonelectrolytes in dilute solution as revealed by computer simulation and X-ray diffraction studies. *J. Incl. Phenom.* **1984**, *2*, 119-126.
29. D'Arrigo, G.; Teixeira, J. Small-angle neutron scattering study of D₂O-alcohol solutions. *J. Chem. Soc. Faraday Trans.* **1990**, *86*, 1503-1509.
30. Kusalik, P, G.; Lyubartsev, A, P.; Bergman, D, L.; Laaksonen, A. Computer simulation study of *tert*-butyl alcohol. 1. Structure in the pure liquid. *J. Phys. Chem. B* **2000**, *104*, 9526-9532.
31. Kusalik, P, G.; Lyubartsev, A, P.; Bergman, D, L.; Laaksonen, A. Computer simulation study of *tert*-butyl alcohol. 2. Structure in aqueous solution. *J. Phys. Chem. B* **2000**, *104*, 9533-9539.
32. Fornili, A.; Civera, M.; Sironi, M.; Fornili, S, L. Molecular dynamics simulation of aqueous solutions of trimethylamine-N-oxide and *tert*-butyl alcohol. *Phys. Chem. Chem. Phys.* **2003**, *5*, 4905-4910.

33. Paul, S.; Patey, G. N. Why *tert*-butyl alcohol associates in aqueous solution but trimethylamine-*N*-oxide does not. *J. Phys. Chem. B* **2006**, *110*, 10514-10518.
34. Nakanishi, K.; Ikari, K.; Okazaki, S.; Touhara, H. Computer experiments on aqueous solutions. III Monte Carlo calculation on the hydration of tertiary butyl alcohol in an infinitely dilute aqueous solutions with a new water-butanol pair potential. *J. Chem. Phys.* **1984**, *80*, 1656-1670.
35. Tanaka, H. Nakanishi, K.; Touhara, H. Computer experiments on aqueous solutions. VI Potential energy function for *tert*-butyl alcohol dimer and molecular dynamics calculation of 3 mol % aqueous solution of *tert*-butyl alcohol. *J. Chem. Phys.* **1984**, *81*, 4065-4073.
36. Bowron, D. T.; Finney, J. L.; Soper, A. K. The structure of pure tertiary butanol. *Mol. Phys.* **1998**, *93*, 531-543.
37. Bowron, D. T.; Finney, J. L.; Soper, A. K. Structural investigation of solute-solute interactions in aqueous solutions of tertiary butanol. *J. Phys. Chem. B* **1998**, *102*, 3551-3563.
38. Bowron, D. T.; Moreno, S. D. The structure of a concentrated aqueous solution of tertiary butanol: Water pockets and resulting perturbations. *J. Chem. Phys.* **2002**, *117*, 3753-3763.
39. Bowron, D. T.; Moreno, S. D. Structural correlations of water molecules in a concentrated alcohol solution. *J. Phys.: Condens. Matter* **2003**, *15*, S121-S127.

40. Finney, J. L.; Bowron, D. T.; Daniel, R. M.; Timmins, P. A.; Roberts, M. A. Molecular and mesoscale structures in hydrophobically driven aqueous solutions. *Biophys. Chem.* **2003**, *105*, 391-409.
41. Harris, K. R.; Newitt, P. J. Diffusion and structure in water-alcohol mixtures: Water + *tert*-butyl alcohol (2-methyl-2-propanol). *J. Phys. Chem. A* **1999**, *103*, 6508-6513.
42. Lee, M. E.; van der Vegt, N. F. A. A new force field for atomistic simulations of aqueous tertiary butanol solutions. *J. Chem. Phys.* **2005**, *122*, 114509 1-13.
43. Yoshida, K.; Yamaguchi, T.; Kovalenko, A.; Hirata, F. Structure of *tert*-butyl alcohol – water mixtures studied by RISM theory. *J. Phys. Chem. B* **2002**, *106*, 5042-5049.
44. Yinnon, C, A.; Yinnon, T, A. Domains in aqueous solutions: Theory and experimental evidence. *Mod. Phys. Lett. B* **2009**, *23*, 1959-1973.
45. Desnoyers, J. Colloids. In *AccessScience* © McGraw-Hill Companies, 2002. Retrieved from <http://www.accessscience.com/content/Colloids/YB020175>
46. Georgalis, Y.; Kierzek, A. M.; Saenger, W. Cluster formation in aqueous electrolyte solutions observed by dynamic light scattering. *J. Phys. Chem. B* **2000**, *104*, 3405-3406.
47. Yang, C.; Lei, W.; Wu, C. Laser light-scattering study of solution dynamics of water/cycloether mixtures. *J. Phys. Chem. B* **2004**, *108*, 11866-11870.
48. Sedláč, M. Large-scale supramolecular structure in solutions of low molar mass compounds and mixtures of liquids: I. Light scattering characterization. *J. Phys. Chem. B* **2006**, *110*, 4329-4338.

49. Sedláč, M. Large-scale supramolecular structure in solutions of low molar mass compounds and mixtures of liquids: II. Kinetics of the formation and long-time stability. *J. Phys. Chem. B* **2006**, *110*, 4339-4345.
50. Sedláč, M. Large-scale supramolecular structure in solutions of low molar mass compounds and mixtures of liquids: III. Correlation with molecular properties and interactions. *J. Phys. Chem. B* **2006**, *110*, 13976-13984.
51. Kistler, M. L.; Bhatt, A.; Liu, G.; Casa, D.; Liu, T. A complete macroion – “blackberry” assembly – macroion transition with continuously adjustable assembly sizes in {Mo₁₃₂} water/acetone systems. *J. Am. Chem. Soc.* **2007**, *129*, 6453 – 6460.
52. Jin, F.; Ye, J.; Hong, L.; Lam, H.; Wu, C. Slow relaxation mode in mixtures of water and organic molecules: Supramolecular structures or nanobubbles? *J. Phys. Chem. B* **2007**, *111*, 2255-2261.
53. Jin, F.; Ye, X.; Wu, C. Observation of kinetic and structural scalings during slow coalescence of nanobubbles in an aqueous solution. *J. Phys. Chem. B* **2007**, *111*, 13143-13146.
54. Kostko, A. F.; Anisimov, M. A.; Sengers, J. V. Criticality in aqueous solutions of 3-methyl pyridine and sodium bromide. *Phys. Rev. E* **2004**, *70*, 026118.
55. Subramanian, D.; Ivanov, D. A.; Yudin, I. K.; Anisimov, M. A.; Sengers, J. V. Mesoscale inhomogeneities in aqueous solutions of 3-methylpyridine and tertiary butyl alcohol. *J. Chem. Eng. Data* **2011**, *56*, 1238-1248.

56. Sadakane, K.; Onuki, A.; Nishida, K.; Koizumi, S.; Seto, H. Multilamellar structures induced by hydrophilic and hydrophobic ions added to a binary mixture of D₂O and 3-methylpyridine. *Phys. Rev. Lett.* **2009**, *103*, 167803.
57. Coffman, R. E.; Kildsig, D. O. Self-association of nicotineamide in aqueous solutions: Light scattering and vapor pressure osmometry studies. *J. Pharm. Sci.* **1996**, *85*, 848-853.
58. Balasubramanian, D.; Rodley, G. A. Incorporation of chemical oscillators into organized surfactant assemblies. *J. Phys. Chem.* **1988**, *92*, 5995-5998.
59. Ott, J. B.; Goates, J. R.; Waite, B, A. (Solid+liquid) phase equilibria and solid-hydrate formation in water + methyl, + ethyl, + isopropyl, and + tertiary butyl alcohols. *J. Chem. Thermodyn.* **1979**, *11*, 739-746.
60. Darwish, N, A.; Al-Anber, Z. A. Vapor-liquid equilibrium measurements and data analysis of *tert*-butanol-isobutanol and *tert*-butanol-water binaries at 94.9 kPa. *Fluid Phase Equilibr.* **1997**, *131*, 287-295.
61. Woznyj, M.; Lüdemann, H, -D. The pressure dependence of the phase diagram t-butanol/water. *Z. Naturforsch* **1985**, *40a*, 693-698.
62. Franks, F.; Ives, D. G. The structural properties of alcohol-water mixtures. *Q. Rev. Chem. Soc.* **1966**, *20*, 1-44.
63. Frank, H. S.; Evans, M. W. Free volume and entropy in condensed systems. III Entropy in binary liquid mixtures; Partial molal entropy in dilute solutions; Structure and thermodynamics in aqueous electrolytes. *J. Chem. Phys.* **1945**, *13*, 507-532.

64. Pratt, L. R.; Chandler, D. Theory of hydrophobic effect. *J. Chem. Phys.* **1977**, *67*, 3683-3704.
65. Kipkemboi, P. K.; Eastal, A, J. Densities and viscosities of binary aqueous mixtures of nonelectrolytes: *tert*-Butyl alcohol and *tert*-Butylamine. *Can. J. Chem.* **1994**, *72*, 1937-1945.
66. Nakanishi, K. Partial molal volumes of butyl alcohols and of related compounds in aqueous solution. *Bull. Chem. Soc. Jpn.* **1960**, *33*, 793-797.
67. Roux, G.; Roberts, D.; Perron, G.; Desnoyers, J, E. Microheterogeneity in aqueous organic solutions: Heat capacities, volumes and expansibilities of some alcohols, aminoalcohol and tertiary amines in water. *J. Solution Chem.* **1980**, *9*, 629-647.
68. Anisimov, M. A.; Esipov, V. S.; Zaprudskii, V. M.; Zaugol'nikova, N. S.; Ovodov, G. I.; Ovodova, T. M.; Seifer, A.L. Anomaly in the heat capacity and structural phase transformation of the ordering type in an aqueous solution of *t*-butanol. *J. Struct. Chem.* **1977**, *18*, 663-670.
69. Anisimov, M. A. *Critical Phenomena in Liquids and Liquid Crystals*; Gordon & Breach Science Publishers: New York, 1991.
70. Visser, de C.; Perron, G.; Desnoyers, J, E. The heat capacities, volumes and expansibilities of *tert*-butyl alcohol – water mixtures from 6 to 65 °C. *Can. J. Chem.* **1977**, *55*, 856-862.
71. Koga, Y. Excess partial molar enthalpies of water in water-*tert*-butanol mixtures. *Can. J. Chem.* **1988**, *66*, 3171-3175.

72. Koga, Y. Differential heats of dilution of *tert*-butanol in water-*tert*-butanol mixtures at 26.90 °C. *Can. J. Chem.* **1986**, *64*, 206-207.
73. Koga, Y. Excess partial molar enthalpies of *tert*-butanol in water-*tert*-butanol mixtures. *Can. J. Chem.* **1988**, *66*, 1187-1193.
74. Koga, Y.; Siu, W, Y, U.; Wong, T, Y, H. Excess partial molar free energies and entropies in aqueous *tert*-Butyl alcohol solutions. *J. Phys. Chem.* **1990**, *94*, 7700-7706.
75. Knight, W. S. Ph. D. Dissertation. *Princeton University* **1962**.
76. Glew, D. N.; Mak, H. D.; Rath, N. S. Aqueous non-electrolyte solutions: Part VII Water shell stabilization by interstitial nonelectrolytes. In: Covington, A. K.; Jones, P. *Hydrogen bonded solvent system*; Taylor and Francis: London, **1998**, 195-210.
77. Burton, C, J. A study of ultrasonic velocity and absorption in liquid mixtures. *J. Acoust. Soc. Am.* **1948**, *20*, 186-199.
78. Blandamer, M, J.; Clarke, D, E.; Hidden, N, J.; Symons, M, C, R. Ultrasonic absorption properties of solutions. Part 4 – *t*-Butyl alcohol + water mixtures. *Trans. Faraday Soc.* **1968**, *64*, 2691-2697.
79. Baumgartner, E, K.; Atkinson, G. Ultrasonic velocity in non-electrolyte-water mixtures. *J. Phys. Chem.* **1971**, *75*, 2336-2340.
80. Tamura, K.; Maekawa, M.; Yasunaga, T. Ultrasonic absorption studies of aqueous solutions of *tert*-butyl alcohol. *J. Phys. Chem.* **1977**, *81*, 2122-2126.

81. Tamura, K.; Osaki, A.; Koga, Y. Compressibilities of aqueous *tert*-butanol in water-rich region at 25 °C: Partial molar fluctuations and mixing schemes. *Phys. Chem. Chem. Phys.* **1999**, *1*, 121-126.
82. Sabirov, L. M.; Semenov, D. I.; Utarova, T. M.; Khaidarov, Kh. S. Some features of the temperature dependence of the hypersonic velocity in an aqueous solution of tertiary butyl alcohol. *Phys. Wave Phenom.* **2011**, *19*, 177-183.
83. Molecular dynamics simulations carried out by Professor J. B. Klauda at the University of Maryland, College Park.
84. Vega, C.; Abascal, J. L.; Nezbeda, I. Vapor-liquid equilibria from the triple point up to the critical point for the new generation of TIP4P-like models: TIP4P/Ew, TIP4P/2005, and TIP4P/ICE. *J. Chem. Phys.* **2006**, *125*, 034503.
85. Vuks, M. F.; Shurupova, L. V. The scattering of light and phase transition in solutions of tertiary butyl alcohol in water. *Opt. Commun.* **1972**, *5*, 277-278.
86. Beer, Jr.; C. W.; Jolly, D. J. Comments on “the scattering of light and phase transition in solutions of tertiary butyl alcohol in water”. *Opt. Commun.* **1974**, *11*, 150-151.
87. Iwasaki, K.; Fujiyama, T. Light scattering study of clathrate hydrate formation in binary mixtures of *tert*-butyl alcohol and water. *J. Phys. Chem.* **1977**, *81*, 1908-1912.
88. Iwasaki, K.; Fujiyama, T. Light-scattering study of clathrate hydrate formation in binary mixtures of *tert*-butyl alcohol and water: 2. Temperature effect. *J. Chem. Phys.* **1979**, *83*, 463-468.

89. Euliss, G. W.; Sorensen, C. M. Dynamic light scattering studies of concentration fluctuations in aqueous *t*-butyl alcohol solutions. *J. Chem. Phys.* **1984**, *80*, 4767-4773.
90. Bender, T. M.; Pecora, R. A dynamic light scattering study of the *tert*-butyl alcohol-water system. *J. Phys. Chem.* **1986**, *90*, 1700-1706.
91. Bender, M. T.; Pecora, R. Dynamic light scattering measurements of mutual diffusion coefficients of water-rich 2-butoxyethanol/water systems. *J. Phys. Chem.* **1988**, *92*, 1675-1677.
92. Li, Z.; Cheng, H.; Li, J.; Hao, J.; Zhang, L.; Hammouda, H.; Han, C, C. Large-scale structures in tetrahydrofuran – water mixture with a trace amount of antioxidant butylhydroxytoluene (BHT). *J. Phys. Chem. B* **2011**, *115*, 7887-7895.
93. Berne, B. J.; Pecora, R. *Dynamic Light Scattering: With Applications to Chemistry, Biology, and Physics*; Wiley: New York, 1976; Dover Publ.: Mineola, New York, 2000.
94. Fabelinskii, I. L. *Molecular Scattering of Light*. Plenum Press, New York, 1968.
95. Van de Hurst, H. C. *Light Scattering by Small Particles*. Dover Publications, New York, 1981.
96. Trent, D. L. *Propylene Oxide*. Kirk-Othmer Encyclopedia of Chemical Technology. John Wiley and Sons, Inc., published online 4 June 2001.
97. Sloan, E. D.; Koh, C. A. *Clathrate Hydrates of Natural Gases*; Taylor and Francis: Boca Raton, 2008.

98. Subramanian, D.; Anisimov, M. A. Resolving the mystery of aqueous solutions of tertiary butyl alcohol. *J. Phys. Chem. B* **2011**, *115*, 9179-9183.
99. Wickert, J. N.; Tamplin, W. S.; Shank, R. L. Phase equilibria in the system propylene oxide-water. *Chem. Eng. Prog. Sym. Serv. No. 2*. **1958**, *48*, 92-96.
100. Othmer, D. F.; White, R. E.; Trueger, E. Liquid-liquid extraction data. *Ind. Eng. Chem.* **1941**, *33*, 1240-1248.
101. Novák, J. P.; Matouš, J.; Pick, J. *Liquid-liquid Equilibria*. Elsevier, New York, 1987.
102. Moriyoshi, T.; Kaneshina, S.; Aihara, K.; Yabumoto, K. Mutual solubility of 2-butanol + water under high pressures. *J. Chem. Thermodyn.* **1975**, *7*, 537-545.
103. Jacob, J.; Anisimov, M. A.; Sengers, J. V.; Oleinikova, A.; Weingärtner, H.; Kumar, A. Novel phase-transition behavior near liquid-liquid critical points of aqueous solutions: Formation of a third phase at the interface. *Phys. Chem. Chem. Phys.* **2001**, *3*, 829-831.
104. Yoshida, K.; Yamaguchi, T.; Otomo, T.; Nagao, M.; Seto, H.; Takeda, T. Concentration fluctuations and cluster dynamics of 2-butoxyethanol-water mixtures by small-angle neutron scattering and neutron spin echo techniques. *J. Mol. Liq.* **2005**, *119*, 125-131.
105. Gupta, R.; Patey, G. N. Association and microheterogeneity in aqueous 2-butoxyethanol solutions. *J. Phys. Chem. B* **2011**, *115*, 15323-15331.

106. Yoshida, K.; Yamaguchi, T.; Otomo, T.; Nagao, M.; Seto, H.; Takeda, T. Concentration fluctuations and cluster dynamics of 2-butoxyethanol – water mixtures by small-angle neutron scattering and neutron spin echo techniques. *J. Mol. Liq.* **2005**, *119*, 125-131.
107. Schubert, K. -V.; Strey, R.; Kline, S. R.; Kaler, E. W. Small angle neutron scattering near Lifshitz lines: Transition from weakly structured mixtures to microemulsions. *J. Chem. Phys.* **1994**, *101*, 5343-5355.
108. Koehler, R. D.; Schubert, K. -V.; Strey, R.; Kaler, E. W. The Lifshitz line in binary systems: Structures in water/C₄E₁ mixtures. *J. Chem. Phys.* **1994**, *101*, 10843-10849.

Additional References:

109. Kiselev, M.; Ivlev, I. The study of hydrophobicity in water-methanol and water-*tert*-butanol mixtures. *J. Mol. Liq.* **2004**, *110*, 193-199.
110. Ferrari, E. S.; Burton, R. C.; Davey, R. J.; Gavezotti, A. Simulation of phase separation in alcohol/water mixtures using two-body force field and standard molecular dynamics. *J. Comput. Chem.* **2006**, *27*, 1211-1219.
111. D'Arrigo, G.; Giordano, R.; Teixeira, J. Temperature and concentration dependence of SANS spectra of aqueous solutions of short-chain amphiphiles. *Eur. Phys. J. E.* **2009**, *29*, 37-43.

112. Mallamace, F.; Micali, N.; Vasi, C.; D'Arrigo, G. Large supramolecular structures in water-alcohol mixtures evidenced by elastic light scattering. *Il Nuovo Cimento D* **1991**, *14*, 333-341.
113. Demangeat, J. L. NMR water proton relaxation in unheated and heated ultrahigh aqueous dilutions of histamine: Evidence for an air-dependent supramolecular organization of water. *J. Mol. Liq.* **2009**, *144*, 32-40.
114. Hunter, C. A.; Sanders, J. K. M. The nature of pi-pi interactions. *J. Am. Chem. Soc.* **1990**, *112*, 5525-5534.
115. Lydon, J. E. Chromonic mesophases. *Curr. Opin. Colloid & Interface Sci.* **2004**, *8*, 480-490.
116. Liu, T.; Diemann, E.; Li, H.; Dress, A. W. M.; Müller, A. Self-assembly in aqueous solution of wheel-shaped Mo₁₅₄ oxide clusters into vesicles. *Nature* **2003**, *426*, 59-62.
117. Bowron, D. T.; Finney, J. L.; Soper, A. K. Structural characteristics of a 0.23 mole fraction aqueous solution of tetrahydrofuran at 25 °C. *J. Phys. Chem. B* **2006**, *110*, 20235-20245.
118. Sorensen, C. M. Dynamic light-scattering study of tetrahydrofuran and water solutions. *J. Phys. Chem.* **1988**, *92*, 2367-2370.
119. Price, W. S.; Ide, H.; Arata, Y. Solution dynamics in aqueous monohydric alcohol systems. *J. Phys. Chem. A* **2003**, *107*, 4784-4789.
120. Zana, R.; Elijebari, M. J. Fluorescence probing investigation of the self-association of alcohols in aqueous solutions. *J. Phys. Chem.* **1993**, *97*, 11134-11136.

121. Cataliotti, R. S.; Palombo, F.; Paolantoni, M.; Sassi, P.; Raudino, A. Concentration fluctuations and collective properties in mixed liquid systems: Rayleigh-Brillouin spectra of *tert*-butyl alcohol/2,2'-dimethylbutane liquid mixture. *J. Chem. Phys.* **2007**, *126*, 044505.
122. Nishikawa, K.; Hayashi, H.; Iijama, T. Temperature dependence of the concentration fluctuation, the Kirkwood-Buff parameters, and the correlation length of *tert*-butyl alcohol and water mixtures studied by small-angle X-ray scattering, *J. Phys. Chem.* **1989**, *93*, 6559-6565.
123. Fukasawa, T.; Tominaga, Y.; Wakisaka, A. Molecular association in binary mixtures of *tert*-butyl alcohol – water and tetrahydrofuran – heavy water studied by mass spectrometry of clusters from liquid droplets. *J. Phys. Chem. A* **2004**, *108*, 59-63.
124. Vasquez, D.; Tora, J.; Lozsan, A.; Garcia-Sucre, M.; Urbina-Villalba, G. Interfacial properties of *tert*-butyl alcohol solutions and their relation to clathrate formation. *J. Phys. Chem. B* **2002**, *106*, 2649-2655.
125. Pradhan, T.; Ghoshal, P.; Biswas, R. Structural transition in alcohol-water binary mixtures: A spectroscopic study. *J. Chem. Sci.* **2008**, *120*, 275-287.
126. Mizuno, K.; Kimura, Y.; Morichika, H.; Nishimura, Y.; Shimada, S.; Maeda, S.; Imafuji, S., Ochi, T. Hydrophobic hydration of *tert*-butyl alcohol probed by NMR and IR. *J. Mol. Liq.* **2000**, *85*, 139-152.

127. Anderson, R. G.; Symons, M. C. R. Solvation spectra. Part 28 – NMR studies of aqueous tertiary butyl alcohol in the presence and absence of various solutes. *Trans. Faraday Soc.* **1969**, *65*, 2550-2558.
128. Goldammer, E. v.; Hertz, H. G. Molecular motion and structure of aqueous mixtures with nonelectrolytes as studied by nuclear magnetic relaxation methods. *J. Phys. Chem.* **1970**, *74*, 3734-3755.
129. Park, Y.; Cha, M.; Shin, W.; Lee, H.; Ripmeester, J. A. Spectroscopic observation of critical guest concentration appearing in *tert*-butyl alcohol clathrate hydrate. *J. Phys. Chem. B* **2008**, *112*, 8443-8446.
130. Broadwater, T. L.; Kay, R. L. Solvent structure in aqueous mixtures. II Ionic mobilities in *tert*-butyl alcohol – water mixtures at 25 °C. *J. Phys. Chem.* **1970**, *74*, 3734-3755.
131. Murthy, S. S. N. Detailed study of ice clathrate relaxation: Evidence for the existence of clathrate structures in some water – alcohol mixtures. *J. Phys. Chem. A* **1999**, *103*, 7927 – 7937.
132. Blandamer, M. J.; Engberts, J. B. F. N.; Gleeson, P. T.; Reis, C. R. Activity of water in aqueous systems; A frequently neglected property. *Chem. Soc. Rev.* **2005**, *34*, 440-458.
133. Chaplin, M. F. The memory of water: An overview. *Homeopathy* **2007**, *96*, 143-150.

134. Turner, J.; Soper, A. K. The effect of apolar solutes on water structure: Alcohols and tetraalkylammonium ions. *J. Chem. Phys.* **1994**, *101*, 6116-6125.
135. Kabeya, T.; Tamai, Y.; Tanaka, H. Structure and potential surface of liquid methanol in low temperature: Comparison of the hydrogen bond network in methanol with water. *J. Phys. Chem. B* **1998**, *102*, 899-905.
136. Ljunggren, S.; Eriksson, J. C. The lifetime of a colloid-sized gas bubble in water and the cause of the hydrophobic attraction. *Colloids Surfaces A* **1997**, *129-130*, 151-155.
137. Guillot, B.; Guissani, Y. A computer simulation study of the temperature dependence of the hydrophobic hydration. *J. Chem. Phys.* **1993**, *99*, 8075-8094.
138. Lum, K.; Chandler, D.; Weeks, J. D. Hydrophobicity at small and large length scales. *J. Phys. Chem. B* **1999**, *103*, 4570-4577.
139. Smith, D. E.; Haymet, A. D. J. Free energy, entropy, and internal energy of hydrophobic interactions: Computer simulations. *J. Chem. Phys.* **1993**, *98*, 6445-6454.
140. Choudhury, N.; Pettitt, B. M. On the mechanism of hydrophobic association of nanoscopic solutes. *J. Am. Chem. Soc.* **2005**, *127*, 3556-3567.
141. Besseling, N. A. M.; Lyklema, J. Molecular thermodynamics of hydrophobic hydration. *J. Phys. Chem. B* **1997**, *101*, 7604-7611.
142. Silverstein, K. A. T.; Haymet, A. D. J.; Dill, K. A. Molecular model of hydrophobic solvation. *J. Chem. Phys.* **1999**, *111*, 8000-8009.

143. Bertrand, G. L.; Millero, F. J.; Wu, C. -H.; Hepler, L. G. Thermochemical investigations of the water-ethanol and water-methanol solvent systems. I. Heats of mixing, heats of solutions, and heats of ionization of water. *J. Phys. Chem.* **1966**, *70*, 699-705.
144. Chechko, V. E.; Gotsulskiy, V. Ya.; Zaremba, V. G. On the nature of relaxation processes in dilute water-glycerol solutions. *J. Mol. Liq.* **2003**, *10*, 211-214.
145. Fukasawa, T.; Amo, Y.; Tominaga, Y. Low-frequency Raman scattering study of *tert*-butyl alcohol – water and tetrahydrofuran – water binary mixtures. *J. Chem. Phys.* **2003**, *118*, 6387-6393.
146. Malomuzh, N. P.; Slinchak, E. L. The cluster structure of dilute aqueous-alcoholic solutions and molecular light scattering in them. *Russ. J. Phys. Chem. A* **2007**, *81*, 1777-1782.
147. Bowron, D. T.; Moreno, S. D. The structure of a trimolecular liquid: *tert*-Butyl alcohol: Cyclohexene: Water. *J. Phys. Chem. B* **2005**, *109*, 16210-16218.
148. Koga, Y.; Nishikawa, K.; Westh, P. “Icebergs” or no “icebergs” in aqueous solutions?: Composition-dependent mixing schemes. *J. Phys. Chem. A* **2004**, *108*, 3873-3877.
149. Davidson, D. W. *Clathrate hydrates in Water: A comprehensive treatise*, Volume 2, Chapter 3, ed. Franks, F. 115-234, Plenum Press, New York-London (1973).

150. Franks, F. *Water: A Comprehensive Treatise*; Volumes 2 and 7. Plenum Press, New York, 1982.
151. Franks, F. *Water*. Royal Society of Chemistry Paperbacks; Royal Society of Chemistry, 1983; Revised ed. 1984.
152. Gompper, G.; Schick, M. *Self-assembling Amphiphilic Systems*. Academic Press Limited, London, 1994.
153. Rosano, H. L.; Clause, M. *Microemulsion Systems*. Marcel Dekker Inc., New York, 1997.
154. Jones, R. A. L. *Soft Condensed Matter*. Oxford University Press, Oxford, 2002.